AD_____

Award Number: W81XWH-07-1-0020

TITLE: Dual-Modality Prostate Imaging with PET and Transrectal Ultrasound

PRINCIPAL INVESTIGATOR: Jennifer Huber

CONTRACTING ORGANIZATION: The University of California
Berkeley, CA 94720

REPORT DATE: September 2011

TYPE OF REPORT: Final

PREPARED FOR: U.S. Army Medical Research and Materiel Command
Fort Detrick, Maryland 21702-5012

REPORT DOCUMENTATION PAGE

Form Approved
OMB No. 0704-0188

1. REPORT DATE *(DD-MM-YYYY)*	**2. REPORT TYPE**	**3. DATES COVERED** *(From - To)*
01-09-2011	Final	15 MAR 2007 - 30 AUG 2011

4. TITLE AND SUBTITLE
Dual-Modality Prostate Imaging with PET and Transrectal Ultrasound

5a. CONTRACT NUMBER

5b. GRANT NUMBER
W81XWH-07-1-0020

5c. PROGRAM ELEMENT NUMBER

6. AUTHOR(S)
Jennifer Huber

E-Mail: jshuber@lbl.gov

5d. PROJECT NUMBER

5e. TASK NUMBER

5f. WORK UNIT NUMBER

7. PERFORMING ORGANIZATION NAME(S) AND ADDRESS(ES)
The University of California
Berkeley, CA 94720

8. PERFORMING ORGANIZATION REPORT NUMBER

9. SPONSORING / MONITORING AGENCY NAME(S) AND ADDRESS(ES)
U.S. Army Medical Research and Materiel Command
Fort Detrick, Maryland 21702-5012

10. SPONSOR/MONITOR'S ACRONYM(S)

11. SPONSOR/MONITOR'S REPORT NUMBER(S)

12. DISTRIBUTION / AVAILABILITY STATEMENT
Approved for Public Release; Distribution Unlimited

13. SUPPLEMENTARY NOTES

14. ABSTRACT

We developed the hardware and software tools needed for dual Positron Emission Tomography-Transrectal Ultrasound(PET-TRUS) imaging of the prostate. We modified the TRUS equipment to work when mounted on a scanner table in conjunction withboth the LBNL prostate-optimized and Siemens EXACT HR PET scanners. We developed software to: determine the location of pointsources and calculate the corresponding location of the TRUS probe tip (both in PET coordinates), reconstruct PET data, reslice PETimaging data into TRUS coordinates, and display fused PET-TRUS images. We validated methods for positioning a subject's prostate inthe center of the PET scanner. We also constructed and imaged one-of-a-kind PET-TRUS phantoms, using these phantoms to evaluate ourdual PET-TRUS imaging techniques. Based on this phantom imaging, we currently have a PET-TRUS registration error of -2.1 ± 1.7 mmin the x direction, 1.9 ± 1.6 mm in the y direction, and 0.6 ± 0.2 mm in the z direction. We also performed extensive point source, phantomand mechanical tests to investigate our PET-TRUS registration accuracy. Finally, we updated our IRB approval for human subject studiesto improve subject recruitment, unfortunately without success.

15. SUBJECT TERMS
positron emission tomography, transrectal ultrasound imaging, prostate cancer, image registration

16. SECURITY CLASSIFICATION OF:			**17. LIMITATION OF ABSTRACT**	**18. NUMBER OF PAGES**	**19a. NAME OF RESPONSIBLE PERSON**
a. REPORT	**b. ABSTRACT**	**c. THIS PAGE**			USAMRMC
U	U	U	UU	54	**19b. TELEPHONE NUMBER** *(include area code)*

Table of Contents

Introduction

The overall goal of this project was to develop dual Positron Emission Tomography–Transrectal Ultrasound (PET-TRUS) imaging of the prostate and validate the technology with phantom and "proof of principle" human subject studies. Newly developed PET radiopharmaceuticals (e.g., [^{11}C] choline) have recently demonstrated outstanding results in the sensitive detection of prostate cancer, detecting malignant tumors in the prostate region and determining tumor "aggressiveness" based on metabolic uptake levels. However, the relative uptake in a tumor is so great that few other anatomical landmarks are visible in the PET images. PET imaging would therefore be greatly enhanced if its functional information could be accurately fused with anatomical information. Transrectal ultrasound imaging of the prostate is a standard imaging technique widely used for prostate cancer diagnosis, biopsy, treatment planning and brachytherapy seed placement. Transrectal ultrasound imaging provides high resolution anatomical detail in the prostate region that can be accurately co-registered with the sensitive functional information from PET imaging, if the PET and TRUS prostate imaging are performed sequentially during the same imaging session. Hence, dual PET-TRUS prostate imaging will help determine the location and aggressiveness of cancer within the prostate region. This novel dual-modality prostate imaging should help confirm initial diagnosis, guide biopsy, guide treatment decisions, monitor response to therapy, and detect local reoccurrence. Ultimately it should help provide better detection and treatment of prostate cancer. The goals of this research focused on developing the hardware and software tools needed for a validated dual PET-TRUS prostate imaging system. These tools are necessary for future clinical research.

Body

The development of dual PET-TRUS prostate imaging was focused on three research tasks: (1) develop methods to position a subject's prostate near the center of the PET scanner, (2) develop methods to accurately co-register PET and TRUS images, and (3) validate our ability to position human subjects in the PET scanner and to acquire co-registered PET and TRUS images with 10 "proof of principle" human subject studies.

Task 1: Develop methods for positioning the prostate at the center of the prostate-optimized PET scanner

Task 1a) Mount transrectal ultrasound stabilizer arm to scanner table, and mount transrectal ultrasound probe-stepper onto stabilizer arm.

During Year 1, we acquired the necessary transrectal ultrasound equipment – probe, stabilizer arm and stepper. The main ultrasound system (Hitachi Hi-Vision 5500 digital system) was borrowed as needed from UCSF Radiation Oncology Department in accordance with the UCSF sub-contract. As established in Year 2, the LBNL transportation group was used to transport the transrectal ultrasound system between LBNL and UCSF at an hourly cost to the project during Years 2-5.

During Year 1, we made all necessary modifications to the TRUS equipment to allow dual PET-TRUS imaging with the prostate-optimized PET scanner. Figure 1 shows the TRUS system mounted onto the scanner table of the prostate-optimized PET scanner. In Year 2, we made modifications to allow dual PET-TRUS imaging with the alternate Siemens EXACT HR PET scanner. In Year 3, we further modified the TRUS support setup to allow the point sources and TRUS probe to move farther into the EXACT HR PET scanner bore. A longer custom aluminum plate was designed, built and added beneath the commercial linear stepper in order to extend the probe-stepper motion (so both point sources can be imaged easily in the PET field of view). No modifications were necessary in Years 4-5. Figure 2a shows the completed PET-TRUS system with the new mechanical support and the EXACT HR PET scanner. Hence, Task 1a was completed for both available PET scanners.

Task 1b) Attach two 511 keV ^{68}Ge point sources to TRUS stepper (to define axial line of probe).

During Year 1, a custom point source holder was designed, built and mounted onto the TRUS stepper, as shown in figures 1 and 2. The holder is an acrylic bar with two machined cylindrical cavities that hold the two ^{68}Ge point sources (at the same height and 60.0 mm apart). The bar mounts on top of the TRUS stepper with positioning pins and screws, accurately aligning two ^{68}Ge point sources along the axial line of the TRUS probe

at a known distance from the TRUS probe tip. The point source holder was completed in Year 1 and required no modifications in Years 2-5.

Task 1c) Mount low-powered lasers on PET gantry along minor and major axes.

During Year 1, two low-powered lasers were mounted along the minor and major axes of the prostate-optimized PET scanner. We did not have to mount additional lasers in Years 2-5, since the EXACT HR PET scanner already had positioning lasers. These lasers are used to visually position objects, such as the two point sources, near the center of the PET scanner (*i.e.*, PET-center).

(a) (b)

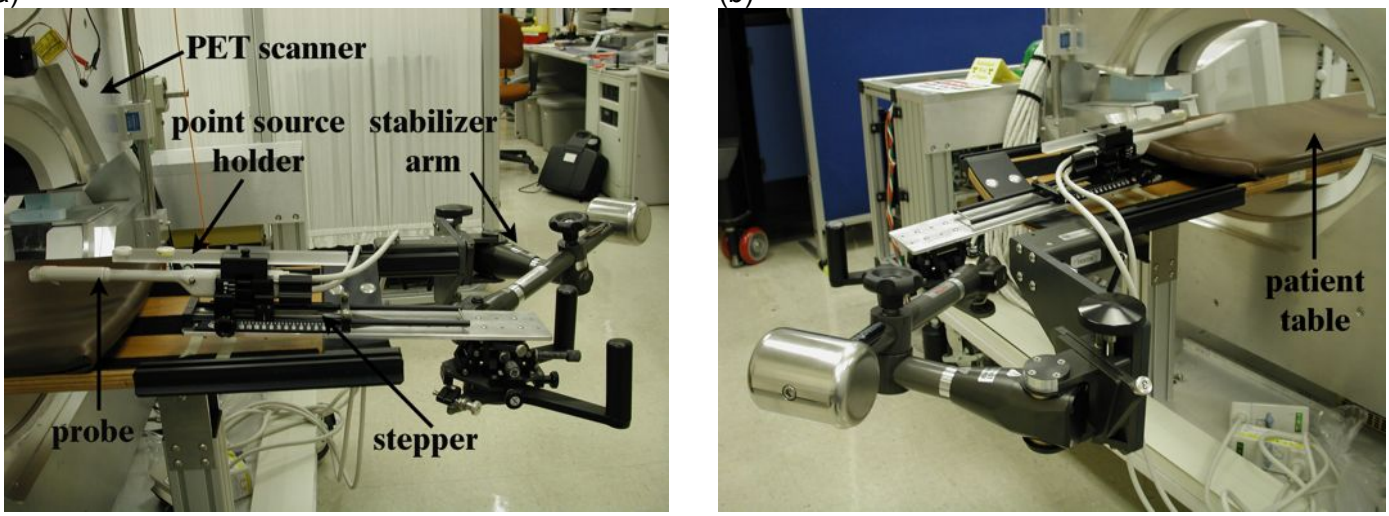

Figure 1. (a) Photograph (left side view) of the dual PET-TRUS system including prostate-optimized PET scanner, scanner table, TRUS stabilizer arm, TRUS modified stepper, TRUS ultrasound probe, and point source holder. (b) Photograph (right side view) of dual PET-TRUS system with the prostate-optimized PET scanner, focusing on the heavy counter-weight of the TRUS stabilizer arm.

(a) (b)

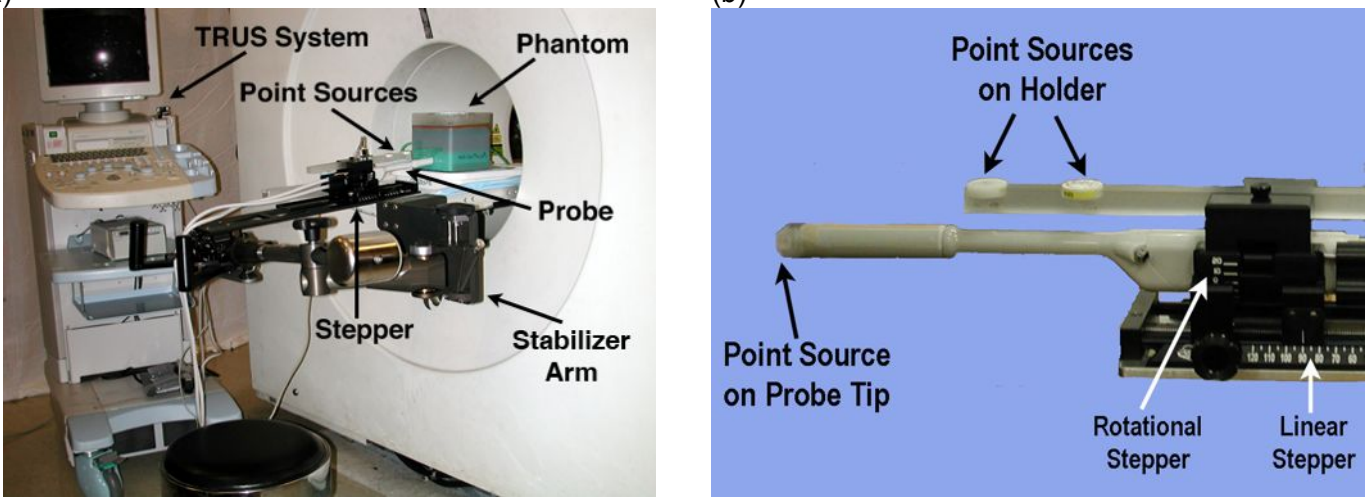

Figure 2. (a) Photograph of the dual PET-TRUS system using the Siemens EXACT HR PET scanner. (b) Photograph close-up of the TRUS ultrasound probe and point source holder. Two ^{68}Ge point sources are mounted on the holder, which are used to measure the position of the axial line of the TRUS probe. A third PET point source is taped to the TRUS probe tip, which is used for validation measurements (see Task 1e).

Task 1d) Develop software to rebin PET data into a single 2D sinogram and determine point source locations.

During Year 1, software was developed to quickly analyze point source PET data and determine the point source locations. An alternate technique was chosen over our originally proposed method (of rebinning the PET data into a single 2D sinogram). We acquired 1-5 minutes of PET data with ^{68}Ge point sources in the PET

scanner and quickly reconstructed the data with a two-iteration expectation-maximum algorithm (with a simplified model of the PET scanner geometry). The resulting PET images were then quickly processed to determine the point source locations in PET coordinates, using modified ImageJ software to determine the brightness-weighted average (over all pixels in the image planes) for each point source in the 3D volumetric PET imaging data set.

During Years 2-5, a standard filtered backprojection or iterative OSEM algorithm was used to reconstruct the point source PET data for the EXACT HR PET scanner. The software used to determine the point source locations was replaced with a streamlined Matlab program based on more statistically rigorous methods. We now use an iterative Powell search method to perform 2D Gaussian fitting, in order to determine the projection of the point sources in each PET image slice. We then find the axial z coordinate of the point sources using a 1D Gaussian fit of the signal amplitude parameter. We find the transaxial x and y coordinates of the point sources using a 1D linear interpolation fit. The (x,y,z) PET coordinate of the two point sources are then used to calculate the position of the TRUS probe tip (in PET coordinates). This software was used for all tasks related to point source imaging during Years 3-5.

Task 1e) Validate prostate positioning by PET imaging a 511 keV point source attached to the TRUS probe tip.

In Year 1 we developed a method to position a prostate near the PET-center, and this method was also used for phantom imaging in Years 2-5. The TRUS probe is rigidly attached to the TRUS stepper that allows calibrated linear displacement along its axis. The point source holder, with two ^{68}Ge point sources (see Task 1b), is attached to the TRUS stepper. The TRUS probe-stepper-point source holder unit is mounted onto the moveable TRUS stabilizer arm that is rigidly attached to the scanner table. This stabilizer arm moves to allow correct positioning of the TRUS probe in a human subject (or phantom), then its position is fixed by tightening a single knob. Once the TRUS probe is inserted and positioned inside a human subject (or phantom) at the prostate and the stabilizer arm is fixed, a series of 2D TRUS images in the transverse plane (*i.e.*, perpendicular to the TRUS probe axis) are acquired from base to apex using the linear stepper. After the TRUS imaging is complete, the TRUS probe tip is positioned at the center of the prostate using the stepper. The scanner table is then moved so the two ^{68}Ge point sources are visually positioned near the PET-center using visible low-powered lasers (see Task 1c). PET data are acquired for 1-5 minutes, quickly reconstructed, and the location of the point sources determined in PET coordinates (see Task 1d). Since the two ^{68}Ge point sources are placed along the axial line of the TRUS probe at a known location from the TRUS probe tip, the two point source locations are represented by two position vectors and vector algebra is used to calculate the actual location of the TRUS probe tip (in PET coordinates). The scanner table is then moved to axially position the TRUS probe tip (*i.e.*, prostate) at the PET-center. After the prostate is positioned in the PET scanner, the point sources can be removed for the remainder of the study or the point sources can be left in place (since they are outside the PET imaging volume and have such low activity that human subject dose is negligible). PET data of the prostate region (or phantom) is then acquired.

Our ability to position a prostate in the PET scanner was validated in Year 1 for the prostate-optimized PET scanner and in Year 2 for the EXACT HR PET scanner, by imaging a point source that represents the prostate location. As figure 2b shows, we attached a third 511 keV ^{68}Ge point source on the TRUS probe tip. We positioned the TRUS probe tip using the procedure described above, acquired (for 5 minutes) and reconstructed PET data of this third point source, and determined the third point source location in PET coordinates (see Task 1d). This procedure was repeated several times for each TRUS probe position, and multiple different probe angles were measured. As predicted, we were able to reproducibly position the TRUS probe tip within 1 mm from the PET-center in the axial direction (*i.e.*, direction of scanner table motion). A subject's prostate only needs to be positioned within the optimum central field of view of the scanner – 3 cm from the PET-center in the transaxial plane and 1 cm from the PET-center in the axial plane. Hence, we achieved greater accuracy than required for subject positioning.

However, it should be noted that this task is not sensitive to scanner table motion that is not level, since the "prostate" point source is repeatedly measured at the same scanner table position. This issue will be discussed below (see Task 2e). Various additional measurements were made using this point source setup in Years 4-5, in order to evaluate the error sources for PET-TRUS image co-registration.

Task 1f) Modify a commercial TRUS phantom to include a 511 keV point source on the "prostate" and validate prostate positioning by PET imaging the point source.

As detailed in Year 1's report, this second validation technique was deemed unnecessary and was not performed. It would only provide redundant information (to Task 1e) at additional cost.

Task 2: Develop methods for co-registering PET and TRUS images.

Task 2a) Construct TRUS-PET prostate phantom

PET-TRUS-CT-MRI Phantoms:

In Years 1 and 2, we developed a multi-modality PET-TRUS-CT-MRI phantom [1]. In Year 2, we constructed multi-modality PET-TRUS-CT-MRI phantoms using a finalized selection of tissue mimicking materials (TMM) and phantom construction procedures. These custom phantoms had structures that simulated the acoustical properties for TRUS and 511 keV activity concentrations for PET, as well as structures that simulated the nuclear magnetization for MRI and radiographic density for CT. We used tissue mimicking mixtures of agar, gelatin, $CuCl_2$-$2H_2O$, EDTA-tetra Na Hydrate, NaCl, HCHO, Germall-Plus^{TM}, glass beads, $BaSO_4$, deionized water, and 511 keV radioactive solutions. Although only PET and TRUS properties are required for this project, we developed this tissue mimicking mixture because similar agar-gelatin mixtures were proven to have long-term mechanical, ultrasound and MRI properties for at least one year [2]. As a result, our novel multi-modality phantom has many applications beyond this project. A more complete description of this phantom development is provided elsewhere [1], including a summary of the primary role for each TMM ingredient.

We constructed and imaged two-region PET-TRUS-CT-MRI phantoms with a "prostate" tapered cylinder within a "pelvis" rectangular cuboid, using the Pelvis TMM and Prostate TMM mixtures outlined in Table 1. The two regions were clearly distinguishable by all four imaging modalities [1]. The phantoms demonstrated long-term stability of imaging and mechanical properties, when stored at room temperature for over a year. We originally planned to repeatedly use the PET-TRUS-CT-MRI phantom that was constructed with long-lived $^{68}GeCl_4$. However, the ^{68}Ge tetrachloride molecules in the "prostate" migrated into the "pelvis" to become roughly uniformly distributed throughout the phantom in less than 57 days. We believe that the ^{68}Ge tetrachloride molecules were small enough to penetrate the gel pores, slowly reaching an equilibrium in radioactive concentration throughout the "prostate" and "pelvis." Hence, the evaluation of our PET-TRUS co-registration using this phantom was compromised by this $^{68}GeCl_4$ migration. We should be able to prevent this $^{68}GeCl_4$ migration by using a barrier, such as a female latex condom, between the "prostate" and "pelvis" so the radioactivity instead reaches an uniform equilibrium within the "prostate" and "pelvis" separately. However, due to the safety issue of handling the long-lived ^{68}Ge radioactivity, we decided to build a different kind of TRUS-PET phantom (that does not require ^{68}Ge handling). The development and testing of this new phantom was performed in Year 3, as discussed below in the Multi-Line Source Phantoms section.

	Agar	Gelatin	$CuCl_2$-$2H_2O$	EDTA	NaCl	HCHO	Germall-Plus	Glass Beads	$BaSO_4$
Pelvis TMM	1.17	5.52	0.11	0.33	0.77	0.24	1.45	4.4	0.50
Prostate TMM	3.64	5.70	0.12	0.34	0.80	0.25	1.50	0	0

Table I. Dry-weight percents of the various components in the PET-TRUS-CT-MRI custom phantom. The remaining weight percent is deionized water, with a trace amount of radioactive solution (^{18}F-Fluoride or $^{68}GeCl_4$).

Multi-line Source Phantoms:

We designed a new custom Multi-line Source Phantom, which was constructed and imaged in Years 3-5 [3]. The previously described PET-TRUS-CT-MRI phantoms had “prostate” and “pelvis” structures that simulated

511 keV (^{18}F or ^{68}Ge) radioactivity concentrations for PET imaging. However, our phantom does not need to have radioactive anatomical structures, because its only purpose is to evaluate image co-registration for PET and TRUS imaging. Hence, we instead designed a Multi-line Source Phantom specifically to assess PET-TRUS image registration accuracy. This phantom contains a fillable tube that winds through a non-radioactive tissue mimicking gel (Fig. 3). The tubing is distinguishable from the gel using TRUS, CT and MRI imaging, and the tube can be filled with radioactive solution (*e.g.*, ^{18}F-FDG or ^{11}C-choline) for PET imaging. This permits us to image the cross-section of several small diameter line sources (*i.e.*, tubes) in the new phantom with both PET and TRUS, allowing us to fully evaluate our co-registration accuracy for PET and TRUS images (e.g., when following our image protocol described in Task 1e).

The phantom was constructed based on the tissue mimicking gels and construction techniques described above [1]. A single piece of 20 ml silicon tube (with ID 5/32″, OD 7/32″) was accurately placed through a plastic box to create four line sources that can be filled with a single injection of radioactive solution. Three of the line sources are in a single horizontal plane in a “N” pattern. The fourth line source is within a plane angled relative to the other three line sources (Fig. 3). Once the tube was positioned, we partially filled the container with a non-radioactive dense gel (“Prostate TMM”) while creating a hole for the TRUS probe (Fig. 4d). This dense gel was selected for its imaging properties and mechanical strength, since the TRUS probe can tear softer gels. Finally, we filled the container with a second non-radioactive gel (“Pelvis TMM”) that was selected so that the tube was distinguishable from the gel in TRUS, CT and MRI images. This phantom is reusable; we simply have to inject new radioactive solution into the tube prior to imaging for each use. Figure 4 shows multimodality images of this phantom, including TRUS, resliced PET, CT and MRI images. A second Multi-line Source Phantom was also constructed and imaged, which utilized water as the second layer instead of the “Pelvis TMM”. However, artifacts in the TRUS images due to water motion made this phantom more difficult to use. In Year 4, an additional Multi-Line Source phantom of the 2 gel-layer design was constructed and imaged to provide additional results for registration accuracy assessment.

(a) (b)

Figure 3. Design drawing of a Multi-line Source Phantom from the (a) front and (b) side view. The plastic container has dimensions 15 cm x 15 cm x 15 cm, with a 2.5 cm diameter hole (centered 3 cm below the A-B-C plane) to allow access for the probe for TRUS imaging. The four line sources are embedded in a “Pelvis TMM” gel. As seen in the front view, the three white-colored line sources A-B-C are in the same horizontal plane in a N pattern with line sources A and C parallel to each other. The distance between line sources B and A (C) varies from 6.5 cm (1.5 cm) at the front face to 1.5 cm (6.5 cm) at the back face. The fourth dark-colored line source D is within a plane angled relative to the A-B-C plane, as seen in the side view. The distance between line sources C and D varies from 4 cm at the front face to 1.5 cm at the back face. Line sources C-D are coplanar, and the C-D plane is perpendicular to the A-B-C plane.

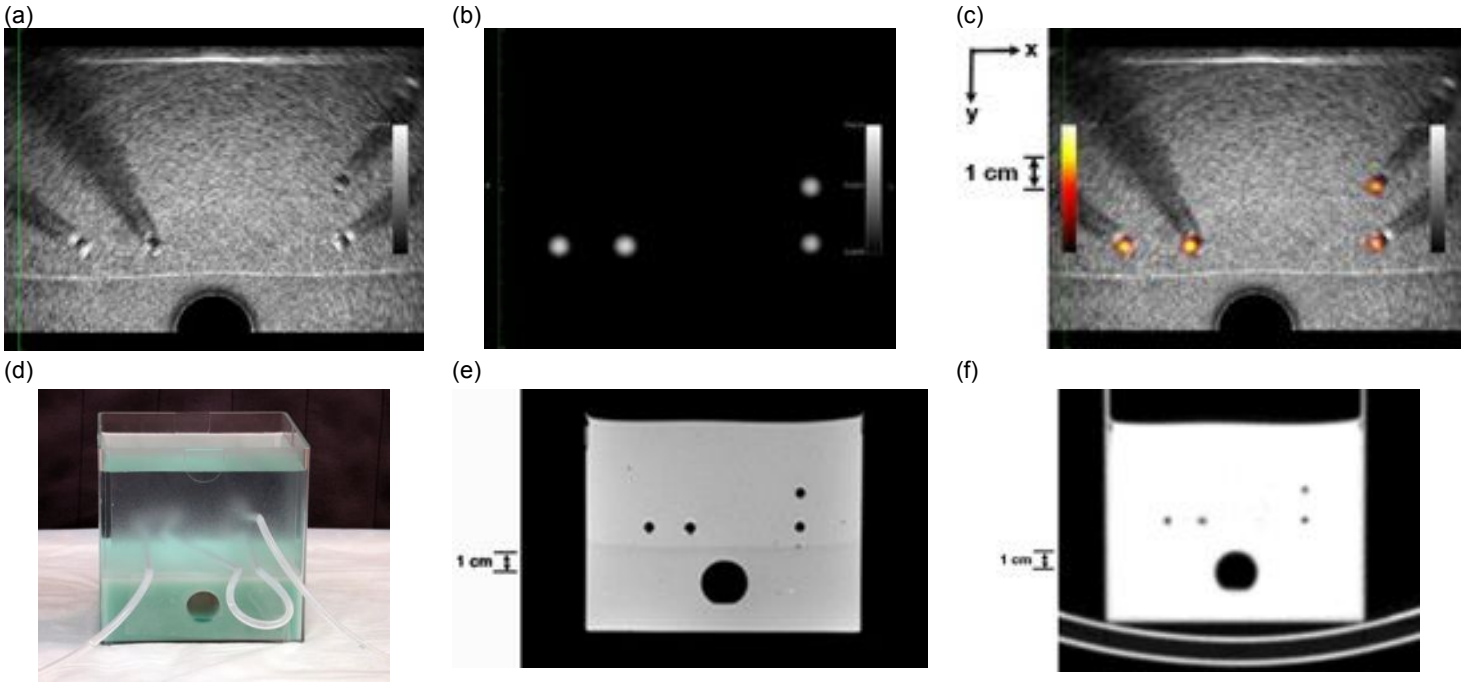

Fig. 4 (a) Transverse TRUS image of the Multi-line Source Phantom. All 4 line sources and the probe location are visible. Phantom imaged on a Hitachi Hi-Vision 5500 digital ultrasound system, using a B mode bi-plane TRUS probe in a linear stepper. Image slice was acquired with the probe inserted 2.5 cm into the phantom. (b) Reconstructed, resliced transverse PET image of the phantom acquired during the same PET-TRUS study and image slice. All 4 line sources are clearly visible. Phantom was imaged on a Siemens EXACT HR PET scanner. (c) Fused transverse image of TRUS and resliced PET image. All 4 line sources are clearly visible for both imaging modalities. Pixel size is 0.289 mm in both x and y direction. (d) Photograph of the Multi-line Source Phantom taken before the second gel layer was poured. The dense gel, hole, and fillable tube are shown within the clear plastic box. (e) Transverse reconstructed MRI T1-weighted image of the phantom. Phantom was imaged without the probe in place, using a 1.5 T Avanto Siemens MRI scanner with a head coil and a standard MPRage brain protocol. The 4 line sources are clearly visible. (f) Transverse reconstructed CT image of the phantom when the tube was filled with non-radioactive water without the probe in place. All 4 line sources are clearly visible. The phantom was imaged with a Hawkeye CT scanner (140 keV; 2.5 mAmps) on a Millennium VG3 SPECT gantry and reconstructed with filtered backprojection.

Task 2b) Attach 511 keV point source onto rear of TRUS probe. Image and reconstruct 3 point sources using PET, then determine 3D location of TRUS probe tip relative to PET-center.

In Year 1, we determined that we do not need the 511 keV point source attached to the rear of the TRUS probe. This point source was intended to track the TRUS probe's rotational motion. However, Dr. Hsu only plans to use the TRUS probe in the upright (*i.e.*, rotational angle of 0 degrees) position based on his extensive TRUS imaging experience. In the event that a rotational angle is needed for human subject imaging, the probe angle is accurately known from the rotational component of the TRUS stepper (see Fig. 2b). In Years 3-5, we also developed an alternate method to measure angular changes of the TRUS probe using an accelerometer (see Task 2e), which could be used to measure the rotational motion of the probe if necessary. Otherwise, the determination of the 3D location of the TRUS probe tip relative to the PET-center was described previously under Tasks 1d and 1e.

Task 2c) Optimize PET image reconstruction and develop image display algorithms.

PET Image Reconstruction:

In Years 1 and 2, we optimized the PET image reconstruction for the prostate-optimized PET scanner. We developed a 3D iterative penalized maximum likelihood PET reconstruction algorithm that modeled our unusual prostate-optimized PET scanner geometry, with a pre-conditioned conjugate gradient optimization algorithm and an improved detector efficiency and randoms estimate technique. However, personnel issues concerning PET image reconstruction for the prostate-optimized PET scanner developed in Year 2. We are now dependent on one person to perform this PET reconstruction, and he retired and works very limited hours as a consultant. Hence, we proceeded with this research using the EXACT HR PET scanner instead of the prostate-optimized PET scanner in Years 2-5. The development of dual PET-TRUS prostate imaging was not

dependent on which PET scanner was used. As primary investigator, I trained and repeatedly used the EXACT HR PET scanner's commercially provided software for data acquisition and image reconstruction. Hence, optimized PET image reconstruction software was developed for this project for both available PET scanners.

Reslicing Software:

In Years 2 and 3, we developed software to reslice transrectal ultrasound imaging data into PET coordinates or reslice the 3D PET imaging data into TRUS coordinates. Either of these coordinate transformations are based on our measurement of the 3D location of the TRUS probe tip in PET coordinates (calculated from the two 511 keV point source data). Although the reslicing software allows us to reslice either PET or TRUS imaging data, we focused primarily on reslicing the PET imaging data (since this provided the best co-registered image display). This software was used without modifications in Years 4-5. In Year 4, the scientist responsible for reslicing the data retired, so I was trained and performed this task for the remaining time of this project.

Functional PET image information is overlaid on anatomical TRUS images with use of the following image registration method. First, a preliminary reference position and orientation for the TRUS probe is measured while the probe is in the PET scanner. This is accomplished by using the PET scanner to image radioactive fiducial markers (*i.e.*, two 511 keV point sources) attached to the TRUS probe at known positions relative to the probe tip. Given this preliminary probe position information, the scanner table is then moved so that the TRUS probe tip is centered in the axial field of view of the PET scanner; it is assumed that the table motion direction is parallel to the axis of the PET scanner. PET images acquired for a phantom (or human subject) at this table position can now be registered with TRUS images acquired by the probe. The 3D geometric relationship between PET image pixels and TRUS image pixels is calculated based on the 511 keV point source images and the known amount of linear table motion. The 3D position in the PET coordinates is calculated for each TRUS pixel, and the PET image intensity at each TRUS pixel position is obtained via trilinear interpolation of the PET images. This yields registered sets of TRUS images and (resliced) PET images that have common pixel size and 3D pixel positions.

Image Display Software:

In Years 2 and 3, we developed the method for image display of co-registered TRUS and re-sliced PET images. This method was used in Years 4-5 for all phantom studies. We first use ImageJ to convert a resliced 3D PET imaging volume data set into an acceptable raw data format (e.g., from 32-bit real to 16-bit integer). We can converted PET image data sets from both the prostate-optimized PET scanner and the EXACT HR PET scanner using this ImageJ software. The TRUS system provides the series of 2D images in an acceptable TIFF format directly. However, we crop these images (deleting text and keeping only the image area) and convert them into the same raw data format as the PET (e.g., 16-bit integer) using ImageJ. Once we have both the TRUS and resliced converted PET images in acceptable formats, we use the OSIRIX software. This software allows us to import the resliced converted PET and TRUS images separately, then create a fused PET-TRUS image. We are able to translate (in real time) one image set relative to the other, allowing both linear translations and rotations, but such translations are intentionally not used. We have chosen the OSIRIX software for data fusion in part because it is free software that is readily available without a license. In the unlikely event that OSIRIX doesn't work well for data fusion of the human subject images, we also have a number of commercial platforms (e.g., Occentra-MasterPlan, Nucletron, and RTT Coherence and Leonardo Workstation), applications tools (e.g., Matlab), and alternate open source software (e.g., AMIDE) that could be used for co-registered image display in future work.

Task 2d) Acquire TRUS and PET "prostate" image of the custom phantom.

In Year 2, we performed dual PET-TRUS imaging of two custom phantoms, following the data acquisition imaging protocol described in Task 1e. Dual PET-TRUS data were acquired, reconstructed and fused for both the PET-TRUS-CT-MRI phantom using $^{68}GeCl_4$ (see Task 2a) and a modified commercial TRUS phantom (with a fillable tube added for ^{18}F PET imaging). These results are described in the Year 2 annual report. However, neither of these phantoms were truly optimized for the task of evaluating PET-TRUS image registration.

In Years 3-5, we performed dual PET-TRUS imaging of the new Multi-line Source Phantoms (see Task 2a) using the EXACT HR PET scanner and UCSF's TRUS system. We performed this dual PET-TRUS imaging protocol six times with Multi-Line Source Phantoms, filling the phantom tubing with 100 μCi – 537 μCi of new ^{18}F solution for each dual imaging study. We acquired TRUS and PET data for each phantom during the same imaging session, using the data collection procedure outlined previously (see Task 1e). The two 511 keV point source PET data were reconstructed (with the optimized PET reconstruction software) and used to accurately determine the 3D location of the TRUS probe tip in PET coordinates (with the Matlab software). The optimized PET reconstruction software was also used to reconstruct a 3D PET imaging volume of the custom phantom. This reconstructed 3D PET imaging volume data set was resliced into TRUS coordinates and fused with the series of 2D TRUS images taken during the same phantom imaging session (see Task 2c). We used these images to accurately evaluate our ability to acquire and co-register PET and TRUS images [3], prior to initiating human subject studies, as discussed below in Task 2e.

Task 2e) Co-register the PET and TRUS phantom images, exploring how to present the dual-modality data.

In Years 3-5, we co-registered 3D TRUS and resliced 3D PET imaging volume data sets of the Multi-Line Source Phantoms, using the reslicing and image display software described in Task 2c. We determined that this is the best way to present the dual-modality co-registered images, when evaluating the accuracy of phantom image co-registration. We also contoured the series of 2D TRUS phantom images and co-registered these contours onto the corresponding PET image planes. We will further explore this second contouring display method for PET-TRUS images of human subjects in future work, if necessary.

In Years 3-5, we used the Multi-line Source Phantom images (see Task 2d) to more accurately evaluate our ability to acquire and co-register PET and TRUS images. Figure 4a shows a transverse TRUS image of the Multi-line Source Phantom that was acquired during a dual PET-TRUS imaging study. All four line sources are clearly visible, along with dark shadows caused by each tube. The black semi-circle shows the TRUS probe location. The white horizontal line (just above the TRUS probe) shows the transition layer between the two gels (*i.e.*, between the Prostate TMM and Pelvis TMM layers). Figure 4b shows the corresponding reconstructed, resliced transverse PET image of the phantom, acquired during the same study. The entire tube was filled with 502 μCi of [^{18}F]FDG solution. PET data were acquired with a 10 minute transmission scan and a 30 minute emission scan in 3-D mode. Image reconstruction was performed with attenuation and scatter correction. Using the point source information, the 3-D volumetric PET image was then resliced into TRUS image coordinates. The four line sources are clearly visible in the PET image, as small white-colored circles from the ^{18}F radioactivity inside the tubes. Figure 4c shows a fused transverse image of the TRUS and resliced PET data, demonstrating an example of our PET-TRUS image registration capability. The resliced PET image is shown in color overlaid onto a grayscale TRUS image.

Based on these multi-line source phantom studies, our PET-TRUS registration error is 1 mm axially and 1-5 mm in the transaxial plane depending on the image study, image slice and line source measured. When calculating our average PET-TRUS registration error, we averaged the PET-TRUS difference in line source position (*i.e.*, center of line source) for a 3 cm "prostate" section of all four line sources as measured during the six multi-line source phantom studies [3]. Our average PET-TRUS registration error is –2.1 ± 1.7 mm (mean ± standard deviation) in the x direction, 1.9 ± 1.6 mm in the y direction, and 0.6 ± 0.2 mm in the z direction (see Fig. 4c for axes). The mean transaxial distance between the PET and TRUS line source position is 3.67 ± 0.86 mm. Hence, our transaxial PET-TRUS registration error is similar to the transaxial spatial resolution of 3.6 mm FWHM for the Siemens EXACT HR PET scanner. Our current registration accuracy should be sufficient for the clinical applications of detecting early recurrence and guiding prostate biopsies, but it is not sufficient for treatment planning.

In Years 4-5, we also performed a variety of phantom, point source and mechanical tests in order to evaluate the sources of this co-registration error. For instance, we repeatedly imaged two point sources (which were aligned and mounted in the standard TRUS setup, Fig. 2b) as the scanner table was moved in steps, in order to evaluate whether the table moved parallel to the axis of the scanner. Similarly, we imaged the point sources at many stepper positions (with the table position fixed and the stepper aligned along z direction), in order to

identify whether the mechanical stepping motion in the axial direction caused small changes in point source locations in the transaxial plane. We also evaluated the mechanical setup, using a precision height gauge to measure the deformation of each component (*e.g.*, probe, point source holder, and extension plate) when a variable force was applied at the TRUS probe transducer. As a result of our phantom, point source and mechanical tests, we have identified a few "real world" systematic error sources for these research methods:

(1) We assumed that the TRUS probe assembly remained rigid and the probe's angle of inclination remained fixed while the probe was stepped during the TRUS imaging. However, the probe was physically constrained by the phantom's hole (*i.e.*, "rectum"), which applied a force on the TRUS transducer that varied with stepper position. This force caused a small change in the probe's angle of inclination and a slight flexing of the probe assembly components (Fig. 6a). Although the probe had only a small deformation depending on the TRUS stepper position, the PET data were acquired at only one stepper position. This caused an error in the PET-TRUS image registration that varied with stepper position (*i.e.*, image slice). Namely, line sources in the transverse resliced PET images are consistently lower than the corresponding TRUS images by 4 ± 1 mm in the vertical direction for PET slice 19 (when the TRUS transducer is 9.5 cm into the phantom) relative to PET slice 1 (when the TRUS transducer is just entering the phantom), see Figure 5. More importantly, the PET images are lower than the corresponding TRUS images by 1.3 ± 0.4 mm for slices at the edge of a "prostate" section (*i.e.*, 3 cm section of phantom that begins 3 cm into the phantom). These "prostate section" results are compatible with the deformation observed in clinical prostate imaging as the probe steps through the rectum.

We have measured the angular deflection of the probe holder during phantom studies, using an ADXL327 accelerometer with a 12 bit ADC, dithering method and non-linear regression calibration algorithm. We have correlated these angular deflection measurements (acquired outside the subject) with the physical deformation of the probe transducer (placed inside the subject). Hence, we can now use external calibrated accelerometer measurements to accurately estimate the vertical displacement of the TRUS probe transducer as a function of stepper position, with an accuracy of 0.2 mm. These calibration measurements are based on applying a variable known force on the transducer, so they are applicable to both phantom and human subject studies. Therefore, we can correct for this known systematic error during future human subject studies, utilizing this information when resampling the PET data into TRUS coordinates.

(2) The fiducial point sources are far from the TRUS transducer because we do not want to insert the point sources inside the subject (see Fig. 2b). As a result, an error of <1 mm in measuring their location caused a PET-TRUS image registration error of up to 2 mm. In addition, this required the PET scan of the point sources to be acquired at a different table position than the phantom. It is assumed that the table motion direction is parallel to the axis of the PET scanner and that the table does not deflect, but the table motion of the PET scanner may not be level or rigid to our required precision. We found that the table re-positioning caused the point source locations to move slightly, causing a registration error of up to 1 mm in the transaxial plane. If necessary, we could develop an alternate radioactive source that can be inserted into the channel within the TRUS probe which is designed for a biopsy needle (Fig. 6b). This radioactive needle source would consist of three custom ^{22}Na-tungsten PET radioactive seeds that are spaced within a small-diameter non-radiopaque needle. However, we did not have sufficient funds remaining to purchase these custom radioactive seeds for this project.

(3) The TRUS probe-stepper unit is mounted onto a long extension plate that attaches to the stabilizer arm (Fig. 2). This plate creates some probe vibration and component flexing. Ideally, we would use an entirely new stabilizer arm that can fit through the scanner bore. This would allow for easier dual TRUS-PET imaging using commercial PET-CT scanners with long scanner bores. However, this task was beyond the resources for this project.

(4) Determination of the line source position in the TRUS images can be challenging and a source of error (Fig. 4a). In Year 3, we developed a more rigorous method for this localization. We now determine the center of each line source in a 2-D TRUS image with an automated method that: (1) calculates the sum of the pixel value along the radius (for a selected range of radius), (2) calculates the derivative of the sum and determines the two boundary angles ($\theta 1$ and $\theta 2$) with peak sum values, (3) calculates the sum pixel

value along the arc with different R and finds the position R0 of local minimum, and (4) calculates the center of the tube as ((θ1+θ2)/2,R0). In Years 3-5, we used this automated algorithm to determine the line source locations in every 2-D TRUS image, for improved evaluation of the PET-TRUS co-registration.

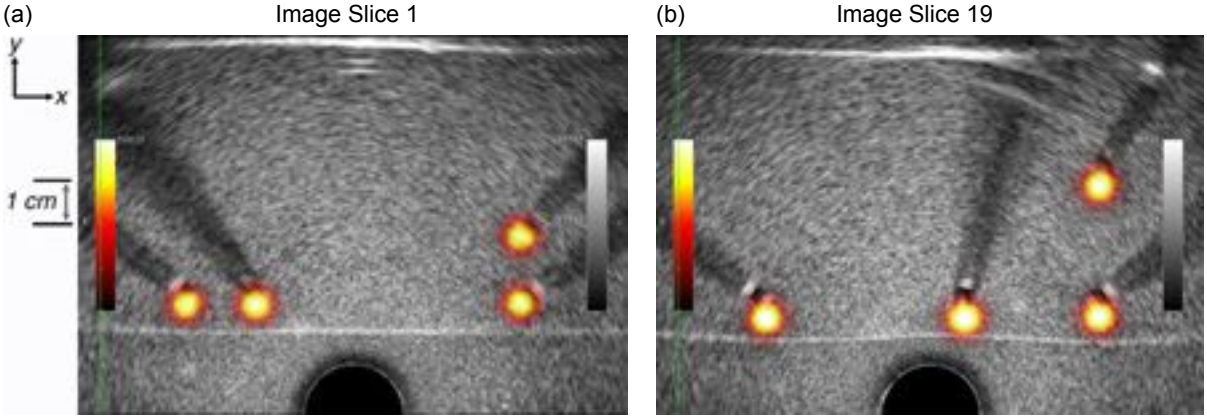

Fig. 5 Fused transverse TRUS image and resliced PET image of a Multi-line Source Phantom. All 4 line sources are clearly visible for both imaging modalities. Phantom was imaged as described above in Task 2e. The pixel size in these images are 0.289 mm in both the x and y direction. (a) Fused PET-TRUS image slice 1, which was acquired just inside the container at the end closest to the point sources (Figs. 2b and 4d). (b) Slice 19, acquired away from the point sources near the center of the phantom.

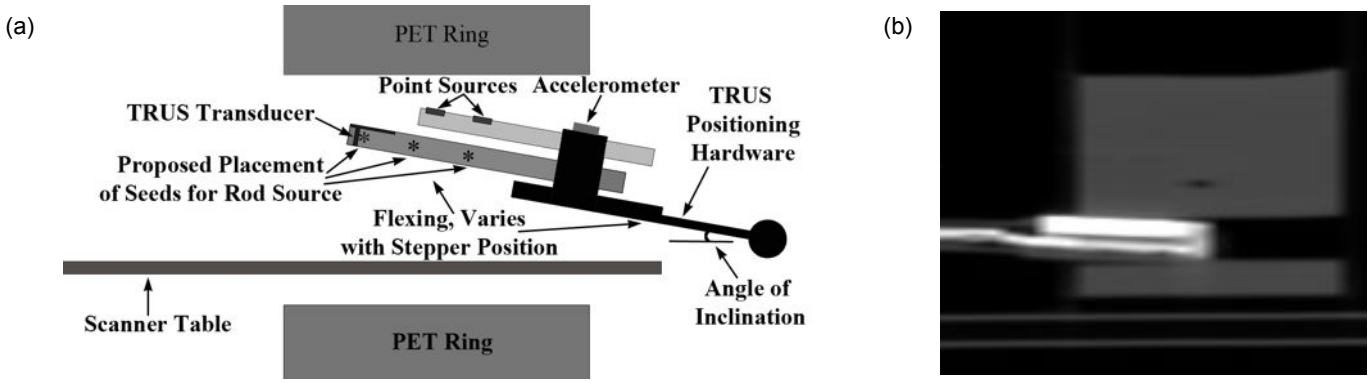

Fig. 6 (a) Simplified drawing of the TRUS-PET setup, showing current and proposed future radioactive source placement. Drawing also indicates the components that are flexing, the accelerometer position, and the angle of inclination. (b) Saggital reconstructed CT image of the TRUS probe partially inserted into the Multi-line Source Phantom, showing the asymmetric internal structure of the probe (including the dark channel where the radioactive needle source could be inserted).

Task 3: Validate our ability to position human subjects in the PET scanner and to acquire co-registered PET and TRUS images.

Task 3a) Write human subjects protocol, and get approval from LBNL, UCSF and DOD.

In Year 1, initial human subject approval was received ahead of schedule. This was updated and renewed in Years 2-3, primarily to allow the use of the EXACT HR PET scanner and to add personnel. In Year 4, further modifications to the human subjects documentation were approved to: (1) include alternate personnel for catheter insertion and radiopharmaceutical injection, (2) update the contact phone number on the recruitment flyer, and (3) allow $100 compensation per subject for his time, effort and local travel expenses. We are currently approved to perform human subjects studies through January 2012 using either available PET scanner.

Task 3b) Recruit 10 human subjects with confirmed prostate cancer.

We initiated human subject recruitment at UCSF, without success. In order to facilitate recruitment, the human subjects protocol was modified in Year 4 to provide subjects $100 reimbursement for their time, effort and

travel expenses. In addition, more aggressive subject recruitment at UCSF Comprehensive Cancer Center was initiated, including emails to all UCSF prostate cancer physicians alerting them of our subject recruitment and subject criteria.

Task 3c) Perform human subject studies with TRUS system and PET scanner (using ^{11}C choline) during the same exam.

Human subject studies were not performed. No suitable human subjects were recruited for this study, despite aggressive attempts to do so through UCSF. For future human subject studies, recruitment will also be initiated through physicians at hospitals and clinics other than UCSF (as allowed by a revised protocol). However, extensive additional phantom studies (beyond those initially proposed) were performed in order to improve PET-TRUS prostate image registration, in anticipation of human subject studies performed in future work.

Task 3d) Reconstruct PET images, identify 3D contours from TRUS images, and co-register.

Human subject studies were not performed. However, image reconstruction, contouring, and registration is discussed in Task 2e for phantoms.

Task 3e) Optimize image co-registration.

Human subject studies were not performed. However, optimization of image co-registration for phantoms is discussed in Task 2e.

Key Research Accomplishments

Our key research accomplishments for this project are summarized as follows:

Task 1: We developed hardware and software tools to position the prostate at the center of a PET scanner (for the LBNL prostate-optimized and Siemens EXACT HR PET scanners) with 1 mm accuracy.

Task 2: We developed and imaged novel Multi-line Source Phantoms, consisting of a single fillable tube that winds through a non-radioactive tissue mimicking gel. These phantoms were specifically designed to evaluate our ability to acquire and co-register PET-TRUS images, but these phantoms have many applications beyond the scope of this project.

We performed repeated dual PET-TRUS imaging studies with the custom Multi-line Source Phantoms and evaluated our PET-TRUS co-registration error. Our average PET-TRUS registration error is –2.1 ± 1.7 mm (mean ± standard deviation) in the x direction, 1.9 ± 1.6 mm in the y direction, and 0.6 ± 0.2 mm in the z direction. Our current registration accuracy should be sufficient for clinical applications, such as detecting early recurrence and guiding prostate biopsies.

We performed various additional tests in order to (1) identify our sources of PET-TRUS co-registration error and (2) investigate how to reduce the co-registration error. For instance, we built improved accelerometer instrumentation and used it to measure TRUS probe motion (*i.e.*, a small change in the probe's angle of inclination as the probe is stepped during TRUS imaging). We also used a precision height gauge to measure the deformation of each component (probe, point source holder and extension plate) when a variable force was applied at the TRUS probe transducer. As a result of correlating these measurements, we can now use external calibrated accelerometer measurements to accurately estimate TRUS probe displacement during a phantom or human subject study, and this will allow us to correct for this known systematic error in future work.

Task 3: We modified our human subjects documentation to facilitate subject recruitment (e.g., provide compensation of $100 per subject) and instigated more aggressive subject recruitment at UCSF Comprehensive Cancer Center. However, we were unable to recruit a suitable human subject in time.

Reportable Outcomes

Bibliography.

- DOD IDEA grant proposal, titled "Multimodality Prostate Imaging Using Transrectal Ultrasound and PET/CT," submitted August 21, 2011 (in review).
- Peer-reviewed journal article: J. S. Huber, Q. Peng, W. W. Moses, B.W. Reutter, J. Pouliot and I.C. Hsu, "Development of a PET-Transrectal Ultrasound Prostate Imaging System," *IEEE Trans. Nucl. Sci.*, NS-58, 674-681 (2011).
- Conference Presenter: J.S. Huber, "Dual-Modality Imaging with Positron Emission Tomography and Transrectal Ultrasound," at the 2011 IMPact Conference, March 10, 2011, Orlando, FL.
- Invited Speaker: J.S. Huber, "Registration Methods for a Dual PET-TRUS Prostate Imaging System," at the 9th Thematic Workshop on Advanced Multimodality Instruments in the Detection, Diagnosis, Therapy and Follow-up of Diseases, January 13, 2011, Marseilles, France.
- Conference Record: J. S. Huber, Q. Peng, W. W. Moses, B.W. Reutter, J. Pouliot, and I.C. Hsu, "Dual PET-TRUS Prostate Image Registration," *2010 Nuclear Science Symposium Conference Record*, 3414-3421, 2010.
- Conference Presenter: J.S. Huber, "Dual PET-TRUS Prostate Image Registration," at the IEEE Nuclear Science and Medical Imaging Conference, November 6, 2010, Knoxville, TN.
- NIH R01 grant proposal, titled "Registration Methods for Multimodality Prostate Imaging," re-submitted October 28, 2010 (scored but not funded).
- U.S. Provisional Patent Application 12/622,335, Attorney Docket JIB-2420; Title "Multi-Modality Phantoms and Methods for Co-registration of Dual PET-Transrectal Ultrasound Prostate Imaging;" Inventors Jennifer S. Huber, William W. Moses, Jean Pouliot, I-Chow Hsu, Qiyu Peng, Ronald H. Huesman, and Thomas F. Budinger; File Date November 19, 2009.
- Peer-reviewed journal article: J. S. Huber, Q. Peng, and W. W. Moses, "Multi-Modality Phantom Development," *IEEE Trans. Nucl. Sci.*, NS-56, 2722-2727 (2009).
- NIH R01 grant proposal, titled "Registration Methods for Multimodality Prostate Imaging," submitted February 1, 2010 (not scored).
- Conference Speaker: J.S. Huber, "Dual-Modality Prostate Imaging with PET and Transrectal Ultrasound" at the IEEE Medical Imaging and Nuclear Science Symposium Conference, October 2008, Dreseden Germany.
- International patent application: Patent Application Ser. No. PCT/US2008/064160; Title "Co-registration for Dual PET-Transrectal Ultrasound (PET-TRUS) Prostate Imaging;" Inventors Jennifer S. Huber, William W. Moses, Jean Pouliot, I-Chow Hsu, Qiyu Peng, Ronald H. Huesman, and Thomas F. Budinger; File Date May 19, 2008.
- Workshop Speaker: J.S. Huber, "Dual PET-Transrectal Ultrasound Prostate Imaging" at the Community of Bay Area Radionuclide Imagers Workshop, February 2008, Berkeley, CA.
- Conference Record: J. S. Huber, Q. Peng, and W. W. Moses, "Multi-Modality Phantom Development," *Nuclear Science Symposium Conference Record*, vol. 4, pp. 2944-2948, 2007.
- Conference Presenter: J.S. Huber, "Multi-Modality Phantom Development" at the IEEE Medical Imaging and Nuclear Science Symposium Conference, October 2007, Honolulu, Hawaii.
- Provisional patent application: Application No. 60/939,051; Title "Co-registration for Dual PET-Transrectal Ultrasound (PET-TRUS) Prostate Imaging;" Inventors Jennifer S. Huber, William W. Moses, Jean Pouliot, I-Chow Hsu, Qiyu Peng, and Thomas F. Budinger; File Date May 19, 2007.

List of Personnel receiving pay from the research effort:

LBNL personnel:
Jennifer S. Huber

Shelley A. Caras
Steven L. Ferreira
David Fraser
Jaspal Gill
John S. Haugrud
Luster D. Howard
Ronald H. Huesman
Robert T. Kelley
William W. Moses
Kit Man Mui
James P. O'Neil
Qiyu Peng
Dennis Paiva
David R. Paulson
Chris Redding
Bryan W. Reutter
James Tobias
Tim S. Williams
David S. Wilson
John C. Wool

UCSF personnel:
Jean Pouliot
I-Chow Joe Hsu
Zhongxia Hu

Conclusions

We fully developed a working PET-TRUS imaging system that utilizes either the prostate-optimized PET scanner or the Siemens EXACT HR PET scanner for our dual-modality prostate imaging studies. We have the necessary software to: (1) determine point source locations and calculate the 3D geometric relationship between PET image pixels and TRUS image pixels, (2) position a prostate at the PET-center, (3) reconstruct PET data, (4) reslice PET imaging data (into TRUS coordinates), and (5) display co-registered resliced PET - TRUS images.

We developed novel PET-TRUS-CT-MRI phantoms and performed dual PET-TRUS imaging studies with them. In particular, we performed dual-modality imaging studies with our custom Multi-line Source Phantoms and evaluated our ability to acquire and co-register PET-TRUS images. Based on these phantom imaging studies, our average PET-TRUS registration error is –2.1 ± 1.7 mm (mean ± standard deviation) in the x direction, 1.9 ± 1.6 mm in the y direction, and 0.6 ± 0.2 mm in the z direction. The mean transaxial distance between the PET and TRUS line source position is 3.67 ± 0.86 mm. Hence, our transaxial PET-TRUS registration error is similar to the transaxial spatial resolution of 3.6 mm FWHM for the Siemens EXACT HR PET scanner. Our current registration accuracy should be sufficient for the clinical applications of detecting early recurrence and guiding prostate biopsies, but it may not be sufficient for treatment planning.

We also performed various phantom, point source and mechanical tests to fully investigate our PET-TRUS registration accuracy. Our overall registration error includes a systematic error in the vertical direction of 1.3 ± 0.4 mm due to mechanical effects as the probe is inserted and stepped into the phantom (or subject). Using external accelerometer measurements, we can accurately estimate and correct this vertical deformation of the TRUS probe transducer as a function of stepper position. This information can be utilized when resampling the PET data into TRUS coordinates, thereby reducing the overall registration error. We will perform this correction for human subject studies in future work.

Based on our results, our dual PET-TRUS imaging still appears to be a promising new technology for prostate imaging. Accurately co-registered PET and TRUS images should accurately guide subsequent diagnosis and treatment procedures. For instance, dual PET-TRUS prostate imaging could be used to: (1) increase the diagnostic accuracy of biopsy, (2) determine where higher dose is needed for external beam irradiation and

brachytherapy treatment, and (3) detect early failure response to external beam irradiation, brachytherapy, prostatectomy, or androgen ablation.

References

[1] J. S. Huber, Q. Peng, and W. W. Moses, "Multi-Modality Phantom Development," *IEEE Trans. Nucl. Sci.*, NS-56, 2722-2727 (2009).

[2] E. L. Madsen, M. A. Hobson, S. Hairong, T. Varghese and G. R. Frank, "Tissue-mimicking agar/gelatin material for use in heterogeneous elastography phantoms," *Phys. Med. Biol.*, vol. 50, pp. 5597-5618, 2005.

[3] J.S. Huber, Q. Peng, W. W. Moses, B.W. Reutter, J. Pouliot and I.C. Hsu, "Development of a PET-Transrectal Ultrasound Prostate Imaging System," *IEEE Trans. Nucl. Sci.*, NS-58, 674-681 (2011).

List of Documents Included as Appendices

- DOD IDEA grant proposal technical abstract, titled "Multimodality Prostate Imaging Using Transrectal Ultrasound and PET/CT," submitted August 21, 2011 (in review).
- J. S. Huber, Q. Peng, W. W. Moses, B.W. Reutter, J. Pouliot and I.C. Hsu, "Development of a PET-Transrectal Ultrasound Prostate Imaging System," *IEEE Trans. Nucl. Sci.*, NS-58, 674-681 (2011).
- Conference abstract: J.S. Huber presenter, "Dual-Modality Imaging with Positron Emission Tomography and Transrectal Ultrasound," at the 2011 IMPact Conference, March 10, 2011, Orlando, FL.
- Invited abstract: J.S. Huber speaker, "Registration Methods for a Dual PET-TRUS Prostate Imaging System," at the 9th Thematic Workshop on Advanced Multimodality Instruments in the Detection, Diagnosis, Therapy and Follow-up of Diseases, January 13, 2011, Marseilles, France.
- J. S. Huber, Q. Peng, W. W. Moses, B.W. Reutter, J. Pouliot, and I.C. Hsu, "Dual PET-TRUS Prostate Image Registration," *2010 Nuclear Science Symposium Conference Record*, 3414-3421, 2010.
- Conference abstract: J.S. Huber presenter, "Dual PET-TRUS Prostate Image Registration," at the IEEE Nuclear Science and Medical Imaging Conference, November 6, 2010, Knoxville, TN.
- NIH R01 grant proposal project summary, titled "Registration Methods for Multimodality Prostate Imaging," re-submitted October 28, 2010 (scored but not funded).
- U.S. provisional patent application abstract: Title "Multi-Modality Phantoms and Methods for Co-registration of Dual PET-Transrectal Ultrasound Prostate Imaging;" Inventors Jennifer S. Huber, William W. Moses, Jean Pouliot, I-Chow Hsu, Qiyu Peng, Ronald H. Huesman, and Thomas F. Budinger; File Date November 19, 2009.
- J. S. Huber, Q. Peng, and W. W. Moses, "Multi-Modality Phantom Development," *IEEE Trans. Nucl. Sci.*, NS-56, 2722-2727 (2009).
- Conference abstract: J.S. Huber speaker, "Dual-Modality Prostate Imaging with PET and Transrectal Ultrasound" at the IEEE Medical Imaging and Nuclear Science Symposium Conference, October 2008, Dreseden Germany.
- Workshop schedule: Jennifer Huber speaker, "Dual PET-Transrectal Ultrasound Prostate Imaging" at the Community of Bay Area Radionuclide Imagers Workshop, February 2008, Berkeley, CA.
- J. S. Huber, Q. Peng, and W. W. Moses, "Multi-Modality Phantom Development," *Nuclear Science Symposium Conference Record*, vol. 4, pp. 2944-2948, 2007.
- Conference abstract: J.S. Huber presenter, "Multi-Modality Phantom Development" at the IEEE Medical Imaging and Nuclear Science Symposium Conference, October 2007, Honolulu, Hawaii.

TECHNICAL ABSTRACT

Background: It is critical to develop a new imaging technology that can distinguish between indolent and aggressive prostate cancer, in order to improve the diagnostic accuracy of biopsies and guide treatment planning. Transrectal ultrasound (TRUS) imaging is a standard anatomical imaging technique widely used for prostate cancer diagnosis, biopsy guidance, treatment planning and brachytherapy seed placement. Positron Emission Tomography (PET) is a sensitive and specific functional imaging technique that can identify biochemical states associated with prostate cancer using newly developed radiopharmaceuticals, as well as determine the aggressiveness of the cancerous tumors based on the metabolic uptake levels. Recent advances in PET technology have improved the diagnostic performance (*e.g.*, new clinical PET scanners have a spatial resolution ~3 mm). Hence, we believe that merging these prostate-imaging technologies will have a significant clinical impact, once techniques for accurate TRUS-PET image registration have been fully developed. This multimodality prostate imaging will help identify both the location and aggressiveness of prostate cancer.

Objective: The goal of this project is to develop TRUS-PET-CT prostate imaging and evaluate the technology with initial human subjects. We will acquire high-resolution anatomical detail from TRUS imaging that is accurately registered with the sensitive metabolic information from PET. The low dose X-ray computed tomography (CT) will be used for improved PET image reconstruction and TRUS-PET image registration. The tools and protocols developed in this project are necessary for future clinical prostate cancer research.

Specific Aims: The aims of this project focus on developing hardware and software tools: (1) to comfortably position the TRUS probe inside a subject using a TRUS controller that can move with the subject through a PET-CT scanner bore, (2) to develop a method to acquire and accurately register 3-D volumetric TRUS, PET and CT images using phantom studies, and (3) to evaluate this registration method with TRUS-PET-CT human subject studies. Our goal is to acquire and register TRUS-PET prostate images with 2 mm accuracy.

Study Design: We will perform multimodality prostate imaging sequentially during the same imaging session in the order of: TRUS, low dose CT and PET. The subject will remain in the same position with the TRUS probe in place for all imaging, since the TRUS probe significantly distorts the local anatomy. The PET-CT images are already routinely co-registered, so the critical task is to register the TRUS images to either the CT or PET images. We will explore two methods for doing this: (1) using CT to determine the position of the TRUS probe and (2) using PET to find the position of ^{22}Na radioactive seeds that are inserted at a known location inside the TRUS probe (via the hollow channel that is designed for a biopsy needle). Since the position of the TRUS images is well known with respect to the physical position of the probe, this gives sufficient information for image registration. We will quantitatively evaluate these two methods by performing phantom studies, using custom phantoms designed to test TRUS-PET-CT image registration accuracy, and will select the best method. We will then perform initial human subject studies in order to identify issues that would affect the clinical utility of the techniques. Subjects will have prostate cancer that has been confirmed by biopsy. Each subject will participate in our study after standard gold radiopaque markers have been implanted into his prostate in preparation for his radiation therapy. These gold fiducial markers will be used to evaluate our multimodality image registration accuracy.

Innovation: This project is novel because it integrates new clinical PET-CT and TRUS technologies for the first time. PET is fundamentally different than most imaging technologies currently used for prostate cancer detection, because it is based on metabolic function (*e.g.*, whether or not radiopharmaceutical is taken up by the prostate tumors and at what level) rather than anatomical structure (*e.g.*, whether or not a lesion is observed using CT or TRUS imaging, which may not be cancerous). We will perform novel functional PET imaging using [^{11}C]choline. We will also acquire anatomical imaging using TRUS and CT during the same imaging session, allowing for accurate TRUS-PET image registration. Hence, we will develop a unique diagnostic imaging tool to identify the location and aggressiveness of prostate cancer tumors.

Impact: TRUS-PET-CT imaging will help localize prostate cancer tumors and distinguish between indolent and aggressive disease. As a result, this multimodality prostate imaging technology can be used to improve many aspects of prostate cancer detection and management, such as (1) guiding biopsy to increase its diagnostic accuracy, (2) targeting where higher dose is needed for external beam radiotherapy and brachytherapy treatment, and (3) monitoring and predicting response to therapy.

Development of a PET-Transrectal Ultrasound Prostate Imaging System

Jennifer S. Huber, *Member, IEEE*, Qiyu. Peng, *Member, IEEE*, William W. Moses, *Fellow, IEEE*, Bryan W. Reutter, *Senior Member, IEEE*, Jean Pouliot, and I. Chow Hsu

***Abstract*—Multimodality imaging has an increasing role in the management of a large number of diseases, particularly if both functional and structural information are acquired and accurately registered. Transrectal ultrasound (TRUS) imaging is currently an integral part of prostate cancer diagnosis and treatment procedures, providing high-resolution anatomical detail of the prostate region. Positron Emission Tomography (PET) imaging with ^{11}C-choline is a sensitive functional imaging technique that can identify biochemical states associated with prostate cancer. We believe that merging these prostate imaging technologies will help identify the location and aggressiveness of prostate cancer. We envision using dual PET-TRUS prostate imaging to guide biopsy, guide treatment procedures, and detect local recurrence earlier than is currently possible. Hence, we have developed a dual PET-TRUS prostate imaging system and protocol designed to allow accurate 3-D image registration. We have evaluated this PET-TRUS system by performing dual PET-TRUS imaging of custom phantoms. We describe here our dual-modality imaging system, custom phantoms and phantom study results. We also discuss our investigation of the PET-TRUS registration accuracy. We measure an average PET-TRUS registration error for our phantom studies of 2.1 ± 1.7 mm in the x direction, 1.9 ± 1.6 mm in the y direction, and 0.6 ± 0.2 mm in the z direction. This registration accuracy is sufficient for some clinical applications such as biopsy guidance and early detection of recurrence.**

***Index Terms*—Cancer, image registration, positron emission tomography, ultrasound.**

I. Introduction

MULTIMODALITY imaging plays an increasingly important role in the management of a large number of diseases. Combining modalities that provide both functional and structural information is particularly important. For instance, functional information can be acquired with single photon emission computed tomography (SPECT), positron emission tomography (PET) or functional magnetic resonance imaging (fMRI), whereas anatomical information can be acquired using x-ray computed tomography (CT), ultrasound (US) or magnetic resonance imaging (MRI).

Combining PET and CT has recently revolutionized the role of imaging in the management of many types of cancer. However, PET-CT imaging is not the preferred modality combination for all cancers. For instance, transrectal ultrasound (TRUS) imaging is an integral part of diagnosis and treatment procedures for prostate cancer [1]. Transrectal ultrasound provides good anatomical detail of the prostate region and accurately measures the prostate volume, whereas CT has poor contrast for soft-tissue (like the prostate) and it over-estimates prostate volume [2]–[4].

TRUS is the anatomical imaging modality of choice for most prostate cancer clinicians. PET with $[^{11}\mathrm{C}]\mathrm{choline}$ is a sensitive functional imaging technique that can identify biochemical states associated with prostate cancer. Hence, we believe that imaging the prostate using a dual PET-TRUS system will help determine the location and aggressiveness of cancer within the prostate region. We envision that dual PET-TRUS prostate imaging could be used to guide biopsy, guide treatment procedures, and detect local recurrence earlier than is currently possible. We estimate that the clinical applications of biopsy guidance and detection of local recurrence both require a PET-TRUS registration accuracy of 5 mm or less [5], whereas treatment guidance (e.g., radiation therapy or brachytherapy planning) requires a PET-TRUS registration accuracy of 2-3 mm [6], [7].

Therefore, we have developed a dual imaging system that acquires PET and TRUS data sets during the same imaging session, using methods that should allow us to accurately register these 3-D volumetric images. PET-TRUS image registration based on prostate image features is inaccurate, since few anatomical features are seen in the PET images. Our image registration method instead depends on precisely determining the mechanical location and orientation of the TRUS probe within the PET scanner directly, by performing an additional fast PET scan of fiducial 511 keV point sources that determine the probe position. In order to evaluate our PET-TRUS image registration accuracy (prior to human subject studies), we have performed dual PET-TRUS imaging studies of custom phantoms. This paper describes our dual PET-TRUS system and presents our phantom study results.

II. Prostate Imaging With Nuclear Medicine

Currently the functional imaging technique most commonly used for prostate cancer is $[^{111}\mathrm{In}]\mathrm{ProstaScint}$ SPECT imaging, which is generally indicated for patients suspected of residual or recurrent disease following treatment and for patients suspected of metastatic disease. However, interpretation of these

Manuscript received September 27, 2010; revised February 18, 2011; accepted March 21, 2011. Date of publication May 12, 2011; date of current version June 15, 2011. This work was supported in part by the Director, Office of Science, Office of Biological and Environmental Research, Medical Science Division of the U.S. Department of Energy under Contract DE-AC02-05CH11231 and in part by Department of Defense Grant W81XWH-07-1-0020.

J. S. Huber, Q. Peng, W. W. Moses, and B. W. Reutter are with the Lawrence Berkeley National Laboratory, Berkeley, CA 94720 USA (e-mail: jshuber@lbl.gov; qpeng@lbl.gov; wwmoses@lbl.gov; bwreutter@lbl.gov).

J. Pouliot and I. C. Hsu are with the Department of Radiation Oncology, UCSF Comprehensive Cancer Center, San Francisco, CA 94143 USA (e-mail: pouliot@radonc.ucsf.edu; ihsu@radonc.ucsf.edu).

Color versions of one or more of the figures in this paper are available online at http://ieeexplore.ieee.org.

Digital Object Identifier 10.1109/TNS.2011.2136387

SPECT images is challenging because the radiopharmaceutical demonstrates nonspecific uptake in the normal vasculature, bowel, bone marrow, and prostate gland [8].

PET was not commonly used for prostate imaging in the past, because the standard radiotracer [^{18}F]fluorodeoxyglucose (FDG) is not very specific and bladder accumulation of this radiopharmaceutical often obscures prostate tumors [9]–[11]. However, newly developed PET radiopharmaceuticals have demonstrated outstanding results in the sensitive detection of prostate cancer. Hara and co-workers find that: [^{11}C]choline clears the blood quickly; its uptake in prostate tumors provides excellent tumor/normal contrast; and bladder accumulation is minimal [12]. Therefore, [^{11}C]choline is an attractive PET radiopharmaceutical for detecting prostate tumors and following treatment efficacy [13]–[28].

Several other ^{11}C radiopharmaceuticals are also under investigation, including [^{11}C]acetate [27], [29], [31] and [^{11}C]methionine [32]–[35]. There are also several ^{18}F radiopharmaceuticals currently under investigation for prostate cancer imaging that are expected to have increased commercial viability, including [^{18}F]fluorocholine (^{18}F – FCH) [36]–[40], [^{18}F] – 16β-fluoro-5α-dihydrotestosterone (^{18}F – FDHT) [41], [42], and anti-1-amino-3-^{18}F-fluorocyclobutane-1-carboxylic acid (anti-^{18}F-FACBC) [43], [44].

Many clinical trials are currently investigating the potential role of PET imaging for initial diagnosis, staging and restaging of prostate cancer. PET imaging with choline and acetate radiopharmaceuticals may be helpful in initial diagnosis and staging, but so far clinical findings have been mixed. Sensitivity appears to depend on other factors–such as PSA level and PSA doubling time–that need to be defined [20], [24], [26], [27]. In some cases clinical findings have also been confused by the attempt to find tumors that are smaller than the spatial resolution of their PET scanner. However, PET imaging with [^{11}C]choline or [^{18}F]FCH has already proven to be a sensitive and accurate imaging technique for restaging and identifying the site of recurrence. It is being increasingly used in many centers in Europe and Japan [22], [24], [25], [28]. PET imaging using more novel radiopharmaceuticals may ultimately prove better at detecting primary cancer. Fortunately, our development of PET-TRUS prostate imaging is not dependent on the specific choice of PET radiopharmaceutical. We are planning to use [^{11}C]choline for our human subject studies, but alternate radiopharmaceuticals could be used instead (depending on the clinical application).

The phantom study results presented in this paper are based on dual PET-TRUS imaging using a Siemens EXACT HR PET scanner. The Siemens EXACT HR PET scanner has a transaxial spatial resolution that varies from 3.6 mm full width at half maximum (FWHM) at the center to 4.5 mm FWHM tangentially and 7.4 mm FWHM radially at a radius of 20 cm [45].

III. Transrectal Ultrasound Imaging

Transrectal ultrasound imaging of the prostate is a standard imaging technique widely used for prostate cancer diagnosis, biopsy guidance, treatment planning, brachytherapy seed placement, high dose rate brachytherapy, and transurethral resection of the prostate. The probe is relatively small (2 cm diameter) and generally well tolerated by patients. A volumetric 3-D reconstructed TRUS image of the prostate is generated using a series of 2-D TRUS images. Such 3-D images are currently used to determine the prostate volume and calculate dose for brachytherapy planning [2]–[4], [46].

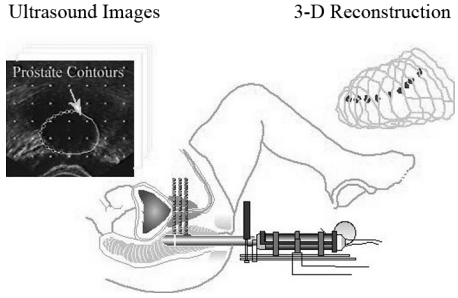

Fig. 1. Transrectal ultrasound probe is attached to a calibrated stepper and a series of 2-D TRUS images are taken as the probe is stepped past the prostate. These 2-D images are then used to reconstruct a single 3-D image.

The transrectal probe is rigidly attached to the table through a calibrated linear stepper that allows displacement along its axis. Ultrasound images in the transverse plane (i.e.,perpendicular to the probe axis) are acquired from base to apex of the prostate. A complete 3-D TRUS image of the prostate, urethra and rectum wall is then reconstructed using a series of 2-D images taken with this step and shoot protocol. Fig. 1 shows a drawing of the TRUS unit with the probe inserted in a patient, as well as a 2-D transverse ultrasound image and the prostate contours from a 3-D reconstruction. The TRUS system provides high-resolution, volumetric images of the prostate region.

The data presented in this paper were acquired using a Hitachi Hi-Vision 5500 digital ultrasound system, using a B mode bi-plane TRUS probe in an EXII classic stepper with a Micro-Touch LP controller. Some modifications were made to these commercial devices, as discussed in Section V. TRUS imaging was performed with a frequency of 9 MHz, an axial distance of 5 mm between 2-D acquisitions, and a transaxial pixel size of 0.2887 mm.

IV. Custom PET-TRUS-CT-MRI Phantoms

Since phantoms for PET-TRUS imaging are not commercially available, we have developed custom PET-TRUS prostate phantoms with structures that simulate the acoustical properties for TRUS and 511 keV activity concentrations for PET. In addition, we have developed custom PET-TRUS-CT-MRI phantoms with structures that also simulate the nuclear magnetization for MRI and radiographic density for CT. Our phantom development, including multimodality images of the phantoms, is described in detail in [47]. We constructed these phantoms using tissue-mimicking mixtures (TMMs) of agar, gelatin, $CuCl_2 - 2H_2O$, EDTA-tetra Na Hydrate, NaCl, formalin, Germall-Plus™, glass beads, $BaSO_4$, radioactive solution (^{18}F-water or ^{68}GeCl), and deionized water (Table I). The imaging and mechanical properties of these phantoms were stable when stored at room temperature (for over a year). These phantoms were useful for investigating multimodality imaging, particularly since they were comprised of tissue mimicking materials. However, their simple two region (*a.k.a.*, "Prostate

TABLE I
DRY-WEIGHT PERCENTS OF COMPONENTS IN THE PET-TRUS-CT-MRI CUSTOM PHANTOM GELS. REMAINING WEIGHT PERCENT IS DEIONIZED WATER WITH A TRACE AMOUNT OF RADIOACTIVITY

	Agar	Gelatin	$CuCl_2$-$2H_2O$	EDTA	NaCl	HCHO	Germall-Plus	Glass Beads	$BaSO_4$
Pelvis TMM	1.17	5.52	0.11	0.33	0.77	0.24	1.45	4.4	0.50
Prostate TMM	3.64	5.70	0.12	0.34	0.80	0.25	1.50	0	0

TMM" and "Pelvis TMM") geometry was not ideal for evaluation of multimodality image registration. Hence, we have also developed a multi-line source phantom that was specifically designed to assess PET-TRUS-CT-MRI image registration accuracy.

Our multi-line source phantom contains a fillable tube that winds through a non-radioactive tissue mimicking gel. The tube is distinguishable from the gel using TRUS, CT and MRI imaging, and the tube can be filled with radioactive solution (e.g., $^{18}\mathrm{F}-\mathrm{FDG}$, $^{11}\mathrm{C}-\mathrm{choline}$, or $^{99\mathrm{m}}\mathrm{Tc}-\mathrm{sodium}$ pertechnetate) for PET or SPECT imaging (Figs. 2–4). The phantom was constructed based on the tissue mimicking gels and construction techniques developed previously [47]. A single 20 ml long piece of silicon tube (with inner diameter 5/32", outer diameter 7/32") was accurately placed through a plastic box to create four line sources that can be filled with a single injection of radioactive solution (Fig. 2). Three of the line sources are in a single horizontal plane in an "N" pattern. The fourth line source is within a plane angled relative to the other three line sources. Once the tube was positioned, we partially filled the container with a non-radioactive dense gel (Prostate TMM) while creating a hole for the TRUS probe (Fig. 2(a)). This dense gel was selected for its imaging properties and mechanical strength, since the TRUS probe can tear softer gels. Finally, we filled the container with a second non-radioactive gel (Pelvis TMM) that was selected so that the tube was distinguishable from the gel in TRUS, CT and MRI images. This phantom is reusable; we simply have to inject new radioactive solution into the tube prior to imaging for each use. Figs. 3 and 4 show multimodality images of this phantom, including TRUS, resampled PET, CT and MRI images. These PET and TRUS images are discussed further in Section VI.

These multi-line source phantoms were only used to assess our multimodality image registration accuracy. The phantom images are not necessarily representative of human subject imaging, in terms of parameters such as tumor-to-background uptake or anatomy.

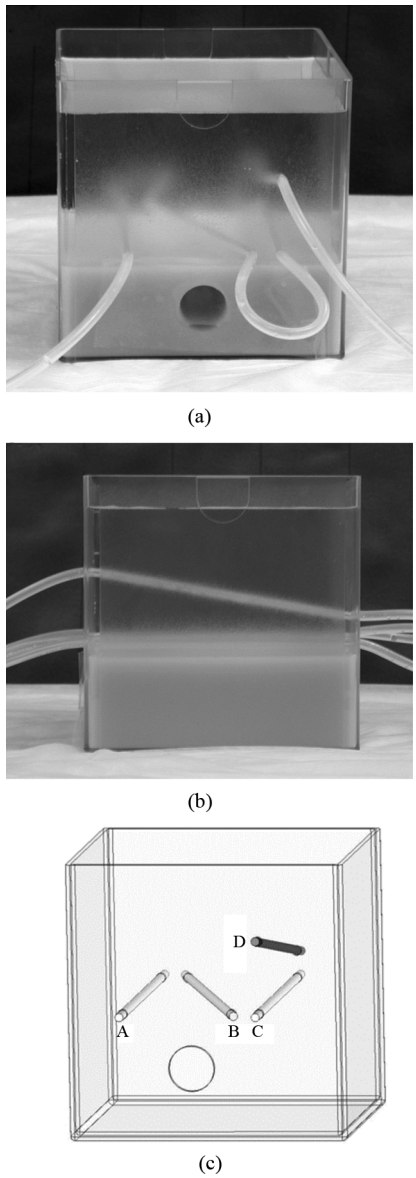

(a)

(b)

(c)

Fig. 2. Photograph of a multi-line source phantom, taken before the second gel layer was poured so the tube is visible. The dense gel, probe hole, and fillable tube are shown within the clear plastic box. The phantom is shown from the (a) front and (b) side. The dimensions of the plastic box are $15\ \mathrm{cm} \times 15\ \mathrm{cm} \times 15\ \mathrm{cm}$. (c) Simplified mechanical drawing of the phantom. Line sources A-B-C are coplanar, forming an N pattern. Line sources A and C are parallel to each other (and 3.5 cm from the nearest vertical plastic wall). The distance between line sources B and A (C) varies from 6.5 cm (1.5 cm) at the front face to 1.5 cm (6.5 cm) at the back face. Line sources C-D are coplanar, and the C-D plane is perpendicular to the A-B-C plane. Line source D is angled relative to the A-B-C plane. The distance between line sources C and D varies from 4 cm at the front face to 1.5 cm at the back face. The hole for the TRUS probe is centered 3 cm below the A-B-C plane.

V. DUAL PET-TRUS PROSTATE IMAGING

Accurate positioning of the TRUS probe inside a phantom (or human) subject utilizes two main mechanical units–a manual stepper and a controller. The probe is rigidly attached to a calibrated stepper that allows both linear displacement along its axis and angular rotation about its axis. For instance, the stepper is used to linearly displace the probe along its axis in steps past the prostate, when acquiring a series of 2-D TRUS images in the transverse plane (Fig. 1). The probe-stepper unit is mounted on to a controller that is rigidly attached to the scanner table (Fig. 5(a)). The controller moves to allow freehand positioning of the probe inside the subject, then the controller is locked to fix the stepper-base location for the multimodality imaging study. This standard commercial TRUS probe-stepper-controller unit was modified for our dual PET-TRUS imaging. Our probe-stepper unit was mounted onto a long extension plate that attached to

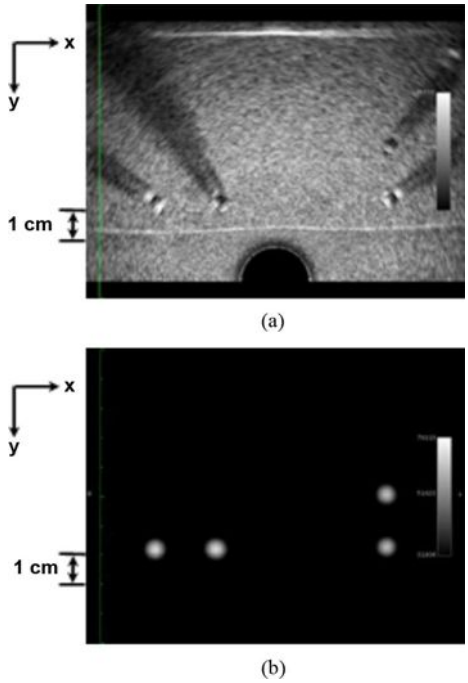

Fig. 3. (a) Transverse TRUS image of a multi-line source phantom, acquired during a dual PET-TRUS study. All 4 line sources are visible. Phantom was imaged on a Hitachi Hi-Vision 5500 digital ultrasound system, using a B mode bi-plane TRUS probe in a linear stepper. Image slice was acquired with the probe inserted 2.5 cm into the phantom. (b) Reconstructed, resampled transverse PET image of the phantom from data acquired during the same dual PET-TRUS study and image slice as Fig. 3(a). All 4 line sources are clearly visible as white circles. Phantom was imaged on a Siemens EXACT HR PET scanner.

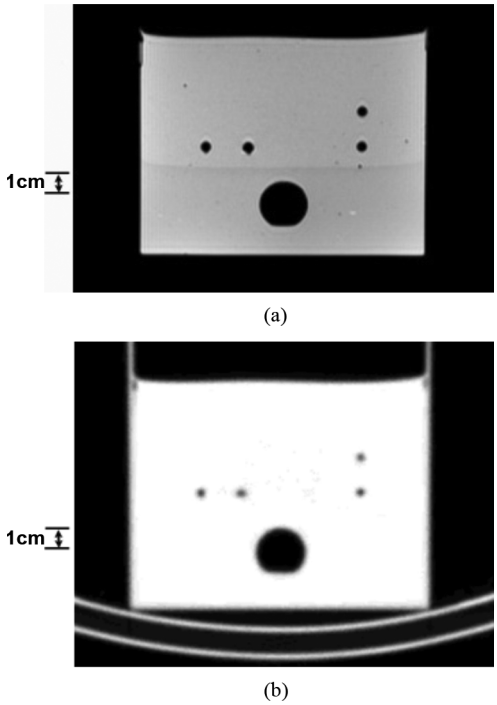

Fig. 4. (a) Transverse reconstructed MRI T1-weighted image of the multi-line source phantom. Phantom was imaged without the probe in place, using a 1.5 T Avanto Siemens MRI scanner with a head coil and a standard MPRage brain protocol. The 4 line sources are clearly visible. (b) Transverse reconstructed CT image of the phantom without the probe in place, when the tube was filled with non-radioactive water. All 4 line sources are clearly visible. The phantom was imaged with a Hawkeye CT scanner (140 keV; 2.5 mAmps) on a Millennium VG3 SPECT gantry and reconstructed with filtered backprojection.

the controller, which in turn was attached to the end of the table. This extra plate was needed to allow the TRUS probe to be imaged near the center of the PET scanner, due to the scanner bore length.

Our methods for PET-TRUS image registration depend on precisely determining the location and orientation of the TRUS probe within the PET scanner directly, by PET scanning fiducial 511 keV point sources that determined the TRUS probe position. Hence, we further modified the TRUS system, mounting two ^{68}Ge PET point sources at known locations with respect to the TRUS transducer. These two point sources were placed in a holder that was attached to the TRUS stepper, so the point sources accurately defined the axial line of the probe. Fig. 5 shows the point source holder and point sources used in the dual PET-TRUS image studies, as well as the stepper-controller mechanical setup. We originally planned to attach a third ^{68}Ge point source at the rear of the probe (placed off the axis defined by the first two point sources) in order to define the probe rotation. However, this proved to be an impractical design for human subjects so the third point source was removed. We instead investigated measuring possible rotational motion using an ADXL327 accelerometer [48], as discussed below.

During a dual PET-TRUS study, the phantom was positioned on the table. The TRUS probe with stepper was mounted onto the controller that was attached to the table. The holder with point sources was attached to the stepper. The controller was moved to position the probe inside the phantom, then its position was fixed. A series of 2-D TRUS images in the transverse plane were acquired every 5 mm using the mechanical linear stepper, then the transducer was re-positioned at the center of the "prostate." For phantom studies, the center of the phantom was used to represent the position for "prostate" imaging. The phantom was left in this position with the probe in place for the subsequent PET scans, since the TRUS probe significantly distorts the local anatomy. The table was moved so the two point sources were visually positioned in the PET scanner and PET data were acquired for 2 minutes. For image registration, these point source PET data were reconstructed after the study. We then removed the point sources, moved the table so the transducer (and hence "prostate") was visually centered in the PET scanner, injected a radiopharmaceutical into the phantom, and acquired PET imaging data of the phantom.

The PET point source data were reconstructed using either a backprojection or iterative OSEM algorithm without attenuation correction. The 3-D location of each point source in the resulting volumetric PET image was determined by fitting a 3-D Gaussian to the reconstructed intensity distribution of each point source. Given the known position of the TRUS transducer relative to the point sources, this provides nearly enough information to determine the position and orientation of the TRUS image planes. There is still ambiguity from the rotation of the TRUS image about the long axis of the probe. However, the dual PET-TRUS studies presented here acquired data with the stepper in a nearly level position (i.e., rotational angle of zero), in agreement with our clinical TRUS imaging experience with

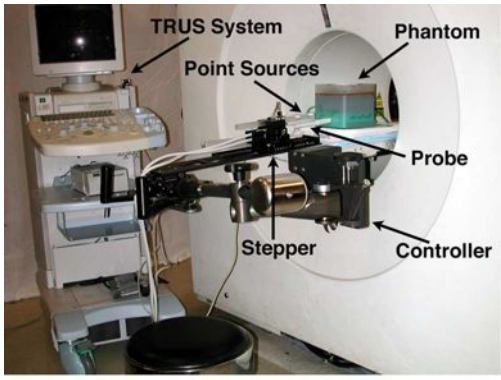

(a)

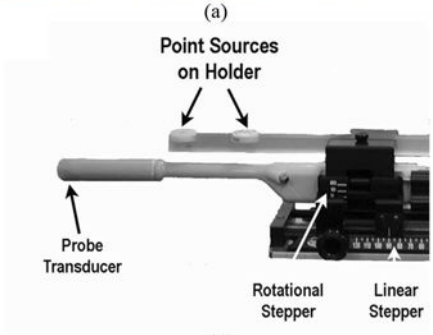

(b)

Fig. 5. (a) Photograph of the dual PET-TRUS system using the EXACT HR PET scanner. (b) Photograph close-up of the TRUS ultrasound probe and point source holder. Two $^{68}\mathrm{Ge}$ point sources, mounted on the holder, are used to measure the position of the axial line of the TRUS probe. The point source holder is mounted on the stepper.

humans. This provides sufficient information for image registration, since the probe is rigidly mounted on the stepper and its position relative to the stepper is tracked.

The PET phantom data were reconstructed using an iterative OSEM reconstruction algorithm with attenuation and scatter correction. The 3-D geometric relationship between PET image pixels and TRUS image pixels was calculated based on the 511 keV point source images and the known amount of linear table motion. The 3-D position in the PET coordinates was calculated for each TRUS pixel, and the PET image intensity at each TRUS pixel position was obtained via trilinear interpolation of the PET images. This yielded registered sets of TRUS images and resampled PET images with common pixel size and 3-D pixel positions. The actual image fusion was performed using OSIRIX [49] software, without any linear or rotational translation between the two image sets.

As Figs. 3 and 6 demonstrate, accurately determining the 3-D location of the line sources in the TRUS images can be challenging. We determined the center of each line source in a 2-D TRUS image with an automated method that: (1) calculated the sum of the pixel value along the radius (for a selected range of radius), (2) calculated the derivative of the sum and determined the two boundary angles ($\theta 1$ and $\theta 2$) with peak sum values, (3) calculated the sum pixel value along the arc with different R and found the position R0 of local minimum, and (4) calculated the center of the tube as $((\theta 1+\theta 2)/2, R0)$. We used this automated algorithm to determine the line source locations in every 2-D TRUS image, for evaluation of the PET-TRUS registration.

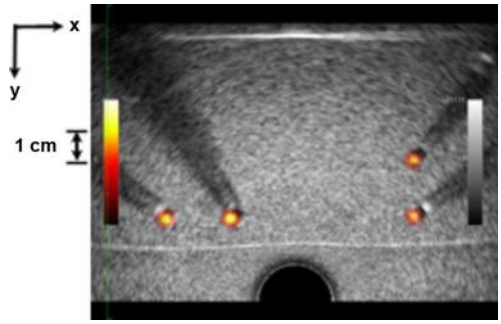

Fig. 6. Fused transverse TRUS image and resampled PET image of a multi-line source phantom. All 4 line sources are clearly visible for both imaging modalities. Pixel size is 0.289 mm in both the x and y direction. Fused image slice was acquired with the probe inserted 2.5 cm into the phantom (same as Figs. 3).

VI. Results and Discussion

We performed dual PET-TRUS imaging of the multi-line source phantoms described in Section IV, following the protocol outlined in Section V. Fig. 3(a) shows a transverse TRUS image of the multi-line source phantom that was acquired during a dual PET-TRUS imaging study. All line sources are clearly visible, along with dark shadows caused by each tube. The black semi-circle at the bottom of the image shows the location of the probe. The white horizontal line (just above the probe) shows the transition layer between the two gels. Fig. 3(b) shows a reconstructed, resampled transverse PET image of the phantom that was acquired during the same study and phantom location. The entire tube was filled with $502\ \mu\mathrm{Ci}$ of $[^{18}\mathrm{F}]\mathrm{FDG}$ solution. PET data were acquired with a 10 minute transmission scan and a 30 minute emission scan in 3-D mode. Iterative OSEM image reconstruction was performed with attenuation and scatter correction. Using the point source information, the 3-D volumetric PET image was then resampled into TRUS image coordinates. Fig. 6 shows a fused transverse image of TRUS and resampled PET data from the same phantom study as Fig. 3, demonstrating our PET-TRUS image registration capability. The resampled PET image is shown in color overlaid onto a grayscale TRUS image.

We performed six multi-line source phantom studies. We injected between $100\ \mu\mathrm{Ci}$ to $537\ \mu\mathrm{Ci}$ of $[^{18}\mathrm{F}]\mathrm{FDG}$ into the 20 ml tube for each study. This radioactivity concentration was significantly higher than what is expected in human PET imaging, but the phantom imaging was solely used to assess the registration accuracy. The phantom (or subject) images were not used for image registration. Registration with our imaging protocol instead utilized the fidicual point source PET images. We used $^{68}\mathrm{Ge}$ point sources with a source strength between $23\ \mu\mathrm{Ci}$ to $150\ \mu\mathrm{Ci}$ for our phantom studies, which were sufficient for use in future human subject studies.

Based on these multi-line source phantom studies, our PET-TRUS registration error is 1 mm axially and 1–5 mm in the transaxial plane depending on the image study, image slice and line source measured. When calculating our average PET-TRUS registration error, we averaged the PET-TRUS difference in line source position (i.e., center of line source) for a 3 cm "prostate" section of all four line sources as measured during six multi-line source phantom studies. The PET-TRUS registration error is

-2.1 ± 1.7 mm (mean $\pm$ standard deviation) in the x direction, 1.9 ± 1.6 mm in the y direction, and 0.6 ± 0.2 mm in the z direction (see Fig. 6 for axes). The mean transaxial distance between the PET and TRUS line source position is 3.67 ± 0.86 mm. Hence, our transaxial PET-TRUS registration error is similar to the transaxial spatial resolution of 3.6 mm FWHM for the Siemens EXACT HR PET scanner. Our current registration accuracy should be sufficient for the clinical applications of detecting early recurrence and guiding prostate biopsies, but it is not sufficient for treatment planning [6], [7].

We performed a variety of point source and phantom tests in order to evaluate the causes of this PET-TRUS registration error. For instance, we repeatedly imaged two point sources (which were aligned and mounted in the standard TRUS setup, Fig. 5(b) as the scanner table was moved in steps, in order to evaluate whether the table moved parallel to the axis of the scanner. Similarly, we imaged the point sources at many stepper positions (with the table position fixed and the stepper aligned along z direction), in order to identify whether the mechanical stepping motion in the axial direction caused small changes in point source locations in the transaxial plane. We also evaluated the mechanical setup, using a precision height gauge to measure the deformation of each component (e.g., probe, point source holder, and extension plate) when a variable force was applied at the TRUS probe transducer. As a result of our phantom, point source and mechanical tests, we have identified a few "real world" systematic error sources for these research methods.

Firstly, we assumed that the TRUS probe assembly remained rigid and the probe's angle of inclination remained fixed while the probe was stepped during the TRUS imaging. However, the probe was physically constrained by the phantom's hole (i.e., "rectum"), which applied a force on the TRUS transducer that varied with stepper position. This force caused a small change in the probe's angle of inclination and a slight flexing of the probe assembly components. Although the probe had only a small deformation depending on the TRUS stepper position, the PET data were acquired at only one stepper position. This caused an error in the PET-TRUS image registration that varied with stepper position (i.e., image slice). Namely, line sources in the transverse resampled PET images are consistently lower than the corresponding TRUS images by 4 ± 1 mm in the vertical direction for PET slice 19 (when the TRUS transducer is 9.5 cm into the phantom) relative to PET slice 1 (when the TRUS transducer is just entering the phantom). Similarly, the PET images are lower than the corresponding TRUS images by 1.3 ± 0.4 mm for slices at the edge of a "prostate" section (i.e., 3 cm section of phantom that begins 3 cm into the phantom). These "prostate section" results are compatible with the deformation observed in clinical prostate imaging as the probe steps through the rectum [5].

We have measured the angular deflection of the probe holder during phantom studies, using an ADXL327 accelerometer with a 12 bit ADC, dithering method and non-linear regression calibration algorithm. We have correlated these angular deflection measurements (acquired outside the subject) with the physical deformation of the probe transducer (placed inside the subject). Hence, we can now use external calibrated accelerometer measurements to accurately estimate the vertical displacement of the TRUS probe transducer as a function of stepper position, with an accuracy of 0.2 mm. These calibration measurements are based on applying a variable known force on the transducer, so they are applicable to both phantom and human subject studies. Therefore, we can correct for this known systematic error during human subject studies, utilizing this information when resampling the PET data into TRUS coordinates.

Secondly, the fiducial point sources are far from the TRUS transducer because we do not want to insert the point sources inside the subject (see Fig. 5(b)). As a result, an error of < 1 mm in measuring their location caused a PET-TRUS image registration error of up to 2 mm. In addition, this required the PET scan of the point sources to be acquired at a different table position than the phantom. It is assumed that the table motion direction is parallel to the axis of the PET scanner and that the table does not deflect, but the table motion of the PET scanner may not be level or rigid to our required precision. We found that the table re-positioning caused the point source locations to move slightly, causing a registration error of up to 1 mm in the transaxial plane. If necessary, we could develop an alternate radioactive source that can be inserted into the channel within the TRUS probe (which is designed for a biopsy needle). This radioactive needle source would consist of three custom ^{22}Na-tungsten PET radioactive seeds that are spaced within a small-diameter non-radiopaque needle.

Thirdly, the TRUS probe-stepper unit is mounted onto a long extension plate that attaches to the controller, as described in Section V. This plate creates some probe vibration and component flexing. Ideally, we would use an entirely new controller that can fit through the scanner bore. This would allow for easier dual TRUS-PET imaging using commercial PET-CT scanners with long scanner bores. We have developed a preliminary design of a new custom controller that attaches to the end of the table, fits within a PET-CT scanner bore, and is easy to maneuver and lock into position. We will build this controller when we receive further funding.

Finally, there are additional potential sources of registration error for PET-TRUS imaging of human subjects, such as internal organ motion and gross subject motion. Since PET imaging will be performed with the TRUS probe fully inserted past the prostate, changes in prostate deformation between the TRUS and PET images (due to the transducer probe pressure) will be minimal. Thus, we plan to use rigid registration techniques, as described. If this is not the case, alternate 3-D or 2-D end-firing TRUS probes could be explored which do not require probe stepping. If organ motion in general is an issue, then we could acquire transverse and sagittal TRUS images during the PET scan to measure the extent of the prostate motion. If necessary, we could explore motion correction algorithms utilizing nonrigid registration [50], [51]. Gross motion of the subject is an issue common to all multimodality imaging. However, we expect this to be minimized in our case because the subject will be placed in a supported position (using knee supports, padding, etc.) with the probe inserted in his rectum. We will assess registration accuracy for human subject studies using standard radiopaque gold fiducial markers that have been implanted in each subject's prostate in preparation of his

scheduled radiation therapy. The use of gold fiducial markers has been established clinically as a "gold standard" registration technique for the prostate [6].

VII. Conclusions

We have successfully developed both a dual PET-TRUS system for prostate imaging and custom multimodality PET-TRUS-CT-MRI phantoms. We have evaluated this dual-modality imaging system, by performing PET-TRUS imaging studies of multi-line source phantoms. We currently have a PET-TRUS registration error of -2.1 ± 1.7 mm in the x direction, 1.9 ± 1.6 mm in the y direction, and 0.6 ± 0.2 mm in the z direction (see Fig. 6 for axes). The mean transaxial distance between the PET and TRUS line source position is 3.67 ± 0.86 mm. We expect this registration accuracy to be sufficient for the clinical applications of detecting early recurrence and guiding biopsies, but it is not yet sufficient to use for treatment planning.

We have also performed various phantom, point source and mechanical tests to investigate our PET-TRUS registration accuracy. Our overall registration error includes a systematic error in the vertical direction of 1.3 ± 0.4 mm due to mechanical effects as the probe is inserted and stepped into the phantom (or subject). Using external accelerometer measurements, we can accurately estimate and correct this vertical deformation of the TRUS probe transducer as a function of stepper position. This information can be utilized when resampling the PET data into TRUS coordinates, thereby reducing the overall registration error. We will perform this correction for our human subject studies.

References

[1] [Online]. Available: http://emedicine.medscape.com/article/457757-overview

[2] M. K. Terris and T. A. Stamey, "Determination of prostate volume by transrectal ultrasound," *J. Urol.*, vol. 145, pp. 984–987, 1991.

[3] S. C. Hoffelt *et al.*, "A comparison of CT scan to transrectal ultrasound-measured prostate volume in untreated prostate cancer," *Int. J. Radiat. Oncol. Biol. Phys.*, vol. 57, pp. 29–32, 2003.

[4] K. M. Kalkner *et al.*, "Prostate volume determination: Differential volume measurements comparing CT and TRUS," *Radiother. Oncol.*, vol. 81, pp. 179–183, 2006.

[5] Data from several urologists, radiation oncologists and nuclear medicine physicians, private communication.

[6] K. Langen *et al.*, "Evaluation of the BAT system for prostate daily localization," *Int. J. Radiat. Oncol. Biol. Phys.*, vol. 57, no. 3, pp. 635–644, 2003.

[7] J. Pouliot, I.-C. Hsu, and Y. Kim, "Registration of MR prostate images with biomechanical modeling and nonlinear parameter estimation," *Med. Phys.*, vol. 32, pp. 446–454, 2006.

[8] Y. Seo, B. L. Franc, R. A. Hawkins, K. H. Wong, and B. H. Hasegawa, "Progress in SPECT/CT imaging of prostate cancer," *Technol. Cancer Res. Treat.*, vol. 5, pp. 329–336, 2006.

[9] E. R. Sigurdson and A. M. Cohen, "Commentary on the applications of PET in clinical oncology," *J. Nucl. Med.*, vol. 32, pp. 649–650, 1991.

[10] M. K. Haseman, N. L. Reed, and S. A. Rosenthal, "Monoclonal antibody imaging of occult prostate cancer in patients with elevated prostate-specific antigen. Positron emission tomography and biopsy correlation," *Clin. Nucl. Med.*, vol. 21, pp. 704–713, 1996.

[11] P. F. Faulhaber, D. B. Sodee, E. Echt, and J. K. O'Donnell, "Staging of prostate adenocarcinoma, comparison of FDG dedicated PET and In-111 capromab pendetide," *J. Nucl. Med.*, vol. 41, p. 116, 2000.

[12] T. Hara, N. Kosaka, and H. Kishi, "PET imaging of prostate cancer using carbon-11-Choline," *J. Nucl. Med.*, vol. 39, pp. 990–995, 1998.

[13] T. Hara, N. Kosaka, T. Kondo, H. Kishi, and O. Kobori, "Imaging of brain tumor, lung cancer, esophagus cancer, colon cancer, prostate cancer, and bladder cancer with [^{11}C]Choline," *J. Nucl. Med.*, vol. 38, p. 250P, 1997.

[14] J. Kotzerke *et al.*, "Carbon-11 choline positron emi ssion tomography (PET) of prostate cancer—first clinical experience," *J. Nucl. Med.*, vol. 41, p. 74, 2000.

[15] M. Picchio *et al.*, "Value of [^{11}C]Choline-Positron emission tomography for re-staging prostate cancer: A comparison with [^{18}F]Fluorodeoxyglucose-Positron emission tomography," *J Urol.*, vol. 169, pp. 1337–1340, 2003.

[16] I. J. De Jong, J. Pruim, P. H. Elsinga, W. Vaalburg, and H. J. Mensink, "Preoperative staging of pelvic lymph nodes in prostate cancer by ^{11}C-Choline PET," *J. Nucl. Med.*, vol. 44, pp. 331–335, 2003.

[17] I. J. De Jong, J. Pruim, P. H. Elsinga, W. Vaalburg, and H. J. Mensink, "^{11}C-Choline positron emission tomography for evaluation after treatment of localized prostate cancer," *Eur. Urol.*, vol. 44, pp. 32–39, 2003.

[18] E. Sutinene *et al.*, "Kinetics of [^{11}C]Choline uptake in prostate cancer: A PET study," *Eur. J. Nucl. Med. Mol. Imag.*, vol. 31, pp. 317–324, 2004.

[19] Q. H. Zheng *et al.*, "[^{11}C]Choline as a PET biomarker for assessment of prostate cancer tumor models," *Bioorg. Med. Chem.*, vol. 12, pp. 2887–2893, 2004.

[20] B. J. Krause *et al.*, "The detection rate of [^{11}C]Choline-PET/CT depends on the serum PSA-value in patient with biochemical recurrence of prostate cancer," *Eur. J. Nucl. Med. Mol. Imag.*, vol. 35, pp. 18–23, 2007.

[21] B. Scher *et al.*, "Value of ^{11}C-Choline PET and PET/CT in patients with suspected prostate cancer," *Eur. J. Nucl. Med. Mol. Imag.*, vol. 34, pp. 45–53, 2007.

[22] A. J. Breeuwsma *et al.*, "Detection of local, regional, and distant recurrence in patients with PSA relapse after external-beam radiotherapy using ^{11}C-Choline positron emission tomography," *Int. J. Radiat. Oncol. Biol. Phys.*, vol. 77, pp. 160–164, 2008.

[23] M. Farsad *et al.*, "Positron-emission tomography in imaging and staging prostate cacner," *Cancer Biomark.*, vol. 4, pp. 277–284, 2008.

[24] L. Rinnab *et al.*, "[^{11}C]Choline PET/CT in prostate cancer patients with biochemical recurrence after radical prostatectomy," *World J. Urol.*, vol. 27, pp. 619–625, 2009.

[25] C. Fuccio, D. Rubello, P. Castellucci, M. C. Marzola, and S. Fanti, "Choline PET/CT for prostate cancer: Main clinical applications," *Eur. J. Radiol.*, vol. EPUB, 2010.

[26] G. Giovacchini *et al.*, "PSA doubling time for prediction of [^{11}C]Choline PET/CT findings in prostate cancer patients with biochemical failure after radical prostatectomy," *Eur. J. Nucl. Med. Mol. Imag.*, vol. 37, pp. 1106–1116, 2010.

[27] H. Jadvar, "Prostate cancer: PET with ^{18}F – FDG, ^{18}F- or ^{11}C-Acetate, and ^{18}F- or ^{11}C-Choline," *J. Nucl. Med.*, vol. 52, pp. 81–89, 2010.

[28] A. Winter, J. Uphoff, R.-P. Henke, and F. Wawroschek, "First results of [^{11}C]Choline PET/CT-guided secondary lymph node surgery I patients with PSA failure and single lymph node recurrence after radicatl retropubic prostatectomy," *Urol. Int.*, vol. 84, pp. 418–423, 2010.

[29] T. Kato *et al.*, "Accumulation of [^{11}C]Acetate in normal prostate and benign prostatic hyperplasia: Comparison with prostate cancer," *Eur. J. Nucl. Med. Mol. Imag.*, vol. 29, pp. 1492–1495, 2002.

[30] E. Fricke *et al.*, "Positron emission tomography with ^{11}C-Acetate and ^{18}F – FDG in prostate cancer patients," *Eur. J. Nucl. Med. Mol. Imag.*, vol. 30, pp. 607–610, 2003.

[31] N. Oyama *et al.*, "^{11}C-Acetate PET imaging of prostate cancer: Detection of recurrent disease at PSA relapse," *J. Nucl. Med.*, vol. 44, pp. 556–558, 2003.

[32] I. Osman *et al.*, "^{11}C methionine and ^{18}F PET imaging: Use in the evaluation of progressive prostate cancer," *Proc. Amer. Soc. Clin Oncol.*, vol. 17, p. 1203, 1998.

[33] H. A. Macapinlac *et al.*, "Differential metabolism and pharmacokinetics of L-(1-^{11}C)Methionine and 2-[^{18}F]Fluoro-2-Deoxy-D-Glucose (FDG) in androgen independent prostate cancer," *Clin. Pos. Imag.*, vol. 2, pp. 173–181, 1999.

[34] R. Nunez *et al.*, "Combined ^{18}F – FDG and ^{11}C-Methionine PET scans in patients with newly progressive metastatic prostate cancer," *J. Nucl. Med.*, vol. 43, no. 1, pp. 46–55, 2002.

[35] G. Toth *et al.*, "Detection of prostate cancer with ^{11}C-Methionine positron emission tomography," *J. Urol.*, vol. 173, no. 1, pp. 66–69, 2005.

[36] T. R. Degrado *et al.*, "Fluorine-18 fluorocholine (FCH) as an oncological PET tracer: Evaluation in murine prostate cancer xenograft model," *J. Nucl. Med.*, vol. 41, p. 231, 2000.

[37] T. R. Degrado *et al.*, "Synthesis and evaluation of ^{18}F-labeled choline as an oncologic tracer for positron emission tomography: Initial findings in prostate cancer," *Cancer Res.*, vol. 61, no. 1, pp. 110–117, 2001.

[38] M. Cimitan *et al.*, "[^{18}F]Fluorochine PET/CT imaging for the detection of recurrent prostate cancer at PSA relapse: Experience in 100 consecutive patients," *Eur. J. Nucl. Med. Mol. Imag.*, vol. 33, pp. 1387–1398, 2006.

[39] C. Steiner *et al.*, "Three-phase ^{18}F-Fluorochine PET/CT in the evaluation of prostate cancer recurrence," *Nuklearmedizin*, vol. 48, pp. 1–9, 2009.

[40] M. Beheshti *et al.*, "[^{18}F]choline PET/CT in the preoperative staging of prostate cancer in patients with intermediate or high risk of extracapsular disease: A prospective study of 130 patients," *Radiology*, vol. 254, pp. 925–933, 2010.

[41] S. M. Larson *et al.*, "Tumor localization of 16B-18F-Fluoro-5A-Dihydrotestosterone versus ^{18}F – FDG in patients with progressive, metastatic prostate cancer," *J. Nucl. Med.*, vol. 45, pp. 366–373, 2004.

[42] B. J. Beattie *et al.*, "Pharmacokinetic assessment of the uptake of 16B-18F-Fluoro-5A-Dihydrotestosterone (FDHT) in prostate tumors as measured by PET," *J. Nucl. Med.*, vol. 51, pp. 183–192, 2010.

[43] D. M. Schuster *et al.*, "Initial experience with the radiotracer anti-1-Amino-3-^{18}F-Fluorocyclobutane-1-Carboxylic acid with PET/CT in prostate carcinoma," *J. Nucl. Med.*, vol. 48, pp. 56–63, 2007.

[44] A. B. Jani, T. H. Fox, D. Whitaker, and D. M. Schuster, "Case study of anti-1-Amino-3-^{18}F flurocyclobutane-1-Carboxylic acid (Anti-[^{18}F] FACBC) to guide prostate cancer radiotherapy target design," *Clin. Nucl. Med.*, vol. 34, pp. 279–284, 2009.

[45] K. Wienhard *et al.*, "The ECAT EXACT HR: Performance of a new high resolution positron scanner," *J. Comp. Asst.*, vol. 18, pp. 110–118, 1994.

[46] G. Kovacs *et al.*, "GEC/ESTRO-EAU recommendations on temporary brachytherapy using stepping sources for localised prostate cancer," *Radiother. Oncol.*, vol. 74, pp. 137–148, 2005.

[47] J. S. Huber, Q. Peng, and W. W. Moses, "Multi-modality phantom development," *IEEE Trans. Nucl. Sci.*, vol. 56, no. 5, pp. 2722–2727, Oct. 2009.

[48] [Online]. Available: http://www.analog.com/en/sensors/inertial-sensors/adxl327/products/product.html

[49] A. Rosset, L. Spadola, and O. Ratbig, "OsiriX: An open-source software for navigating in multimodality DICOM images," *J. Digit Image*, vol. 17, pp. 205–216, 2004.

[50] G. J. Klein, B. W. Reutter, and R. H. Huesman, "Four-dimensional affine registration models for respiratory-gated PET," *IEEE Trans. Nucl. Sci.*, vol. 48, no. 3, pp. 756–760, Jun. 2001.

[51] G. J. Klein and R. H. Huesman, "Four-dimensional processing of deformable cardiac PET data," *Med. Imag. Anal.*, vol. 6, pp. 29–46, 2002.

Dual-Modality Prostate Imaging with Positron Emission Tomograph and Transrectal Ultrasound

J.S. Huber, Q. Peng, W.W. Moses, B.W. Reutter, J. Pouliot, and I.C. Hsu
Lawrence Berkeley National Laboratory, Berkeley, CA 94720 USA, jshuber@lbl.gov
Department of Radiation Oncology, UCSF Comprehensive Cancer Center, San Francisco, CA 94143 USA, pouliot@radonc17.ucsf.edu

Background & Objectives: Although prostate specific antigen blood tests, rectal exams and surgical biopsies are commonly used to detect and stage prostate cancer, the results can be unreliable. In addition, multiple courses of a therapy must be administered before a clear indication of response can be determined. A new imaging technology is needed to accurately detect prostate cancer and to assess treatment efficacy. Functional positron emission tomography (PET) with [C-11]choline detects malignant prostate tumors and helps determine the tumor "aggressiveness," but few anatomical features are visible in the PET images. Transrectal ultrasound (TRUS) imaging identifies lesions but some are not cancerous. By accurately fusing the sensitive functional information from PET with the high-resolution anatomical information from TRUS imaging, dual PET-TRUS imaging can accurately localize prostate cancer and determine its response to treatment. The objective of this project is to develop PET-TRUS prostate imaging and evaluate the technology using phantom and initial human subject studies.

Methods: PET-TRUS image registration based on prostate image features is inaccurate, since few anatomical features are seen in the PET images and the TRUS probe distorts the local anatomy. Our image registration method instead depends on precisely determining the location and orientation of the TRUS probe within the PET scanner directly, by performing an additional fast PET scan of fiducial 511 keV point sources that determine the probe position. The goals of this project focus on developing the necessary hardware and software tools to acquire and accurately register volumetric PET and TRUS images.

Results: We developed phantoms that are compatible with PET, TRUS, x-ray computed tomography (CT), and magnetic resonance imaging (MRI). We evaluated our PET-TRUS image registration accuracy by imaging these phantoms. Our PET-TRUS preliminary registration error is 1 mm axially and 2-5 mm in the transaxial plane (depending on the image study, image slice and line source measured). We also performed various phantom and point source tests to investigate this PET-TRUS registration error. The overall registration error includes a systematic error in the vertical direction of up to 3 mm (that varies with slice) due to the physical constraint of the probe during insertion. This information will soon be utilized when resampling the PET data into TRUS coordinates, and this correction is expected to lower the registration error.

Conclusions: We successfully developed a dual PET-TRUS system for prostate imaging and custom PET-TRUS-CT-MRI phantoms. We evaluated our PET-TRUS imaging system by performing studies of our phantoms. We currently have a PET-TRUS registration error of 1 mm axially and 2-5 mm in the transaxial plane, which is sufficient for some clinical applications such as early detection of recurrence. This error is expected to reduce with further systematic error corrections.

Impact: Our PET-TRUS prostate imaging technology should help guide needle biopsies, confirm initial diagnosis, determine where higher dose is needed for external beam radiation and brachytherapy, evaluate treatment effectiveness, and detect local recurrence earlier than is currently possible. Combining PET and CT has recently revolutionized the role of imaging in diagnosis and treatment planning for many kinds of cancer. We believe that combining PET and TRUS could do the same for prostate cancer.

Invited Speaker: 9th Thematic Workshop on Advanced Multimodality Instruments in the Detection, Diagnosis, Therapy and Follow-up of Diseases

Title– Registration Methods for a Dual PET-TRUS Prostate Imaging System

Abstract–
Multimodality imaging plays an increasingly important role in the diagnosis and treatment of a large number of diseases, particularly if both functional and structural information are acquired and accurately registered. Hence, we have developed a dual-modality imaging system that will help identify the location and aggressiveness of prostate cancer. We acquire high-resolution anatomical detail of the prostate region from transrectal ultrasound (TRUS) imaging that is accurately registered with the sensitive functional information from external positron emission tomography (PET). PET-TRUS image registration based on prostate image features is inaccurate, since few anatomical features are seen in the PET images. Our image registration method instead depends on precisely determining the location and orientation of the TRUS probe within the PET scanner directly, by performing an additional fast PET scan of fiducial 511 keV point sources that determine the probe position. We have evaluated our PET-TRUS image registration accuracy by performing dual-modality imaging of custom phantoms. We describe our PET-TRUS system, custom multi-modality phantom development and phantom study results. Our PET-TRUS preliminary registration error is 1 mm axially and 2-5 mm in the transaxial plane (depending on the image study, image slice and line source measured). The mean transaxial distance between the PET and TRUS line source position is 3.67 ± 0.86 mm. This registration accuracy is sufficient for some clinical applications such as early detection of recurrence and guiding biopsies, but it is not yet sufficient to use for treatment planning. We will also discuss future alternative registration methods for PET-TRUS prostate imaging.

Dual PET-TRUS Prostate Image Registration

J.S. Huber, *Member, IEEE,* Q. Peng, *Member, IEEE,* W.W. Moses, *Fellow, IEEE,* B.W. Reutter, *Senior Member, IEEE*, J. Pouliot, and I. C. Hsu

***Abstract*– Multimodality imaging has an increasingly important role in the diagnosis and treatment of a large number of diseases, particularly if both functional and structural information are acquired and accurately registered. Transrectal ultrasound (TRUS) imaging is currently an integral part of prostate cancer diagnosis and treatment procedures, providing high-resolution anatomical detail of the prostate region. PET imaging with ^{11}C-choline is a sensitive functional imaging technique that can identify biochemical states associated with prostate cancer. We believe that merging these prostate imaging technologies will help identify the location and aggressiveness of prostate cancer. We envision using dual PET-TRUS prostate imaging to guide biopsy, guide treatment procedures, and detect local recurrence earlier than is currently possible. Hence, we have developed a dual PET-TRUS prostate imaging system and protocol designed to allow accurate 3-D image registration. We have evaluated this PET-TRUS system by performing dual PET-TRUS imaging of custom phantoms. We describe here our dual-modality system, custom phantoms and phantom study results. We also discuss our investigation of the PET-TRUS registration accuracy. We currently have a PET-TRUS registration error of 1 mm axially and 1-5 mm transaxially (depending on the image study, image slice, and line source measured), which is sufficient for clinical applications such as biopsy guidance and early detection of recurrence.**

***Index Terms*—Positron Emission Tomography, Ultrasound, Image Registration, Cancer**

I. Introduction

Multimodality imaging plays an increasingly important role in the diagnosis and treatment of a large number of diseases. Combining modalities that provide both functional and structural information is particularly important. For instance, functional information can be acquired with single photon emission computed tomography (SPECT), positron emission tomography (PET) or functional magnetic resonance imaging (fMRI), whereas anatomical information can be acquired using x-ray computed tomography (CT), ultrasound (US) or magnetic resonance imaging (MRI).

Combining PET and CT has recently revolutionized the role of imaging in diagnosis and treatment planning for many kinds of cancer. However, PET-CT imaging is not the preferred modality combination for all cancers. For instance, transrectal ultrasound (TRUS) imaging is an integral part of diagnosis and treatment procedures for prostate cancer [1]. Transrectal ultrasound provides good anatomical detail of the prostate region and accurately measures the prostate volume, whereas CT has poor contrast for soft-tissue (like the prostate) and it over-estimates prostate volume [2-4].

TRUS is the anatomical imaging modality of choice for most prostate cancer clinicians. PET with ^{11}C-choline is a sensitive functional imaging technique that can identify biochemical states associated with prostate cancer. Hence, we believe that imaging the prostate using a dual PET-TRUS system will help determine the location and aggressiveness of cancer within the prostate region. We envision that dual PET-TRUS prostate imaging could be used to guide biopsy, guide treatment procedures, and detect local recurrence earlier than is currently possible. We estimate that the clinical applications of biopsy guidance and detection of local recurrence both require a PET-TRUS registration accuracy of 5 mm or less, whereas treatment guidance (*e.g.*, radiation therapy or brachytherapy planning) requires a PET-TRUS registration accuracy of 2-3 mm.

Therefore, we have developed a dual imaging system that acquires PET and TRUS data sets during the same patient imaging session, using methods that should allow us to accurately register these 3-D volumetric images. PET-TRUS image registration based on prostate image features is inaccurate, since few anatomical features are seen in the PET images. Our image registration method instead depends on precisely determining the mechanical location and orientation of the TRUS probe within the PET scanner directly, by performing an additional fast PET scan of fiducial 511 keV point sources that determine the TRUS probe position. In order to evaluate our PET-TRUS image registration accuracy (prior to human subject studies), we have performed dual PET-TRUS imaging studies on custom phantoms. This paper describes our dual PET-TRUS system and presents our phantom study results.

II. Prostate Imaging With Nuclear Medicine

Currently the functional imaging technique most commonly used for prostate cancer is [^{111}In]ProstaScint SPECT imaging, which is generally indicated for patients suspected of residual or recurrent disease following treatment and for patients suspected of metastatic disease. However, interpretation of these SPECT images is challenging because the radiopharmaceutical demonstrates nonspecific uptake in the normal vasculature, bowel, bone marrow, and prostate gland [5].

PET was not commonly used for prostate imaging in the past, because the standard radiotracer [^{18}F]fluorodeoxyglucose (FDG) is not very specific and bladder accumulation of this

Manuscript received September 27, 2010. This work was supported in part by the Director, Office of Science, Office of Biological and Environmental Research, Medical Science Division of the U.S. Department of Energy under Contract No. DE-AC02-05CH11231, and in part by Department of Defense grant number W81XWH-07-1-0020.

J.S. Huber, Q. Peng, W.W. Moses, and B.W. Reutter are with Lawrence Berkeley National Laboratory, Berkeley, CA 94720 USA (telephone 510-486-6445, e-mail: jshuber@lbl.gov).

J. Pouliot and I.C. Hsu are with the Department of Radiation Oncology, UCSF Comprehensive Cancer Center, San Francisco, CA 94143 USA (telephone: 415-353-7190, e-mail pouliot@radonc.ucsf.edu)

radiopharmaceutical often obscures prostate tumors [6-8]. However, newly developed PET radiopharmaceuticals have demonstrated outstanding results in the sensitive detection of prostate cancer. Hara and co-workers find that: [^{11}C]choline clears the blood quickly; its uptake in prostate tumors provides excellent tumor/normal contrast; and bladder accumulation is minimal [9]. Therefore, [^{11}C]choline is an attractive PET radiopharmaceutical for detecting prostate tumors and following treatment efficacy [10-17]. Several other ^{11}C radiopharmaceuticals are also under investigation, including [^{11}C]acetate [18-20] and [^{11}C]methionine [21-24]. There are also several ^{18}F radiopharmaceuticals currently under investigation for prostate cancer imaging that are expected to have increased commercial viability, including [^{18}F]fluorocholine [25, 26].

We are planning to use [^{11}C]choline for our human subject studies, but alternate radiopharmaceuticals could be used instead. The phantom study results presented in this paper are based on dual PET-TRUS imaging using a Siemens EXACT HR PET scanner. The Siemens EXACT HR PET scanner has a transaxial spatial resolution that varies from 3.6 mm full width at half maximum (FWHM) at the center to 4.5 mm FWHM tangentially and 7.4 mm FWHM radially at a radius of 20 cm [27].

III. Transrectal Ultrasound Imaging

Transrectal ultrasound imaging of the prostate is a standard imaging technique widely used for prostate cancer diagnosis, biopsy guidance, treatment planning, brachytherapy seed placement, high dose rate brachytherapy, and transurethral resection of the prostate. The probe is relatively small (2 cm diameter) and generally well tolerated by patients. A volumetric 3-D reconstructed TRUS image of the prostate is generated using a series of 2-D TRUS images. Such 3-D images are currently used to determine the prostate volume and calculate dose for brachytherapy planning [2-4, 28] .

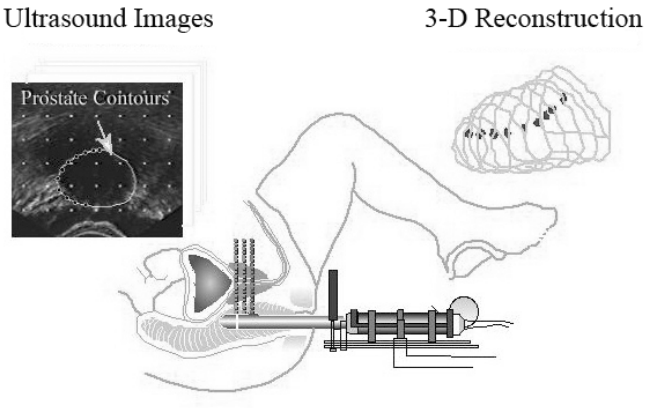

Fig. 1. Transrectal ultrasound probe is attached to a calibrated stepper and a series of 2-D TRUS images are taken as the probe is stepped past the prostate. These 2-D images are then used to reconstruct a single 3-D image.

The transrectal probe is rigidly attached to the table through a calibrated linear stepper that allows displacement along its axis. Ultrasound images in the transverse plane (*i.e.,* perpendicular to the probe axis) are acquired from base to apex of the prostate. A complete 3-D TRUS image of the prostate, urethra and rectum wall is then reconstructed using a series of 2-D images taken with this step and shoot protocol. Figure 1 shows a drawing of the TRUS unit with the probe inserted in a patient, as well as a 2-D transverse ultrasound image and the prostate contours from a 3-D reconstruction. The TRUS system provides high-resolution, volumetric images of the prostate region.

The data presented in this paper were acquired using a Hitachi Hi-Vision 5500 digital ultrasound system, using a B mode bi-plane TRUS probe in an EXII classic stepper with a Micro-Touch LP controller. Some modifications were made to these commercial devices, as discussed in Section V. TRUS imaging was performed with a frequency of 9 MHz, an axial distance of 5 mm between 2-D acquisitions, and a transaxial pixel size of 0.2887 mm.

IV. Custom PET-TRUS-CT-MRI Phantoms

Since phantoms for PET-TRUS imaging are not commercially available, we have developed custom PET-TRUS prostate phantoms with structures that simulate the acoustical properties for TRUS and 511 keV activity concentrations for PET. In addition, we have developed custom PET-TRUS-CT-MRI phantoms with structures that also simulate the nuclear magnetization for MRI and radiographic density for CT. Our phantom development, including multimodality images of the phantoms, is described in detail in [29]. We constructed these phantoms using tissue-mimicking mixtures (TMMs) of agar, gelatin, $CuCl_2$-$2H_2O$, EDTA-tetra Na Hydrate, NaCl, formalin, Germall-Plus^{TM}, glass beads, $BaSO_4$, radioactive solution (^{18}F-water or ^{68}GeCl*)*, and deionized water (Table 1). The imaging and mechanical properties of these phantoms were stable when stored at room temperature (for over a year). These phantoms were useful for investigating multimodality imaging, particularly since they were comprised of tissue mimicking materials. However, their simple two region (*a.k.a.*, Prostate TMM and Pelvis TMM) geometry was not ideal for evaluation of multimodality image registration. Hence, we also developed a multi-line source phantom that was specifically designed to assess PET-TRUS-CT-MRI image registration accuracy.

Table 1: Dry-weight percents of components in the PET-TRUS-CT-MRI custom phantom gels. Remaining weight percent is deionized water with a trace amount of radioactivity.

	Agar	Gelatin	$CuCl_2$-$2H_2O$	EDTA	NaCl	HCHO	Germall-Plus	Glass Beads	$BaSO_4$
Pelvis TMM	1.17	5.52	0.11	0.33	0.77	0.24	1.45	4.4	0.50
Prostate TMM	3.64	5.70	0.12	0.34	0.80	0.25	1.50	0	0

(a)

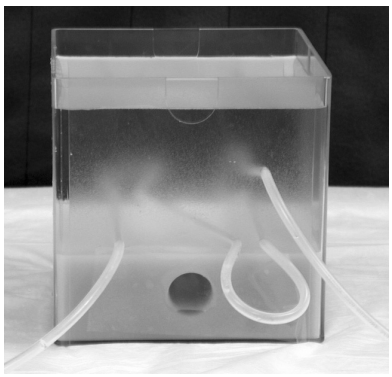

(b)

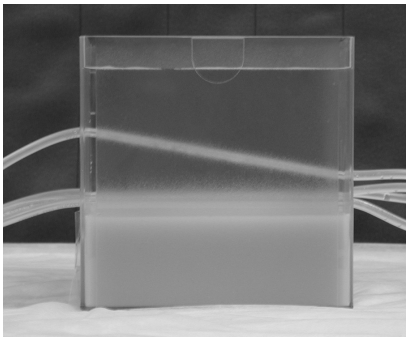

(c)

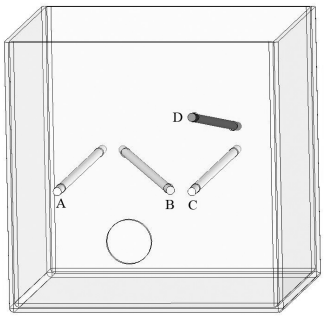

Fig. 2. Photograph of a multi-line source phantom, taken before the second gel layer was poured so the tube is visible. The dense gel, probe hole, and fillable tube are shown within the clear plastic box. The phantom is shown from the (a) front and (b) side. The dimensions of the plastic box are 15 cm x 15 cm x 15 cm. (c) Simplified mechanical drawing of the phantom. Line sources A-B-C are coplanar, forming an N pattern with A and C parallel to each other. Line sources C-D are coplanar, and the C-D plane is perpendicular to the A-B-C plane. Line source D is angled relative to the A-B-C plane.

Our multi-line source phantom contains a fillable tube that winds through a non-radioactive tissue mimicking gel. The tube is distinguishable from the gel using TRUS, CT and MRI imaging, and the tube can be filled with radioactive solution (*e.g.*, ^{18}F-water, ^{11}C-choline, or ^{99m}Tc-sodium pertechnetate) for PET or SPECT imaging (Figs. 2-4). The phantom was constructed based on the tissue mimicking gels and construction techniques developed previously [29]. A single piece of silicon tube (with inner diameter 5/32″, outer diameter 7/32″) was accurately placed through a plastic box to create four line sources that can be filled with a single injection of radioactive solution. Three of the line sources are in a single horizontal plane in an "N" pattern. The fourth line source is within a plane angled relative to the other three line sources. Once the tube was positioned, we partially filled the container with a non-radioactive dense gel (Prostate TMM) while creating a hole for the TRUS probe (Fig. 2a). This dense gel was selected for its imaging properties and mechanical strength, since the TRUS probe can tear softer gels. Finally, we filled the container with a second non-radioactive gel (Pelvis TMM) that was selected so that the tube was distinguishable from the gel in TRUS, CT and MRI images. This phantom is reusable; we simply have to inject new radioactive solution into the tube prior to imaging for each use. Figures 3 and 4 show multimodality images of this phantom, including TRUS, resampled PET, CT and MRI images. These PET and TRUS images are discussed further in Section VI.

(a)

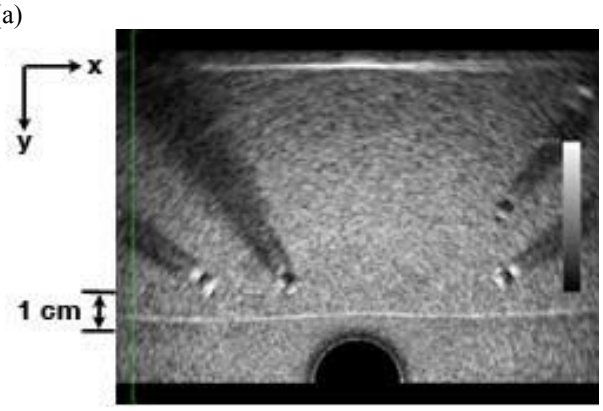

(b)

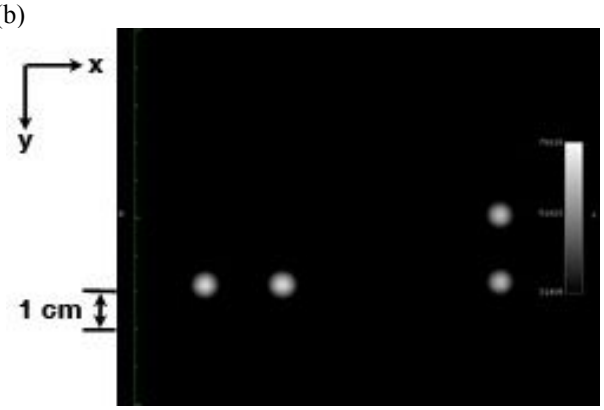

Fig. 3. (a) Transverse TRUS image of a multi-line source phantom, acquired during a dual PET-TRUS study. All 4 line sources and the probe are visible. Phantom was imaged on a Hitachi H-Vision 5500 digital ultrasound system, using a B mode bi-plane TRUS probe in a linear stepper. Image slice was acquired with the probe inserted 2.5 cm into the phantom. (b) Reconstructed, resampled transverse PET image of the phantom from data acquired during the same study and phantom location. All 4 line sources are clearly visible as white circles. Phantom was imaged on a Siemens EXACT HR PET scanner.

(a)

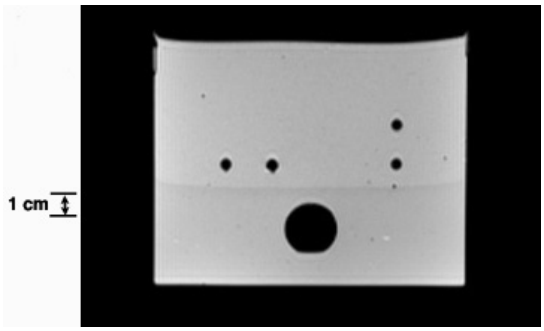

(b)

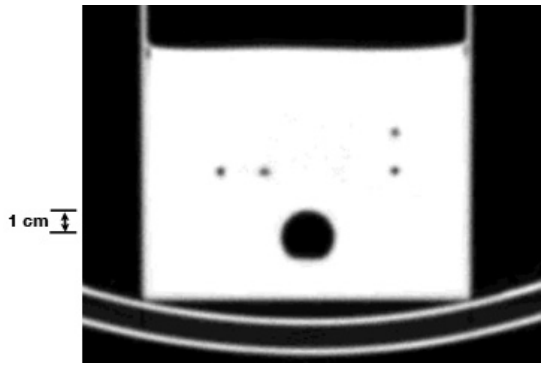

Fig. 4. (a) Transverse reconstructed MRI T1-weighted image of the multi-line source phantom. Phantom was imaged without the probe in place, using a 1.5 T Avanto Siemens MRI scanner with a head coil and a standard MPRage brain protocol. The 4 line sources are clearly visible. (b) Transverse reconstructed CT image of the phantom without the probe in place, when the tube was filled with non-radioactive water. All 4 line sources are clearly visible. The phantom was imaged with a Hawkeye CT scanner (140 keV; 2.5 mAmps) on a Millennium VG3 SPECT gantry and reconstructed with filtered backprojection.

V. Dual PET-TRUS Prostate Imaging

Accurate positioning of the TRUS probe inside a phantom (or human) subject utilizes two main mechanical units – a manual stepper and a controller. The probe is rigidly attached to a calibrated stepper that allows both linear displacement along its axis and angular rotation about its axis. For instance, the stepper is used to linearly displace the probe along its axis in steps past the prostate, when acquiring a series of 2-D TRUS images in the transverse plane (Fig. 1). The probe-stepper unit is mounted on to a controller that is rigidly attached to the scanner table (Fig. 5a). The controller moves to allow freehand positioning of the probe inside the subject, then the controller is locked to fix the stepper-base location for the multimodality imaging study. This standard commercial TRUS probe-stepper-controller unit was modified for our dual PET-TRUS imaging. Our probe-stepper unit was mounted onto a long extension plate that attached to the controller, which in turn was attached to the end of the table. This extra plate was needed to allow the TRUS probe to be imaged near the center of the PET scanner, due to the scanner bore width.

Our methods for PET-TRUS image registration depend on precisely determining the location and orientation of the TRUS probe within the PET scanner directly, by PET scanning fiducial 511 keV point sources that determined the TRUS probe position. Hence, we further modified the TRUS system, mounting two ^{68}Ge PET point sources at known locations with respect to the TRUS transducer. These two point sources were placed in a holder that was attached to the TRUS stepper, so the point sources accurately defined the axial line of the probe. Figure 5 shows the point source holder and point sources used in the dual PET-TRUS image studies, as well as the stepper-controller mechanical setup. We originally planned to attach a third ^{68}Ge point source at the rear of the probe (placed off the axis defined by the first two point sources) in order to define the probe rotation. However, this proved to be an impractical design for human subjects so the third point source was removed. We instead investigated measuring possible rotational motion using an ADXL327 accelerometer [30], as discussed below.

(a)

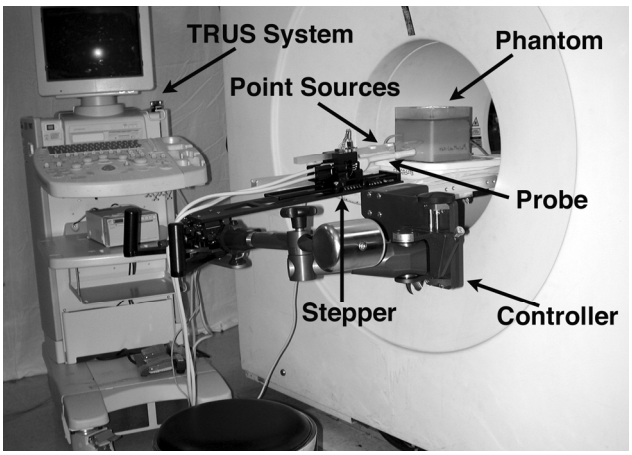

(b)

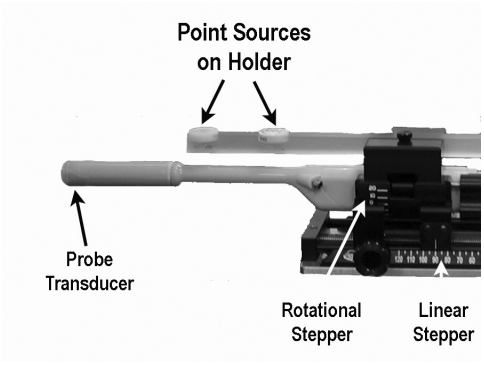

Fig. 5. (a) Photograph of the dual PET-TRUS system using the EXACT HR PET scanner. (b) Photograph close-up of the TRUS ultrasound probe and point source holder. Two ^{68}Ge point sources, mounted on the holder, are used to measure the position of the axial line of the TRUS probe. The point source holder is mounted on the stepper.

During a dual PET-TRUS study, the phantom was positioned on the table. The TRUS probe with stepper was mounted onto the controller that was attached to the table. The holder with point sources was attached to the stepper. The controller was moved to position the probe inside the phantom, then its position was fixed. A series of 2-D TRUS images in the transverse plane were acquired every 5 mm using the mechanical linear stepper, then the transducer was re-positioned at the center of the "prostate." For phantom studies, the center of the phantom was used as the "prostate"

position. The phantom was left in this position with the probe in place for the subsequent PET scans, since the TRUS probe significantly distorts the local anatomy. The table was moved so the two point sources were visually positioned in the PET scanner and PET data were acquired for 2 minutes. For image registration, these point source PET data were reconstructed after the study. We then removed the point sources, moved the table so the transducer (and hence "prostate") was visually centered in the PET scanner, injected a radiopharmaceutical into the phantom, and acquired PET imaging data of the phantom.

The point source PET data were reconstructed using either a backprojection or iterative OSEM algorithm without attenuation correction. The 3-D location of each point source in the resulting volumetric PET image was determined by fitting a 3-D Gaussian to the reconstructed intensity distribution of each point source. Given the known position of the TRUS transducer relative to the point sources, this provides nearly enough information to determine the position and orientation of the TRUS image planes. There is still ambiguity from the rotation of the TRUS image about the long axis of the probe. However, the dual PET-TRUS studies presented here acquired data with the stepper in a level position (*i.e.*, rotational angle of zero), in agreement with our clinical TRUS imaging experience with humans. This provides sufficient information for image registration, since the probe is rigidly mounted on the stepper and its position relative to the stepper is tracked.

The PET phantom data were reconstructed using an iterative OSEM reconstruction algorithm with attenuation and scatter correction. The 3-D geometric relationship between PET image pixels and TRUS image pixels was calculated based on the 511 keV point source images and the known amount of linear table motion. The 3-D position in the PET coordinates was calculated for each TRUS pixel, and the PET image intensity at each TRUS pixel position was obtained via trilinear interpolation of the PET images. This yielded registered sets of TRUS images and resampled PET images with common pixel size and 3-D pixel positions. The actual image fusion was performed using OSIRIX [31] software, without any linear or rotational translation between the two image sets.

As Figs. 3 and 6 demonstrate, accurately determining the 3-D location of the line sources in the TRUS images can be challenging. We determined the center of each line source in a 2-D TRUS image with an automated method that: (1) calculated the sum of the pixel value along the radius (for a selected range of radius), (2) calculated the derivative of the sum and determined the two boundary angles ($\theta 1$ and $\theta 2$) with peak sum values, (3) calculated the sum pixel value along the arc with different R and found the position R0 of local minimum, and (4) calculated the center of the tube as $((\theta 1+\theta 2)/2,R0)$. We used this automated algorithm to determine the line source locations in every 2-D TRUS image, for evaluation of the PET-TRUS registration.

VI. Results and Discussion

We performed dual PET-TRUS imaging of the multi-line source phantoms described in Section IV, following the protocol outlined in Section V. Figure 3a shows a transverse TRUS image of the multi-line source phantom that was acquired during a dual PET-TRUS imaging study. All line sources are clearly visible, along with dark shadows caused by each tube. The black semi-circle at the bottom of the image shows the probe. The white horizontal line (just above the probe) shows the transition layer between the two gels. Figure 3b shows a reconstructed, resampled transverse PET image of the phantom, acquired during the same study and phantom location. The entire tube was filled with 502 μCi of [^{18}F]FDG solution. PET data were acquired with a 10 minute transmission scan and a 30 minute emission scan in 3-D mode. Iterative OSEM image reconstruction was performed with attenuation and scatter correction. Using the point source information, the 3-D volumetric PET image was then resampled into TRUS image coordinates. Figure 6 shows a fused transverse image of TRUS and resampled PET data from the same phantom study as Fig. 3, demonstrating our PET-TRUS image registration capability. The resampled PET image is shown in color overlaid onto a grayscale TRUS image.

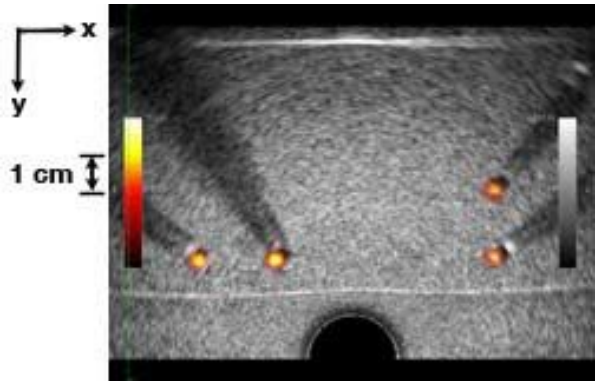

Fig. 6. Fused transverse TRUS image and resampled PET image of a multi-line source phantom. All 4 line sources are clearly visible for both imaging modalities. Pixel size is 0.289 mm in both the x and y direction. Fused image slice was acquired with the probe inserted 2.5 cm into the phantom (same as Fig. 3).

Based on our multi-line source phantom studies, our PET-TRUS registration error is 1 mm axially and 1-5 mm in the transaxial plane depending on the image study, image slice and line source measured. When calculating our PET-TRUS registration error, we averaged the PET-TRUS difference in line source position (*i.e.*, center of line source) for a 3 cm "prostate" section of all four line sources as measured during six multi-line source phantom studies. The PET-TRUS transaxial registration error is -2.1 ± 1.7 mm in the x direction and 1.9 ± 1.6 mm in the y direction. The mean transaxial distance between the PET and TRUS line source position is 3.67 ± 0.86 mm. Hence, our PET-TRUS registration error is similar to the transaxial spatial resolution of 3.6 mm FWHM for the Siemens EXACT HR PET scanner. Our current registration accuracy is sufficient for the clinical applications

of detecting early recurrence and guiding prostate biopsies, but it is not sufficient for treatment planning.

We performed a variety of point source and phantom tests in order to evaluate the causes of this PET-TRUS registration error. For instance, we repeatedly imaged two point sources (which were aligned and mounted in the standard TRUS setup, Fig. 5b) as the scanner table was moved in steps, in order to evaluate whether the table moved parallel to the axis of the scanner. Similarly, we imaged the point sources at many stepper positions (with the table position fixed and stepper aligned along z direction), in order to identify whether the mechanical stepping motion in the axial direction caused small changes in point source locations in the transaxial plane. We also evaluated the mechanical setup, using a precision height gauge to measure the deformation of each component (*e.g.*, probe, point source holder, and plate) when a force was applied to the TRUS probe tip. As a result of our phantom, point source and mechanical tests, we have identified three "real world" systematic error sources for these research methods.

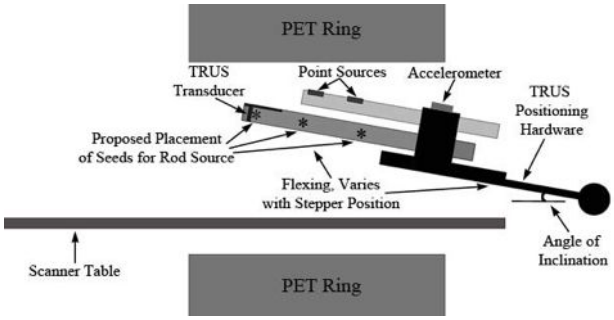

Fig. 7. Simplified drawing of the dual PET-TRUS setup, showing current and proposed radioactive source placement. Drawing also indicates the components that are flexing, the accelerometer position, and the angle of inclination.

Firstly, we assumed that the TRUS probe assembly remained rigid and the probe's angle of inclination remained fixed while the probe was stepped during the TRUS imaging. However, the probe was physically constrained by the phantom's hole (*i.e.*, "rectum"), which applied a force on the TRUS transducer that varied with stepper position. This force caused a small change in the probe's angle of inclination and a slight flexing of the probe assembly components (Fig. 7). Although the probe had only a small deformation depending on the TRUS stepper position, the PET data were acquired at only one stepper position. This caused an error in the PET-TRUS image registration that varied with stepper position (*i.e.*, image slice). Namely, line sources in the resampled PET images become lower than the corresponding TRUS images by 4 ± 1 mm in the vertical direction for PET slice 19 (when the TRUS transducer is 9.5 cm into the phantom) relative to PET slice 1 (when the TRUS transducer is just entering the phantom). Similarly, the PET images become lower than the corresponding TRUS images by 1.3 ± 0.4 mm for slices at the edge of a "prostate" section (*i.e.*, 3 cm section of phantom that begins 3 cm into the phantom).

We have measured the angular deflection of the probe holder during phantom studies, using an ADXL327 accelerometer with a 12 bit ADC, dithering method and non-linear regression calibration algorithm (Fig. 7). We have correlated these angular deflection measurements (acquired outside the subject) with the physical deformation of the probe transducer (placed inside the subject). Hence, we can now use external calibrated accelerometer measurements to accurately estimate the vertical displacement of the TRUS probe transducer as a function of stepper position, with an accuracy of 0.2 mm. Therefore, we can correct for this known systematic error during human subject studies, utilizing this information when resampling the PET data into TRUS coordinates.

Secondly, the fiducial point sources are far from the TRUS transducer because we do not want to insert the point sources inside the subject (see Fig. 5b). As a result, an error of <1 mm in measuring their location caused a PET-TRUS image registration error of up to 2 mm. In addition, this required the PET scan of the point sources to be acquired at a different table position than the phantom. It is assumed that the table motion direction is parallel to the axis of the PET scanner and that the table does not deflect, but the table motion of the PET scanner may not be level or rigid to our required precision. We found that the table re-positioning caused the point source locations to move slightly, causing a registration error of up to 1 mm in the transaxial plane. If necessary, we could develop an alternate radioactive source that can be inserted into the channel within the TRUS probe (which is designed for a biopsy needle). This radioactive needle source would consist of three custom ^{22}Na-tungsten PET radioactive seeds that are spaced within a small-diameter non-radiopaque needle (Fig. 7).

Finally, the TRUS probe-stepper unit is mounted onto a long extension plate that attaches to the controller, as described in Section V. This plate creates some probe vibration and component flexing. Ideally, we would design an entirely new controller that can fit through the scanner bore. This would allow for easier dual TRUS-PET imaging using commercial PET-CT scanners with long scanner bores.

VII. Conclusions

We have successfully developed a dual PET-TRUS system for prostate imaging and custom multi-modality PET-TRUS-CT-MRI phantoms. We have evaluated this dual-modality imaging system, by performing dual PET-TRUS imaging studies of multi-line source phantoms. We currently have a PET-TRUS registration error of 1 mm axially and 1-5 mm in the transaxial plane, depending on the image study, image slice and line source measured. The mean transaxial distance between the PET and TRUS line source position is 3.67 ± 0.86 mm. This registration accuracy is sufficient for the clinical applications of detecting early recurrence and guiding biopsies, but it is not yet sufficient to use for treatment planning.

We have also performed various phantom, point source and mechanical tests to investigate our PET-TRUS registration

accuracy. Our overall registration error includes a systematic error in the vertical direction of 1.3 ± 0.4 mm due to mechanical effects as the probe is inserted and stepped into the phantom (or subject). Using external accelerometer measurements, we can accurately estimate and correct this vertical deformation of the TRUS probe transducer as a function of stepper position. This information can be utilized when resampling the PET data into TRUS coordinates, thereby reducing the overall registration error. We will perform this correction for our human subject studies.

VIII. References

1) http://emedicine.medscape.com/article/457757-overview

2) M. K. Terris and T. A. Stamey, "Determination of prostate volume by transrectal ultrasound," *J. Urol.*, vol. 145, pp. 984-987, 1991.

3) S. C. Hoffelt, L. M. Marshall, M. Garzotto, A. Hung, J. Holland, et al., "A Comparison of CT Scan to Transrectal Ultrasound-Measured Prostate Volume in Untreated Prostate Cancer," *Int. J. Radiation Oncology Biol. Phys.*, vol. 57, pp. 29-32, 2003.

4) K. M. Kalkner, G. Kubicek, J. Nilsson, M. Lundell, S. Levitt, et al., "Prostate volume determination: Differential volume measurements comparing CT and TRUS," *Radiotherapy and Oncology*, vol. 81, pp. 179-183, 2006.

5) Y. Seo, B. L. Franc, R. A. Hawkins, K. H. Wong and B. H. Hasegawa, "Progress in SPECT/CT Imaging of Prostate Cancer," *Technology in Cancer Research & Treatment*, vol. 5, pp. 329-336, 2006.

6) E. R. Sigurdson and A. M. Cohen, "Commentary on the applications of PET in clinical oncology," *J. Nuc. Med.*, vol. 32, pp. 649-650, 1991.

7) M. K. Haseman, N. L. Reed, and S. A. Rosenthal, "Monoclonal antibody imaging of occult prostate cancer in patients with elevated prostate-specific antigen. Positron emission tomography and biopsy correlation," *Clin Nucl Med*, vol. 21, pp. 704-13, 1996.

8) P. F. Faulhaber, D. B. Sodee, E. Echt and J. K. O'Donnell, "Staging of Prostate Adenocarcinoma, comparison of FDG Dedicated PET and In-111 Capromab Pendetide," *J Nucl Med*, vol. 41, pp. 116 (abstract), 2000.

9) T. Hara, N. Kosaka, and H. Kishi, "PET imaging of prostate cancer using carbon-11-choline," *J Nucl Med*, vol. 39, pp. 990-5, 1998.

10) T. Hara, N. Kosaka, T. Kondo, H. Kishi and O. Kobori, "Imaging of brain tumor, lung cancer, esophagus cancer, colon cancer, prostate cancer, and bladder cancer with [C-11]choline," *J Nucl Med*, vol. 38 (suppl), pp. 250P (abstract), 1997.

11) J. Kotzerke, J. U. Prang, B. Neumaier, A. C. Guhlmann, K. Kleinschmidt, et al., "Carbon-11 choline positron emission tomography (PET) of prostate cancer -- first clinical experience," *J. Nucl. Med.*, vol. 41 (5 Suppl), pp. 74, 2000.

12) J. Kotzerke, J. Prang, B. Neumaier, B. Volkmer, A. Guhlmann, et al., "Experience with carbon-11 choline positron emission tomography in prostate carcinoma," *Eur J Nucl Med*, vol. 27, pp. 1415-9, 2000.

13) M. Picchio, C. Messa, C. Landoni, L. Gianolli, S. Sironi, et al., "Value of [11C]choline-positron emission tomography for re-staging prostate cancer: a comparison with [18F]fluorodeoxyglucose-positron emission tomography," *J Urol.*, vol. 169, pp. 1337-1340, 2003.

14) I. J. de Jong, J. Pruim, P. H. Elsinga, W. Vaalburg and H. J. Mensink, "Preoperative staging of pelvic lymph nodes in prostate cancer by 11C-choline PET," *J Nucl Med*, vol. 44, pp. 331-335, 2003.

15) I. J. de Jong, J. Pruim, P. H. Elsinga, W. Vaalburg and H. J. Mensink, "11C-choline positron emission tomography for evaluation after treatment of localized prostate cancer," *Eur Urol*, vol. 44, pp. 32-39, 2003.

16) E. Sutinene, M. Nurmi, A. Roivainen, M. Varpula, T. Tolvanen, et al., "Kinetics of [(11)C]choline uptake in prostate cancer: a PET study," *Eur J Nucl Med Mol Imaging*, vol. 31, pp. 317-324, 2004.

17) Q. H. Zheng, T. A. Gardner, S. Raikwar, C. Kao, K. L. Stone, et al., "[11C]Choline as a PET biomarker for assessment of prostate cancer tumor models," *Bioorg Med Chem*, vol. 12, pp. 2887-2893, 2004.

18) T. Kato, R. Tsukamoto, Y. Kuge, T. Takei, T. Shiga, et al., "Accumulation of [11C]acetate in normal prostate and benign prostatic hyperplasia: comparison with prostate cancer," *Eur J Nucl Med Mol Imaging*, vol. 29, pp. 1492-1495, 2002.

19) N. Oyama, T. R. Miller, F. Dehdashti, B. A. Siegel, K. C. Fischer, et al., "11C-acetate PET imaging of prostate cancer: detection of recurrent disease at PSA relapse," *J. Nuc. Med.*, vol. 44, pp. 556-558, 2003.

20) E. Fricke, S. Machtens, M. Hofmann, J. Van Den Hoff, S. Bergh, et al., "Positron emission tomography with 11C-acetate and 18F-FDG in prostate cancer patients," *Eur J Nucl Med Mol Imaging*, vol. 30, pp. 607-610, 2003.

21) I. Osman, T. Akhurst, H. Macapinlac, H. Yeung, J. Miller, et al., "C-11 methionine and F-18 PET imaging: use in the evaluation of progressive prostate cancer," *Proc Am Soc Clin Oncol*, vol. 17, pp. 1203 (abstract), 1998.

22) H. A. Macapinlac, J. L. Humm, T. Akhurst, I. Osman, K. Pentlow, et al., "Differential metabolism and pharmacokinetics of L- [1-C-11]methionine and 2-[F-18]fluoro-2-deoxy-D-glucose (FDG) in androgen independent prostate cancer," *Clinical Positron Imaging*, vol. 2, pp. 173-81, 1999.

23) R. Nunez, H. A. Macapinlac, H. W. Yeung, T. Akhurst, S. Cai, et al., "Combined 18F-FDG and 11C-methionine PET scans in patients with newly progressive metastatic prostate cancer," *J Nucl Med*, vol. 43(1), pp. 46-55, 2002.

24) G. Toth, Z. Lengyel, L. Balkay, M. A. Salah, L. Tron, et al., "Detection of prostate cancer with 11C-methionine positron emission tomography," *J. Urol.*, vol. 173(1), pp. 66-69, 2005.

25) T. R. Degrado, R. E. Coleman, S. W. Baldwin, M. D. Orr, C. N. Robertson, et al., "Fluorine-18 fluorocholine (FCH) as an oncological PET tracer: evaluation in murine prostate cancer xenograft model," *J Nucl Med*, vol. 41 (5 Suppl), pp. 231, 2000.

26) T. R. Degrado, R. E. Coleman, S. Wang, S. W. Baldwin, M. D. Orr, et al., "Synthesis and Evaluation of F18-labeled Choline as an Oncologic Tracer for Positron Emission Tomography: Initial Findings in Prostate Cancer," *Cancer Research*, vol. 61(1), pp. 110-117, 2001.

27) K. Wienhard, M. Dahlbom, L. Eriksson, C. Michel, T. Bruckbauer, et al., "The ECAT EXACT HR: performance of a new high resolution positron scanner," *J Comp Asst*, vol. 18, pp. 110-118, 1994.

28) G. Kovacs, R. Potter, T. Loch, J. Hammer, I.-K. Kolkman-Deurloo, et al., "GEC/ESTRO-EAU recommendations on temporary brachytherapy using stepping sources for localised prostate cancer," *Radiotherapy and Oncology*, vol. 74, pp. 137-148, 2005.

29) J. S. Huber, Q. Peng, and W. W. Moses, "Multi-Modality Phantom Development," *IEEE Trans Nucl Sci*, vol. 56, pp. 2722-2727, 2009.

30) http://www.analog.com/en/sensors/inertial-sensors/adxl327/products/product.html

31) A. Rosset, L. Spadola, and O. Ratbig, "OsiriX: An open-source software for navigating in multimodality DICOM images," *J. Digit Image.*, vol. 17, pp. 205-216, 2004.

32)

You have one entry in the database.

Abstract #	Abstract Title	Conference	Status
1214	Dual PET-TRUS Prostate Image Registration	MIC	Waiting for reviewer assignment

Add a new abstract to: NSS MIC RTSD Workshops

Abstract #: 1214 **Conference:** MIC **Preferred Pres.:** Either

Tech. Topic: Multi-modality Systems **Presenter:** Jennifer S Huber

Dual PET-TRUS Prostate Image Registration

J. S. Huber[1], Q. Peng[1], W. W. Moses[1], J. Pouliot[2], I.-C. Hsu[2]

[1]Radiotracer Development and Imaging Technology Department, Lawrence Berkeley National Lab, Berkeley, CA, USA
[2]Radiation Oncology Department, University of California, San Francisco, San Francisco, CA, USA

Multimodality imaging plays an increasingly important role in the diagnosis and treatment of a large number of diseases, particularly if both functional and structural information are acquired and accurately registered. Hence, we have developed a dual PET-TRUS imaging system that will help identify the location and aggressiveness of prostate cancer. We acquire high-resolution anatomical detail of the prostate region from transrectal ultrasound (TRUS) imaging that is accurately registered with the sensitive functional information from positron emission tomography (PET). PET-TRUS image registration based on prostate image features is inaccurate, since few anatomical features are seen in the PET images. Our image registration method instead depends on precisely determining the location and orientation of the TRUS probe within the PET scanner directly, by performing an additional fast PET scan of fiducial 511 keV point sources that determine the probe position. We have evaluated our PET-TRUS image registration accuracy by performing dual-modality imaging of custom phantoms. We describe our PET-TRUS system, custom phantom and phantom study results (including registration accuracy and systematic errors). Our PET-TRUS preliminary registration error is 1 mm axially and 2-5 mm in the transaxial plane (depending on the image study, image slice and line source measured), which is sufficient for some clinical applications such as early detection of recurrence. We also discuss our plans to expand this work to multimodality prostate imaging using TRUS and PET-CT or SPECT-CT imaging systems.

This work was supported in part by the Director, Office of Science, Office of Biological and Environmental Research, Medical Science Division of the U.S. Department of Energy under Contract No. DE-AC02-05CH11231, and in part by Department of Defense grant number W81XWH-07-1-0020.

If you need to update the summary file, click on the "My Files" menu above.

If you need to make changes to this abstract, contact the program chairs.

Withdraw This Abstract

Transfer Ownership

Project Summary

Objective: The objective of this project is to develop multimodality prostate imaging and evaluate the technology with initial human subject studies. We will acquire high resolution anatomical detail of the prostate region from transrectal ultrasound (TRUS) imaging that is accurately registered with sensitive functional information from either positron emission tomography (PET) or single photon emission computed tomography (SPECT). This multimodality imaging will help to detect and localize cancer within the prostate region. The accurately registered multimodality images can be used to guide subsequent diagnosis and treatment procedures, *e.g.*, biopsy, surgery, external beam radiotherapy, and brachytherapy. Recent studies have shown the value of multimodality imaging, especially when functional and anatomical data are fused. TRUS is the anatomical imaging modality of choice for most prostate cancer clinicians (*i.e.*, not CT), hence the desire to merge the use of TRUS with PET and SPECT for prostate imaging.

Specific Aims: The goals of this proposal focus on developing hardware and software tools: (1) to comfortably position the TRUS probe inside a human subject using a TRUS controller that can move with the subject through the PET-CT or SPECT-CT scanner bore, (2) to develop a method to accurately register volumetric TRUS, CT, and PET images using phantom studies, (3) to evaluate this registration method with TRUS-CT-PET human subject studies using the radiopharmaceutical [^{11}C]choline, and (4) to repeat Aims 2 and 3 for TRUS-CT-SPECT imaging using the radiopharmaceutical [^{111}In]ProstaScint.

Research Design: We will perform multimodality prostate imaging sequentially during the same imaging session in the order of: TRUS, low dose CT and PET (or SPECT). The subject will remain in the same position with the TRUS probe in place for all imaging, since the TRUS probe significantly distorts the local anatomy. The PET-CT (or SPECT-CT) images are already routinely co-registered, so the critical task is to register the TRUS images to either the CT or the PET (or SPECT) images. We will explore two methods for doing this: (1) using CT to determine the position of the TRUS probe and (2) using PET (or SPECT) to find the position of ^{22}Na (or ^{57}Co) radioactive seeds that are inserted at a known location inside the TRUS probe (via the hollow channel that is designed for a biopsy needle). Since the position of the TRUS images is well known with respect to the physical position of the probe, this gives sufficient information for image co-registration. We will quantitatively evaluate these two methods by performing phantom studies, using custom phantoms designed to test TRUS-CT-PET and TRUS-CT-SPECT image registration accuracy, and will select the best method. We will then perform initial human subject studies in order to identify issues that would affect the clinical utility of the techniques. The tools and protocols developed in this project are necessary for future clinical research.

US 20100198063A1

(19) **United States**

(12) **Patent Application Publication**

Huber et al.

(10) **Pub. No.: US 2010/0198063 A1**

(43) **Pub. Date: Aug. 5, 2010**

(54) **MULTI-MODALITY PHANTOMS AND METHODS FOR CO-REGISTRATION OF DUAL PET-TRANSRECTAL ULTRASOUND PROSTATE IMAGING**

(75) Inventors: **Jennifer S. Huber**, El Sobrante, CA (US); **William W. Moses**, Berkeley, CA (US); **Jean Pouliot**, Mill Valley, CA (US); **I-Chow Hsu**, San Francisco, CA (US); **Qiyu Peng**, Albany, CA (US); **Ronald H. Huesman**, Danville, CA (US); **Thomas F. Budinger**, Berkeley, CA (US)

Correspondence Address:
LAWRENCE BERKELEY NATIONAL LABORATORY
Technology Transfer & Intellectual Propery Managem, One Cyolotron Road MS 56A-120
BERKELEY, CA 94720 (US)

(73) Assignee: **THE REGENTS OF THE UNIVERSITY OF CALIFORNIA**, Oakland, CA (US)

(21) Appl. No.: **12/622,335**

(22) Filed: **Nov. 19, 2009**

Related U.S. Application Data

(63) Continuation-in-part of application No. PCT/US2008/064160, filed on May 19, 2008.

(60) Provisional application No. 60/939,051, filed on May 19, 2007.

Publication Classification

(51) **Int. Cl.**

A61B 8/00	(2006.01)
G09B 23/30	(2006.01)
G01T 1/164	(2006.01)

(52) **U.S. Cl.** **600/437**; 434/267; 250/363.03

(57) **ABSTRACT**

Herein are described methods and tools for acquiring accurately co-registered PET and TRUS images, as well as the construction and use of PET-TRUS prostate phantoms. Ultrasound imaging with a transrectal probe provides anatomical detail in the prostate region that can be accurately co-registered with the sensitive functional information from the PET imaging. Imaging the prostate with both PET and transrectal ultrasound (TRUS) will help determine the location of any cancer within the prostate region. This dual-modality imaging should help provide better detection and treatment of prostate cancer. Multi-modality phantoms are also described.

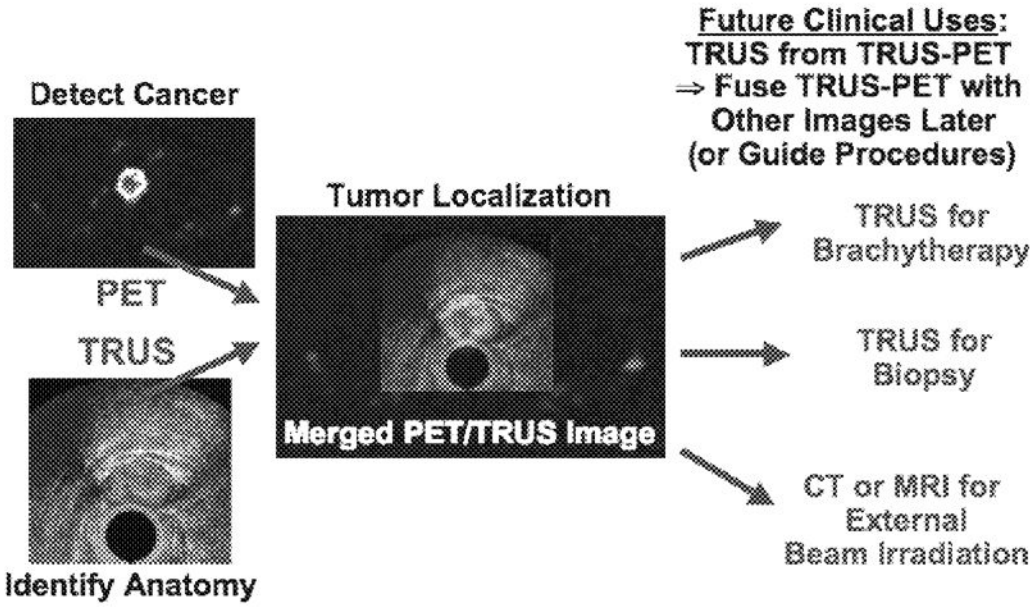

Multi-Modality Phantom Development

Jennifer S. Huber, *Member, IEEE*, Qiyu Peng, and William W. Moses, *Fellow, IEEE*

***Abstract*—Multi-modality imaging has an increasing role in the diagnosis and treatment of a large number of diseases, particularly if both functional and anatomical information are acquired and accurately co-registered. Hence, there is a resulting need for multi-modality phantoms in order to validate image co-registration and calibrate the imaging systems. We present our PET-ultrasound phantom development, including PET and ultrasound images of a simple prostate phantom. We use agar and gelatin mixed with a radioactive solution. We also present our development of custom multi-modality phantoms that are compatible with PET, transrectal ultrasound (TRUS), MRI and CT imaging. We describe both our selection of tissue mimicking materials and phantom construction procedures. These custom PET-TRUS-CT-MRI prostate phantoms use agar-gelatin radioactive mixtures with additional contrast agents and preservatives. We show multi-modality images of these custom prostate phantoms, as well as discuss phantom construction alternatives. Although we are currently focused on prostate imaging, this phantom development is applicable to many multi-modality imaging applications.**

***Index Terms*—Magnetic resonance imaging, positron emission tomography, ultrasound, x-ray computed tomography.**

I. Introduction

MULTI-MODALITY imaging plays an increasingly important role in the diagnosis and treatment of a large number of diseases. Combining modalities that provide both functional and structural information is particularly important. For instance, functional information can be acquired with single photon emission computed tomography (SPECT), positron emission tomography (PET) or functional magnetic resonance imaging (fMRI), whereas anatomical information can be acquired using x-ray computed tomography (CT), ultrasound (US) or magnetic resonance imaging (MRI).

Combining PET and CT has recently revolutionized the role of imaging in diagnosis and treatment planning for many kinds of cancer. As a result, there are commercially available PET-CT phantoms that are used for acceptance testing and routine quality evaluation of the PET-CT systems. For instance, these phantoms are used to determine how accurately the two image sets are aligned and how accurately the CT-based PET attenuation correction works. However, PET-CT imaging is not the preferred modality combination for all diseases or even all cancers. For instance, ultrasound imaging is an integral part of diagnosis and treatment procedures for many diseases, such as prostate cancer. Transrectal ultrasound (TRUS) provides good anatomical detail of the prostate region and accurately measures the prostate volume, whereas CT has poor contrast for soft-tissue (like the prostate) and it over-estimates prostate volume. Hence, phantoms for multi-modality imaging with ultrasound and PET or MRI are needed. Ultrasound phantoms are readily available commercially, but we are not aware of any commercially available US-PET or US-MRI phantoms.

We believe that imaging the prostate with ^{11}C-choline using a dual PET-TRUS system will help locate cancer within the prostate region. We envision that dual PET-TRUS prostate imaging could be used to guide biopsy, guide treatment procedures, and detect local recurrence earlier than is currently possible. Therefore, we are developing a dual imaging system that acquires PET and TRUS data sets during the same patient imaging session, using methods that allow us to accurately determine the 3-D location of the TRUS probe tip relative to the PET scanner. As a result, co-registration of the PET and TRUS patient images will be simple and accurate. However, prior to our patient studies, we must validate our ability to image and accurately co-register PET and TRUS images using a PET-TRUS prostate phantom.

Since the phantom that we need is not commercially available, we have built a custom PET-TRUS prostate phantom with structures that simulate the acoustical properties for TRUS and 511 keV activity concentrations for PET. In addition, we have built custom PET-TRUS-CT-MRI phantoms with structures that also simulate the nuclear magnetization for MRI and radiographic density for CT. We present here our PET-ultrasound phantom and PET-TRUS-CT-MRI phantom development, including multi-modality images of phantoms. We also discuss alternative phantom construction options. This phantom development is applicable to many multi-modality applications.

II. PET-Ultrasound Phantom

We have constructed a simple PET-ultrasound prostate phantom as proof of principle. It was constructed with two basic tissue mimicking materials (TMMs). The "pelvis" was prepared as a high-scatter ultrasound TMM, using 4% agarose mixed with deionized water and heated to 62°C (in a hot water bath on a hot plate and mixed continuously with a magnetic stir rod). The temperature of the agarose-water was kept below 70°C to maintain the high-scatter ultrasound properties. The "prostate" was prepared as a low-scatter ultrasound TMM, using 8% gelatin mixed with deionized water and heated until the gelatin dissolved.

The PET-US phantom was constructed in two stages. We first filled a rectangular plastic box with the 4% agarose TMM, creating a void with a petrolatum-coated plastic rod in the center.

Manuscript received March 20, 2009; revised June 10, 2009 and June 12, 2009. Crrent version published October 07, 2009. This work was supported in part by the Director, Office of Science, Office of Biological and Environmental Research, Medical Science Division of the U.S. Department of Energy under Contract DE-AC02-05CH11231, and in part by Department of Defense under Grant W81XWH-07-1-0020.

The authors are with Lawrence Berkeley Nationial Laboratory, Berkeley, CA 94720 USA (e-mail: jshuber@lbl.gov; qpeng@lbl.gov; wwmoses@lbl.gov).

Color versions of one or more of the figures in this paper are available online at http://ieeexplore.ieee.org.

Digital Object Identifier 10.1109/TNS.2009.2028073

As soon as the rectangular agarose "pelvis" hardened, the rod was removed and we filled the inner cylindrical "prostate" region with the 8% gelatin TMM. Fig. 1(a) shows a photograph of the PET-US phantom. At each stage, the TMM was mixed with $^{18}\mathrm{F}$ radioactivity (potassium fluoride in aqueous solution mixed with a drop of food coloring) before placing it in a refrigerator to harden. We used short-lived [$^{18}\mathrm{F}$]Fluoride (110 minutes half-life), since $^{18}\mathrm{F}$ is readily available from our in-house cyclotron and no long-lived radioactive waste were generated by the tests. As a result, the gel hardening time was important due to the $^{18}\mathrm{F}$ half-life. The "pelvis" gel hardened in 52 minutes (using an ice bath within the refrigerator) and the "prostate" hardened in 31 minutes (without ice bath). The resulting phantom had six times higher 511 keV activity density in the inner cylindrical "prostate" than in the outer rectangular "pelvis."

The phantom was roughly centered in an EXACT HR PET scanner, and PET data were acquired with a 20 minute emission scan in 3-D mode and 10 minute transmission scan. At the start of the emission scan, the $^{18}\mathrm{F}$ activity density was 1.07 $\mu\mathrm{Ci/ml}$ in the cylindrical "prostate" gelatin and 0.17 $\mu\mathrm{Ci/ml}$ in the rectangular "pelvis" agarose. Image reconstruction was performed with attenuation and scatter correction. Fig. 1(b) shows a reconstructed coronal PET image of the phantom, as well as a horizontal profile through the "prostate" center. The $^{18}\mathrm{F}$ activity in the cylindrical "prostate" gelatin is clearly visible within the rectangular "pelvis" background activity, with the expected 6 ("prostate") to 1 ("pelvis") relative activity. The $^{18}\mathrm{F}$ activity is concentrated almost uniformly within the "prostate," but a small asymmetry is seen due to incomplete $^{18}\mathrm{F}$ mixing during the gel hardening process (Fig. 1(b)).

The phantom was then imaged using a 5 MHz external Elektra ultrasound system, as shown in Fig. 1(c). The ultrasound image clearly shows the low-scatter cylindrical "prostate" gelatin, which is surrounded by the high-scatter "pelvis" agarose. Thus, we have demonstrated our ability to construct and image a custom PET-ultrasound phantom. However, the phantom's mechanical and ultrasound properties did not have long-term stability, especially at room temperature. For instance, this phantom (without preservative) was invaded by fungus and bacteria within about a month even when stored in a refrigerator.

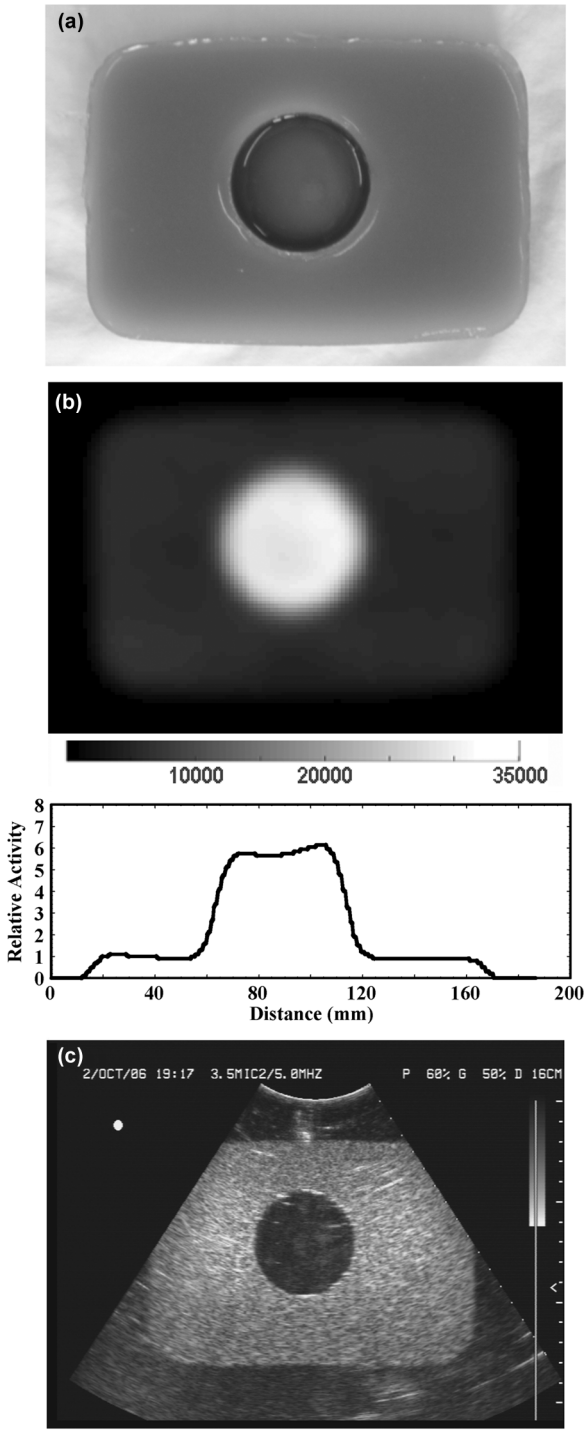

Fig. 1. (a) Photograph of a PET-ultrasound prostate phantom. The agarose "pelvis" has outer dimensions of 16 cm × 11 cm × 3.5 cm. The cylindrical gelatin "prostate" has a 5 cm diameter and 2.5 cm depth. (b) Reconstructed coronal PET image of the phantom. The white circle shows the high $^{18}\mathrm{F}$ activity density in the "prostate," and the dark gray rectangle shows the low $^{18}\mathrm{F}$ activity density in the background "pelvis." Image represents 636 M counts (i.e., 20 minutes of data). The voxel size is 1.47 mm × 1.47 mm × 3.125 mm. Horizontal profile through the "prostate" center is also shown. (c) Ultrasound image of the same phantom using a 5 MHz external ultrasound probe. The dark gray circle shows the low-scatter gelatin "prostate," and the surrounding light gray background shows the high-scatter agarose "pelvis."

III. PET-TRUS-CT-MRI Phantoms

Methods for ultrasound phantom construction are well represented in literature [1]–[5]. Since the phantom described in Section II did not have long-term stability at room temperature, we needed to develop a different phantom construction process. We therefore constructed a multi-modality phantom using tissue mimicking mixtures of agar, gelatin, $\mathrm{CuCl_2 - 2H_2O}$, EDTA-tetra Na Hydrate, NaCl, formalin, Germall-Plus, glass beads, $\mathrm{BaSO_4}$, and deionized water (Table I). Similar agar-gelatin mixtures were proven to have stable mechanical, ultrasound and MRI properties for at least one year [5]. These agar-gelatin-based tissue mimicking materials were mixed with radioactive solutions (with a drop of food coloring). When developing the procedures for this phantom construction, we used short-lived radioactive [$^{18}\mathrm{F}$]Fluoride and a small amount of non-radioactive 0.5 M HCl. Once the phantom construction procedures were finalized, we used long-lived $^{68}\mathrm{GeCl_4}$ radioactivity (271 day half-life) in a 0.5 M HCl solution to allow

TABLE I
DRY-WEIGHT PERCENTS OF THE VARIOUS COMPONENTS IN THE PET-TRUS-CT-MRI CUSTOM PHANTOM. THE REMAINING WEIGHT PERCENT IS DEIONIZED WATER

	Agar	Gelatin	$CuCl_2$-$2H_2O$	EDTA	NaCl	Formalin	Germall-Plus	Glass Beads	$BaSO_4$
Pelvis TMM	1.17	5.52	0.11	0.33	0.77	0.24	1.45	4.4	0.50
Prostate TMM	3.64	5.70	0.12	0.34	0.80	0.25	1.50	0	0

repeated PET imaging of the same phantom. (0.5 M HCl is used to maintain a stable homogenous $^{68}GeCl_4$ solution.) The main purpose of these custom PET-TRUS-CT-MRI phantoms is to develop radioactive TMMs that both approximate the acoustical properties of patients more accurately and have improved long-term stability at room temperature than those developed in Section II.

We constructed two-region PET-TRUS-CT-MRI phantoms with a "prostate" tapered cylinder within a "pelvis" rectangular cuboid. The "pelvis" has outer dimensions of 15 cm $\times$ 15 cm $\times$ 7.5 cm. The "prostate" is 7 cm deep with a tapering diameter ranging from 5 to 3 cm. We first filled the "pelvis" cubic container with the "Pelvis TMM" (Table I), creating two voids with petrolatum-coated plastic rods. A small 2.5 cm diameter cylindrical rod was used to create a hole for the TRUS imaging probe. A larger rod with a tapered end was used to create a void for the "prostate." Once the "pelvis" hardened, we removed both rods. We then filled the tapered cylindrical void with a "Prostate TMM" (Table I), having different multi-modality properties and ^{18}F or ^{68}Ge activity concentrations than the "pelvis." Both TMMs were hardened at room temperature. Theses phantoms are stored with a thin layer of safflower oil on top to minimize dehydration and shrinkage. Fig. 2 shows a photograph of a custom PET-TRUS-CT-MRI phantom.

Table I outlines the dry-weight percentages of the materials used to construct the "Prostate TMM" and "Pelvis TMM" of the custom PET-TRUS-CT-MRI phantoms. For initial tests, only the "Prostate TMM" was mixed with $[^{18}F]$Fluoride due to the time required for gel hardening. For the final phantom, both TMM regions were mixed with $^{68}GeCl_4$ solution. The primary role of each ingredient is summarized below:

- *Agar*: concentration set to achieve tissue-like ultrasound properties, such as ultrasound propagation speed. Higher agar concentration also produces shorter longitudinal (T_1) and transverse (T_2) MRI relaxation times.
- *Gelatin*: concentration set for tissue-like ultrasound properties, such as ultrasound propagation speed. Concentration must be roughly the same for "prostate" and "pelvis" regions to avoid changes in volumes due to osmosis.
- $CuCl_2-2H_2O$ and *EDTA-tetra Na Hydrate*: EDTA forms chelate with the Cu^{2+} ions to allow Cu^{2+} to remain mobile, allowing controlled lowering of the T_1 MRI relaxation time.
- *NaCl*: produces tissue-like MRI coil loading.

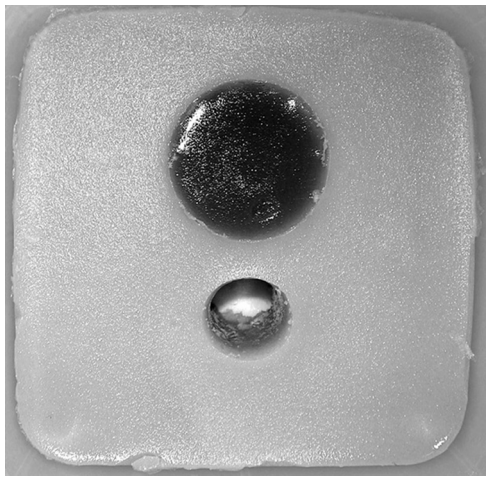

Fig. 2. Photograph of a custom PET-TRUS-CT-MRI phantom. The square "pelvis" has outer dimensions of 15 cm $\times$ 15 cm. The tapered cylindrical "prostate" is seen as a 5 cm diameter dark circle (the diameter of the cylinder tapers, decreasing from 5 cm to 3 cm towards the container bottom). The hole for transrectal ultrasound imaging (seen directly below the dark "prostate" circle) has a diameter of 2.5 cm.

- *Formalin* (37% formaldehyde): cross-links the gelatin, raising the melting point to 78°C where the agar component melts.
- *Germall-Plus*: preservative to prevent fungal and bacterial invasion.
- *Glass Beads* (20 μm average diameter): increases ultrasound attenuation and backscatter to tissue-like levels. Also shortens T_1 and T_2 MRI relaxation times.
- $BaSO_4$: increases radiographic attenuation for CT imaging.
- $[^{18}F]$*Fluoride or* $^{68}GeCl_4$: 511 keV radioactivity for PET imaging.

The expected ultrasound and MRI properties of the phantom are based on previous work by others [5], since precise measurements of these properties were not needed for our application. The expected ultrasound properties include a propagation speed of about 1534 m/s, a density of about 1.04 g/ml, and an attenuation coefficient divided by frequency of about 0.14 dB/cm/MHz for the "Prostate TMM" and 0.38 dB/cm/MHz for the "Pelvis TMM." The MRI T_1 relaxation times are expected to be about 494 ms for the "Prostate TMM" and 423 ms for the "Pelvis TMM." The MRI T_2 relaxation times are expected to be approximately 58 ms. Based on direct region of interest measurements of the CT scans of the phantom, the CT number is expected to be about 50 HU for the "Prostate TMM" and about 140 HU for the "Pelvis TMM."

A custom PET-TRUS-CT-MRI phantom, using ^{18}F in only the "prostate," was imaged with PET, CT and MRI. Using an EXACT HR PET scanner, PET data were acquired with a 60 minute emission scan in 3-D mode and 10 minute transmission scan. At the start of the emission scan, the ^{18}F activity density was 0.33 μCi/ml in the prostate. Image reconstruction was performed with attenuation and scatter correction. Fig. 3 shows a reconstructed coronal PET image of the phantom, as well as a horizontal profile through the "prostate" center. The ^{18}F activity is concentrated almost uniformly within the "prostate," but

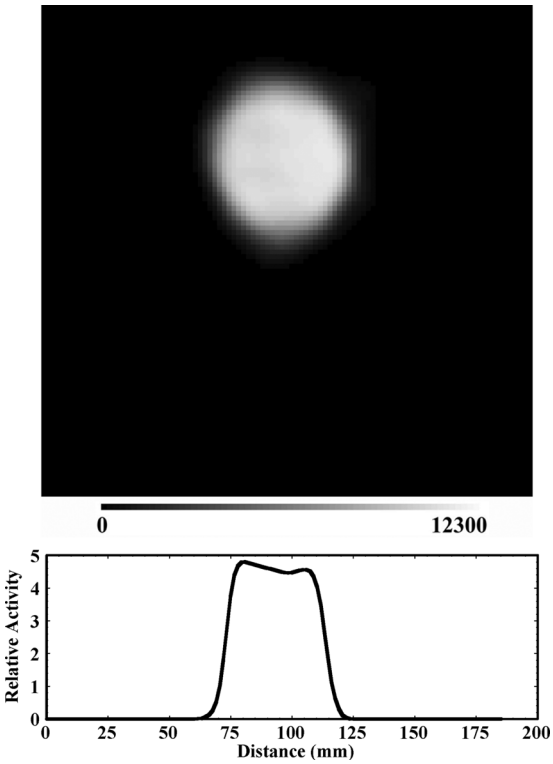

Fig. 3. Reconstructed coronal PET image of a custom PET-TRUS-CT-MRI phantom using $^{18}\mathrm{F}$ (in the "prostate" only). The white circle shows the nearly uniform $^{18}\mathrm{F}$ activity in the "prostate." The $^{18}\mathrm{F}$ initial activity density was 0.33 $\mu\mathrm{Ci/ml}$. Voxel size is 1.47 mm $\times$ 1.47 mm $\times$ 3.125 mm. Horizontal profile through the "prostate" center is also shown.

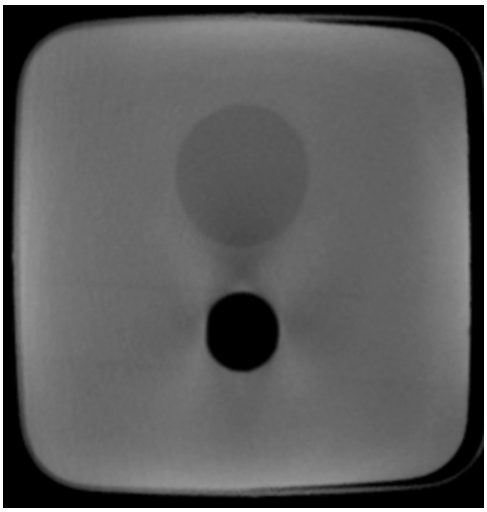

Fig. 4. Reconstructed coronal x-ray CT image of the phantom with 1 mm axial thick slices. The pixel size is 0.5 mm $\times$ 0.5 mm $\times$ 1 mm. The dark gray circle shows lower radiographic attenuation in the "prostate" compared with the surrounding light gray higher-attenuation "pelvis." The black circle shows a hole used for the TRUS imaging probe.

a small asymmetry is seen due to incomplete $^{18}\mathrm{F}$ mixing during the gel hardening process.

The phantom was imaged with a Nucletron KV ConeBeam CT scanner (100 keV; 16 mAmps) after the $^{18}\mathrm{F}$ decayed. Reconstruction was performed with a proprietary SmartScatter algorithm using a Cone-Beam CT wedge filter. Fig. 4 shows a reconstructed coronal CT image of the phantom with increased radiographic attenuation in the "pelvis" due to the $\mathrm{BaSO_4}$.

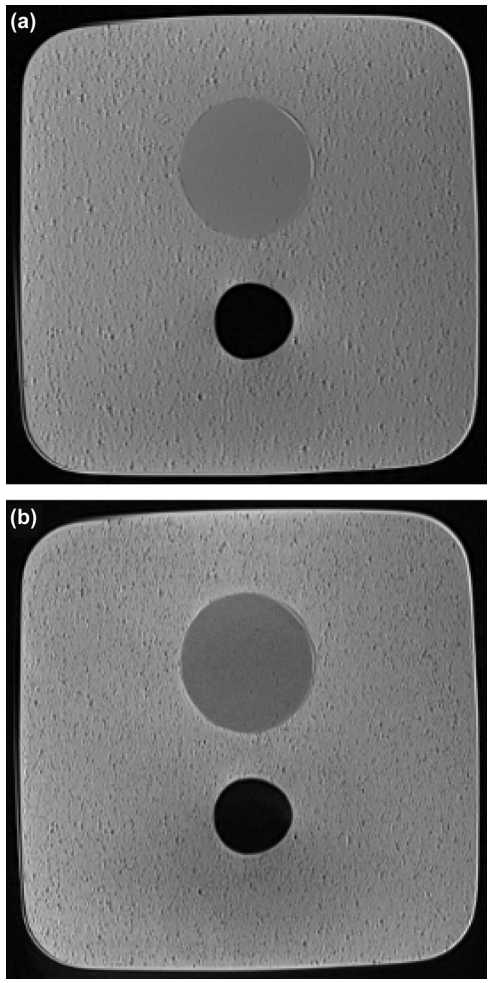

Fig. 5. (a) Reconstructed coronal MRI $\mathrm{T_1}$-weighted image of the custom PET-TRUS-CT-MRI phantom, representing 60 minutes of data. Voxel size is 0.4 mm $\times$ 0.4 mm $\times$ 3 mm. The dark gray circle shows the longer $\mathrm{T_1}$ "prostate" surrounded by the shorter $\mathrm{T_1}$ "pelvis." The black circle shows a hole used for the TRUS imaging probe. (b) Reconstructed coronal MRI $\mathrm{T_2}$-weighted image of the phantom, representing 50 minutes of data. Voxel size is 0.4 mm $\times$ 0.4 mm $\times$ 3 mm.

After the $^{18}\mathrm{F}$ decayed, the phantom was also imaged with an 1.5 T Avanto Siemens MRI scanner using a head coil with a $\mathrm{T_1}$-weighted 2-D spin echo pulse sequence ($\mathrm{TE} = 7.8$ msec; $\mathrm{TR} = 500$ msec; field of view $= 230$ mm $\times$ 230 mm $\times$ 3 mm; voxel size $= 0.4$ mm $\times$ 0.4 mm $\times$ 3 mm). Fig. 5(a) shows a reconstructed $\mathrm{T_1}$-weighted MRI image with a darker "prostate" representing a longer $\mathrm{T_1}$ compared to the "pelvis." The glass beads (used for ultrasound imaging) shortened the $\mathrm{T_1}$ in the "pelvis" despite having a lower agar concentration. The phantom was also imaged with a $\mathrm{T_2}$-weighted 2-D turbo spin echo pulse sequence ($\mathrm{TE} = 89$ msec; $\mathrm{TR} = 5590$ msec; field of view $= 230$ mm $\times$ 230 mm $\times$ 3 mm; voxel size $=$ 0.4 mm $\times$ 0.4 mm $\times$ 3 mm). Fig. 5(b) shows a reconstructed $\mathrm{T_2}$-weighted MRI image with a darker "prostate" representing a shorter $\mathrm{T_2}$ compared to the "pelvis."

A custom PET-TRUS-CT-MRI phantom using $^{68}\mathrm{GeCl_4}$ in a 0.5 M HCl solution was also constructed. The phantom gel is inside a plastic cubic box with a lid that has a hole for TRUS imaging access. In order to prevent $^{68}\mathrm{Ge}$-gel pieces from escaping during TRUS imaging, a condom is used to seal the hole.

(The condom base is fixed around a centering ring on top of the container lid. The condom is held in place using a small washer inside the condom tip and a magnet outside the bottom of the plastic container.) When TRUS imaging the phantom, the TRUS probe is covered by a second condom filled with ultrasound gel and pushed against the phantom to minimize air bubbles. At the time of the phantom construction, the ^{68}Ge activity density was 0.73 μCi/ml in the "prostate" and 0.12 μCi/ml in the "pelvis."

This custom phantom was imaged using an EXACT HR PET scanner 30 hours after phantom construction. PET data were acquired with a 3-D emission scan followed by a 10 minute transmission scan. Iterative image reconstruction was performed with attenuation and scatter correction. Fig. 6(a) shows a reconstructed coronal PET image of the phantom, as well as a horizontal profile through the "prostate" center. The ^{68}Ge activity density was initially six times higher in the "prostate" than the "pelvis." The ^{68}Ge activity in the "prostate" is clearly visible within the "pelvis" background. However, the "prostate" radioactivity in the PET image has a blurrier edge in this case (e.g., compared to Fig. 1(b)), and the relative activity shown in the profile is only 4.8 ("prostate") to 1 ("pelvis"). This is probably due to the initial diffusion of the ^{68}Ge tetrachloride molecules, which is discussed in detail in Section IV. This assumption is supported by the nearly uniform radioactivity seen in the PET image of the previously discussed PET-TRUS-CT-MRI phantom constructed with ^{18}F (Fig. 3).

The phantom was also imaged with a Hitachi Hi-Vision 5500 digital ultrasound system, using a B mode biplane TRUS probe in a linear stepper. Fig. 6(b) shows a transrectal ultrasound image of the phantom with a lower-scatter "prostate" surrounded by a higher-scatter "pelvis."

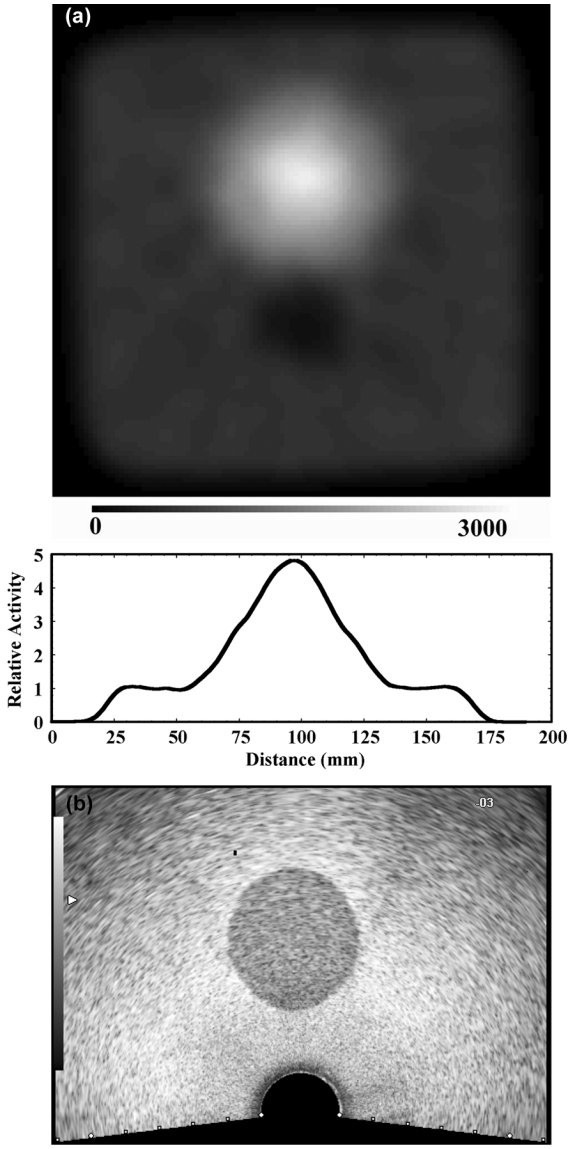

Fig. 6. (a) Reconstructed coronal PET image of a custom PET-TRUS-CT-MRI phantom using ^{68}Ge. The white circle shows the higher ^{68}Ge activity in the "prostate" within the dark gray low ^{68}Ge activity in the "pelvis." The ^{68}Ge activity density was 0.73 μCi/ml in the "prostate" and 0.12 μCi/ml in the "pelvis" during initial construction. Voxel size is 1.47 mm × 1.47 mm × 3.125 mm. Horizontal profile through the "prostate" center is also shown. (b) Ultrasound image of the phantom. The dark gray circle shows the lower-scatter "prostate," directly above the black circular hole used for the TRUS probe. The surrounding light gray background shows the higher-scatter "pelvis."

IV. Discussion

We intended to use this custom PET-TRUS-CT-MRI phantom repeatedly over a year. However, the ^{68}Ge tetrachloride molecules in the "prostate" diffused into the "pelvis" to become roughly uniformly distributed throughout the phantom in less than 57 days. We believe that the ^{68}Ge tetrachloride molecules were small enough to penetrate the gel pores, slowly reaching an equilibrium in radioactive concentration throughout the "prostate" and "pelvis." We should be able to prevent this $^{68}GeCl_4$ diffusion by using a barrier, such as a female latex condom, between the "prostate" and "pelvis" so the radioactivity instead reaches an uniform equilibrium within the "prostate" and "pelvis" separately. This is similar to the latex condom used to seal the TRUS hole (i.e., to prevent $^{68}GeCl_4$-gel pieces from escaping onto the TRUS probe), which successfully prevented diffusion. No $^{68}GeCl_4$ contamination was measured on either the TRUS probe or the probe-side of the condom that was permanently fixed on the phantom, based on swipe tests that were measured accurately with a well gamma counter.

Other tissue mimicking materials could also be used for PET-US phantom construction. Typical ultrasound TMMs include agar, Zerdine, urethanes, epoxies, liquids and natural materials. There are three ultrasound TMMs commercially available: Zerdine from CIRs Inc., condensed-milk-based gel from Gammax RMI, and urethane-rubber-based material from ATS Labs. Alternative PET-US phantom construction could utilize radioactive water in condensed milk-agar-based mixtures [2] or poly(vinyl alcohol) cryogels [4]. However, $^{68}GeCl_4$ diffusion is still expected for these alternative TMMs (due to the relative size of the $^{68}GeCl_4$ molecule), so a diffusion barrier would still be necessary.

We investigated the construction of a PET-TRUS-CT-MRI prostate phantom with a more realistic geometry, using the agar-gelatin mixtures from Section III. The phantom would have structures simulating the prostate, rectal wall and urethra in a background gel with an opening for the TRUS probe (Fig. 7). The urethra is routinely simulated by filling a tube with

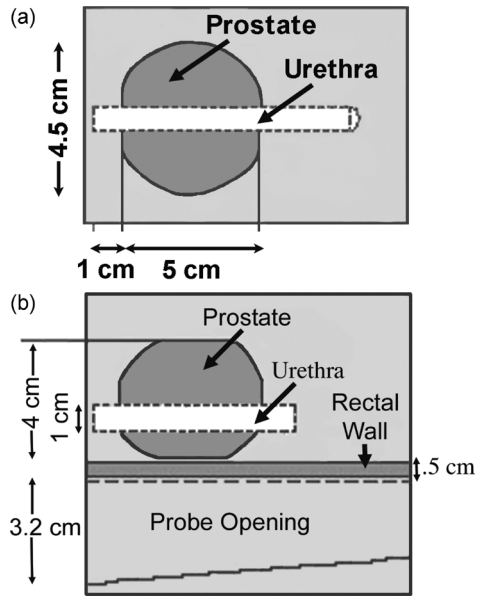

Fig. 7. (a) Top view and (b) side view of design drawing of a PET-TRUS-CT-MRI prostate phantom with more realistic geometry. The phantom structures simulate the prostate, rectal wall and urethra in a background gel with an opening for the TRUS probe.

ultrasound gel with some air bubbles. Since this PET-TRUS prostate phantom would be used only to validate image co-registration, the phantom would not have to exactly mimic the PET and TRUS properties of the prostate region. However, the phantom could be used to validate interventional procedures such a brachytherapy (i.e., radiation therapy where small radiation sources or "seeds" are placed inside or next to the area requiring treatment, such as the prostate).

V. Conclusions

We have successfully developed multi-modality phantoms, including PET-TRUS-CT-MRI phantoms with two regions distinguishable by all four imaging modalities and long-term stability at room temperature. These phantoms had a relatively simple geometry, as their main purpose was to validate image co-registration for PET and TRUS prostate imaging. Long-lived $^{68}\mathrm{Ge}$ was used to allow repeated imaging, but the long-term use of the phantom for PET imaging was unsuccessful due to diffusion of the $^{68}\mathrm{GeCl}_4$ molecules; thus a diffusion barrier between the "prostate" and "pelvis" is required. Based on repeated imaging results, these phantoms appear to have long-term stability otherwise (i.e., except for the $^{68}\mathrm{GeCl}_4$ diffusion). The mechanical properties also appear stable and there are no signs of bacterial or fungal invasion, when stored at room temperature for over ten months.

References

[1] C. L. de Korte, E. I. Cespedes, A. F. W. van der Steen, B. Norder, and K. Te Nijenhuis, "Elastic and acoustic properties of vessel mimicking material for elasticity imaging," *Ultrason. Imaging*, vol. 19, pp. 112–126, 1997.

[2] W. D. D'Souza, E. L. Madsen, O. Unal, K. V. Vigen, and G. R. Frank *et al.*, "Tissue mimicking materials for a multi-imaging modality prostate phantom," *Med. Phys.*, vol. 28, pp. 688–700, 2001.

[3] J. E. Browne, K. V. Ramnarine, A. J. Watson, and P. R. Hoskins, "Assessment of the acoustic properties of common tissue-mimicking test phantoms," *Ultrasound Med. Biol.*, vol. 29, pp. 1053–1060, 2003.

[4] K. J. M. Surry, H. J. B. Austin, A. Fenster, and T. M. Peters, "Poly(vinyl alcohol) cryogel phantoms for use in ultrasound and MR imaging," *Phys. Med. Biol.*, vol. 49, pp. 5529–5546, 2004.

[5] E. L. Madsen, M. A. Hobson, S. Hairong, T. Varghese, and G. R. Frank, "Tissue-mimicking agar/gelatin material for use in heterogeneous elastography phantoms," *Phys. Med. Biol.*, vol. 50, pp. 5597–5618, 2005.

DUAL-MODALITY PROSTATE IMAGING WITH PET AND TRANSRECTAL ULTRASOUND

J.S. Huber, W.W. Moses, Q. Peng, R.H. Huesman, B.W. Reutter, D.S. Wilson, J. Pouliot, and I.C. Hsu
Lawrence Berkeley National Laboratory
University of California, San Francisco

We are developing a dual-modality positron emission tomograph (PET) and transrectal ultrasound (TRUS) prostate imaging system, which allows us to accurately co-register PET and TRUS images that are acquired sequentially during a single imaging session. Functional PET imaging with [^{11}C]choline detects malignant prostate tumors and determines a tumor's aggressiveness based on metabolic uptake level. However, the relative uptake in a prostate tumor can be so great that few other anatomical landmarks are visible in a PET image. Ultrasound imaging with a transrectal probe provides high-resolution anatomical detail in the prostate region that will be accurately co-registered with the sensitive functional information from the PET imaging. This dual-modality PET-TRUS imaging will help localize any cancer within the prostate region.

We have developed initial hardware and software tools for dual PET-TRUS prostate imaging. We have completed the mechanical setup, mechanically modifying the TRUS equipment to work when mounted onto a common patient table in conjunction with the LBNL prostate-optimized PET scanner. We have developed and validated methods for positioning a patient's prostate in the center of the PET scanner, reproducibly positioning the TRUS probe tip (which will be positioned axially at the prostate center) within 1 mm of the PET-center. This prostate positioning is important, since the prostate-optimized PET scanner has optimal resolution and sensitivity near the PET-center and a reduced axial extent. We have also improved the PET image reconstruction software and have developed preliminary image display software. Finally, we have constructed and imaged unique TRUS-PET prostate phantoms that are used to validate PET and TRUS image co-registration. Co-registered PET and TRUS phantom images acquired with this dual-modality system will be presented.

(Currently 1880 characters. Maximum of 2000 characters allowed)

Acknowledgments:
This work was supported in part by the U.S. Department of Energy under Contract No. DE-AC02-05CH11231, and in part by Department of Defense grant number W81XWH-07-1-0020.

Want to be added to the COBRA mailing list? Send email to Carmen Taylor at carmen.taylor@mindspring.com with subject COBRA

Agenda for the Feb 21, 2008 Meeting

Feb 21, 2008
LBNL COBRA Meeting
Ernest Orlando Lawrence Berkeley National Lab

1:30 pm — Arrive at LBNL
Check in at Building 55

1:45 pm
Tours — Budinger, Derenzo, Gullberg, Jagust, & Moses Laboratories
Including:
High-Throughput Facility
Biomedical Isotope Facility

4:00 pm
Talks

Tamara Alliston, PhD
Tough Bones and TGF-β:
Regulation of Bone Matrix Material

Jamie Eberling, PhD
Gene Therapy for Parkinson's Disease

Tom Budinger, MD, PhD
Positron Emitters from Desk-Top Sources:
Carbon-11, Rubidium-82, Iodine-122

Bill Moses, PhD & Jennifer Huber, PhD
Current Instrumentation Projects at LBNL
Dual PET-Transrectal Ultrasound Prostate Imaging

6:00 pm
Dinner — Dinner kindly provided by Philips

COBRA
Community of Bay Area Radionuclide Imagers

Multi-Modality Phantom Development

J.S. Huber, *Member, IEEE,* Q. Peng, and W.W. Moses, *Fellow, IEEE*

***Abstract*–Multi-modality imaging has an increasing role in the diagnosis and treatment of a large number of diseases, particularly if both functional and anatomical information are acquired and accurately co-registered. Although PET-CT has recently revolutionized the role of imaging for many kinds of cancer, ultrasound is the preferred imaging technology for many diseases such as prostate cancer. Transrectal ultrasound (TRUS) is an integral part of diagnosis and treatment for prostate cancer, so we are developing a dual imaging system that will acquire PET and TRUS data during the same patient imaging session and accurately co-register the images. In order to validate our methods prior to patient imaging, we will use a novel custom PET-TRUS prostate phantom. We present our initial PET-ultrasound phantom development, including PET and ultrasound images of a simple phantom, as well as discuss of our future phantom construction plans. We will use agar-gelatin tissue mimicking materials mixed with radioactive water solutions. Although we are currently focused on prostate imaging, this phantom development is applicable to all PET-ultrasound imaging applications. In addition, we discuss how to make a PET-ultrasound phantom also MRI and/or CT compatible.**

I. Introduction

Multi-modality imaging plays an increasingly important role in the diagnosis and treatment of a large number of diseases. Combining modalities that provide both functional and structural information is particularly important. For instance, functional information can be acquired with positron emission tomography (PET) or functional magnetic resonance imaging (fMRI), and anatomical information can be acquired using x-ray computed tomography (CT), ultrasound (US) or magnetic resonance imaging (MRI). Combining PET and CT has recently revolutionized the role of imaging in diagnosis and treatment planning for many kinds of cancer. However, ultrasound is already an integral part of diagnosis and treatment procedures for many diseases, such as prostate cancer. Transrectal ultrasound (TRUS) provides good anatomical detail of the prostate region and accurately measures the prostate volume, whereas CT has poor contrast for soft-tissue (like the prostate) and it over-estimates prostate volume.

We believe that imaging the prostate with ^{11}C-choline using a dual PET-TRUS system will help locate cancer within the prostate region. We envision that dual PET-TRUS prostate imaging could be used to guide biopsy, guide treatment procedures such as external beam radiotherapy and brachytherapy, and detect local recurrence earlier than current clinical practice. Therefore, we are developing a dual imaging system that acquires PET and TRUS data sets during the same patient imaging session using methods that allow us to accurately determine the 3D location of the TRUS probe tip (relative to the PET scanner). As a result, co-registration of the PET and TRUS patient images will be simple and accurate. However, prior to our patient studies, we must validate our ability to image and accurately co-register PET and TRUS images using a PET-TRUS prostate phantom. We will build a custom PET-TRUS prostate phantom with structures that simulate the acoustical properties for TRUS and 511 keV activity concentrations for PET.

We present here our initial PET-ultrasound phantom and PET-US-CT-MRI phantom development, including multi-modality images of simple phantoms. This phantom development is applicable to many multi-modality applications. We will also discuss our future prostate phantom construction plans.

II. Custom PET-Ultrasound Phantom

We have constructed a simple PET-ultrasound prostate phantom as proof of principle. When developing the procedures for our phantom construction, we used short-lived ^{18}F radioactive (110 minutes half-life) water solutions, since ^{18}F is readily available from our in-house cyclotron and no long-lived radioactive waste were generated by the tests. Our simple PET-US phantom was constructed in two stages. We first filled a rectangular plastic box with 4% agarose that was prepared as a high-scatter ultrasound tissue mimicking material (TMM), creating a void with a petrolatum-coated plastic rod in the center. Once the rectangular agarose "pelvis" hardened, the rod was removed and we filled the inner cylindrical "prostate" region with a low-scatter ultrasound 8% gelatin TMM. Fig. 1a shows a photograph of the PET-US phantom. At each stage, the TMM was mixed with ^{18}F radioactive water solution before putting it into a refrigerator to harden. The phantom had six times higher 511 keV activity density in the inner cylindrical "prostate" than in the outer rectangular "pelvis."

The phantom was roughly centered in an EXACT HR PET camera, and PET data were acquired with a 10 minute transmission scan followed by a 20 minute emission scan in 3D mode. At the start of the emission scan, the ^{18}F activity density was 1.07 μCi/ml in the cylindrical "pelvis" gelatin and 0.17 μCi/ml in the rectangular "pelvis" agarose. Image reconstruction was performed with attenuation and scatter correction. Fig. 1b shows a reconstructed coronal PET image of the phantom. The ^{18}F activity uniformly concentrated in the cylindrical "prostate" gelatin is clearly visible within the rectangular "pelvis" background activity, as shown in Fig. 1b.

Manuscript received November 15, 2007. This work was supported in part by the U.S. Department of Energy under Contract No. DE-AC02-05CH11231, and in part by Department of Defense grant number W81XWH-07-1-0020.

J.S. Huber, Q. Peng, and W.W. Moses are all with Lawrence Berkeley National Laboratory, Berkeley, CA 94720 USA (telephone: 510-486-6445, e-mail: jshuber@lbl.gov).

(a)

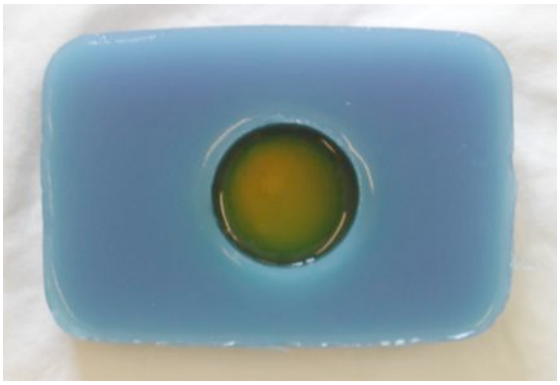

(b)

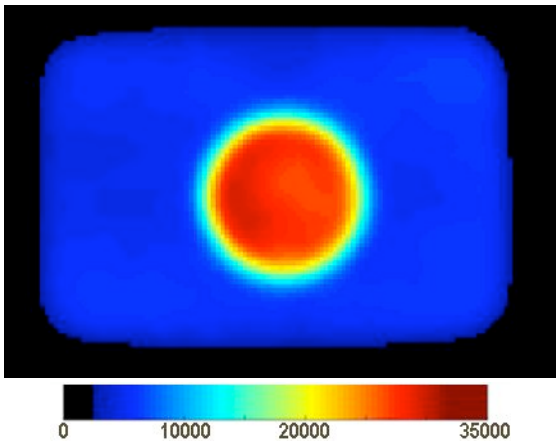

(c)

Fig. 1. (a) Photograph of a simple PET-ultrasound phantom. The blue-colored agarose has outer dimensions of 16 cm x 11 cm x 3.5 cm. The yellow-colored gelatin cylinder has a 5 cm diameter and 2.5 cm depth. (b) Reconstructed coronal PET image of the PET-ultrasound phantom. The red-yellow circle shows the high ^{18}F activity concentration in the "prostate" region, and the blue rectangle shows the low ^{18}F activity concentration in the background "pelvis" region. Image represents 636 M counts (*i.e.,* 20 minutes of data). The voxel size is 1.47 mm x 1.47 mm x 3.13 mm. (c) Ultrasound image of the same phantom using a 5MHz external ultrasound probe. The dark gray circle shows the low-scatter gelatin "prostate," and the surrounding light gray background shows the high-scatter agarose "pelvis."

The phantom was then imaged using a 5 MHz external Elektra ultrasound system, as shown in Fig. 1c. The ultrasound image clearly shows the low-scatter cylindrical "prostate" gelatin, which is surrounded by the high-scatter "pelvis" agarose. Thus, we have demonstrated our ability to construct and image a custom PET-ultrasound phantom. However, the phantom's mechanical and ultrasound properties did not have long-term stability especially at room temperature.

III. Custom PET-US-CT-MRI Phantom

Methods on ultrasound phantom construction are well represented in literature [1-5]. Since the phantom described in section II did not have long-term stability at room temperature, we needed to develop a different phantom construction process. We have constructed a multi-modality phantom using tissue mimicking mixtures of agar, gelatin, $CuCl_2$-$2H_2O$, EDTA-tetra Na Hydrate, NaCl, HCHO, Germall-Plus^{TM}, glass beads, $BaSO_4$, and deionized water (Table I). Similar agar-gelatin mixtures were proven to have long-term mechanical, ultrasound and MRI properties for at least one year [5]. These agar-gelatin-based tissue mimicking materials can be mixed with radioactive water solutions. When developing the procedures for the agar-gelatin-based phantom construction, we used non-radioactive water and short-lived ^{18}F radioactive water solutions. Once the phantom construction procedures are finalized, we will use long-lived ^{68}Ge radioactivity (271 day half-life) for phantom construction to allow repeated PET imaging of the same phantom over at least one year. The main purpose of this phantom is to develop radioactive TMMs, with long-term stability at room temperature, that approximate the acoustical properties of patients more accurately than those developed in section II.

We constructed a two-region PET-US-CT-MRI phantom with an inner cylindrical "prostate" within an outer rectangular "pelvis" (*i.e.*, with the same simple geometry as the PET-US phantom described in section II). We first filled the rectangular "pelvis" container with the "Pelvis TMM" (Table I), creating a void with a petrolatum-coated plastic rod in the center. This rod was removed once the rectangular "pelvis" hardened, then we filled the inner cylindrical "prostate" with a "Prostate TMM" (Table I) having different multi-modality properties and ^{18}F activity. The TMMs were hardened at room temperature. Fig. 2 shows a photograph of the custom PET-US-CT-MRI phantom.

	Agar	Gelatin	$CuCl_2$-$2H_2O$	EDTA	NaCl	HCHO	Germall-Plus	Glass Beads	$BaSO_4$
Pelvis TMM	1.17	5.50	0.11	0.32	0.77	0.24	1.44	4.38	0.50
Prostate TMM	3.64	5.70	0.12	0.34	0.80	0.25	1.50	0	0

Table I. Dry-weight percents of the various components in the PET-US-CT-MRI custom phantom. The weight percent of the deionized water is not shown since it makes up the remainder.

Table I outlines the dry-weight percents for the "Prostate TMM" and "Pelvis TMM" used to construct the custom PET-US-CT-MRI phantom. For these tests, only the cylindrical "prostate" TMM was mixed with a ^{18}F-water solution. The primary role of each ingredient is summarized below:

- *Agar*: concentration set to achieve tissue-like US properties, such as US propagation speed. Higher agar concentration also produces shorter longitudinal (T_1) and transverse (T_2) MRI relaxation times.
- *Gelatin*: concentration set for tissue-like US properties, such as US propagation speed. Concentration must be roughly the same for "prostate" and "pelvis" regions to avoid changes in volumes due to osmosis.
- *$CuCl_2$-2H_2O* and *EDTA-tetra Na Hydrate*: EDTA forms chelate with the Cu^{2+} ions to allow Cu^{2+} to remain mobile, allowing controlled lowering of the T_1 MRI relaxation time.
- *NaCl*: anti-bacterial agent that produces tissue-like MRI coil loading.
- *HCHO* (37% formaldehyde): cross-links the gelatin, raising the melting point to 78 °C where the agar component melts.
- *Germall-Plus^{TM}*: preservative to prevent fungal and bacterial invasion.
- *Glass Beads* (20 μm average diameter): increases ultrasound attenuation and backscatter to tissue-like levels. Also lowers T_1 and T_2 MRI relaxation times.
- *$BaSO_4$*: increases radiographic attenuation for CT.
- *^{18}F*: 511 keV radioactivity for PET imaging.

The expected ultrasound properties include a propagation speed of about 1535 m/s, a density of about 1.04 g/ml, and an attenuation coefficient divided by frequency of about 0.14 dB/cm/MHz for the "Prostate TMM" and 0.38 dB/cm/MHz for the "Pelvis TMM." The MRI T_1 relaxation times are expected to be about 494 ms for the "Prostate TMM" and 423 ms for the "Pelvis TMM" [5].

Fig. 2. Photograph of a custom PET-US-CT-MRI phantom. The aqua-colored rectangular "pelvis" has outer dimensions of 16 cm x 11 cm x 3.5 cm. The dark green-colored cylindrical "prostate" has a 5 cm diameter and 2.5 cm depth (*i.e.* inner cylinder does not go all the way through).

The custom PET-US-CT-MRI phantom was imaged using an EXACT HR PET scanner. PET data were acquired with a 3D emission scan followed by a 10 minute transmission scan. Iterative image reconstruction was performed with attenuation and scatter correction. Fig. 3a shows a reconstructed coronal PET image of the phantom. The ^{18}F activity concentrated in the cylindrical "prostate" is clearly visible. The PET image in the "prostate" region is not uniform in this case (*e.g.*, compared to Fig. 1b) due to PET scanner hardware problems that affected the attenuation map and normalization.

(a)

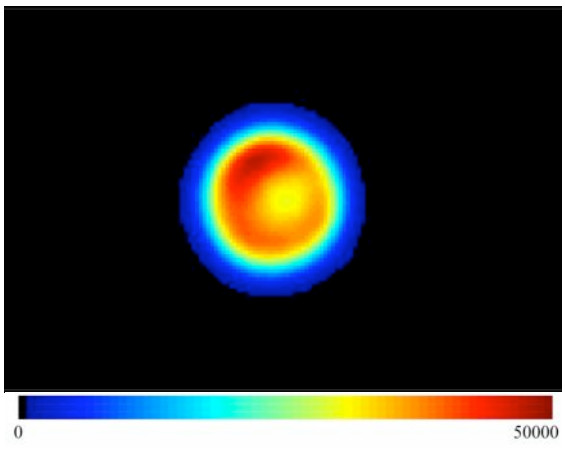

(b)

(c)

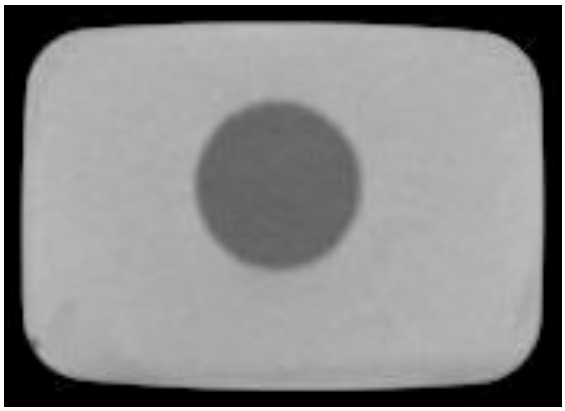

Fig. 3. (a) Reconstructed coronal PET image of the custom PET-US-CT-MRI phantom. The colored circle shows the ^{18}F activity in the "prostate" region; the ^{18}F activity density was 0.8 μCi/ml in the "prostate" at the start of the 60 minute emission scan. Voxel size is 3.6 mm x 3.6 mm x 4 mm. (b) Ultrasound image of the phantom using a 5 MHz external ultrasound probe. The dark gray circle shows the lower-scatter "prostate," and the surrounding gray background shows the higher-scatter "pelvis." (c) Reconstructed coronal x-ray CT image of the phantom with 1 cm axial thick slices. The pixel size is 1 mm x 1 mm x 10 mm. The dark gray circle shows lower radiographic attenuation in the "prostate" compared with the surrounding light gray higher-attenuation "pelvis."

The custom PET-US-CT-MRI phantom was imaged by the other three modalities the following day, after the ^{18}F radioactivity decayed. The phantom was imaged with a 5MHz external Elektra ultrasound system. Fig. 3b shows an ultrasound image of the phantom with a lower-scatter cylindrical "prostate" surrounded by higher-scatter "pelvis." The phantom was then imaged with a Hawkeye CT scanner (140 keV; 2.5 mAmps) on a Millennium VG3 SPECT gantry. Reconstruction was performed with filtered backprojection using a Hann filter with a cutoff frequency of 1. Fig. 3c shows a reconstructed coronal CT image of the phantom with increased radiographic attenuation in the "pelvis" due to the $BaSO_4$.

Finally, the phantom was imaged with an 1.5 T Avanto Siemens MRI scanner using a head coil with a T_1-weighted 2D spin echo pulse sequence (TE = 7.8 msec; TR = 500 msec; field of view = 220 mm x 178.8 mm x 3 mm; voxel size = 0.4 mm x 0.4 mm x 3 mm). Fig. 4a shows a reconstructed T_1-weighted MRI image with a darker "prostate" representing a longer T_1 compared to the "pelvis." The glass beads (used for ultrasound imaging) shortened the T_1 in the "pelvis" to make it brighter, despite the increased agar concentration in the "prostate." The phantom was also imaged with a T_2-weighted 2D turbo spin echo pulse sequence (TE = 91 msec; TR = 4000 msec; field of view = 220 mm x 175.3 mm x 3 mm; voxel size = 0.4 mm x 0.4 mm x 3 mm). Fig. 4b shows a reconstructed T_2-weighted MRI image with a darker "prostate" representing a shorter T_2 compared to the "pelvis."

(a)

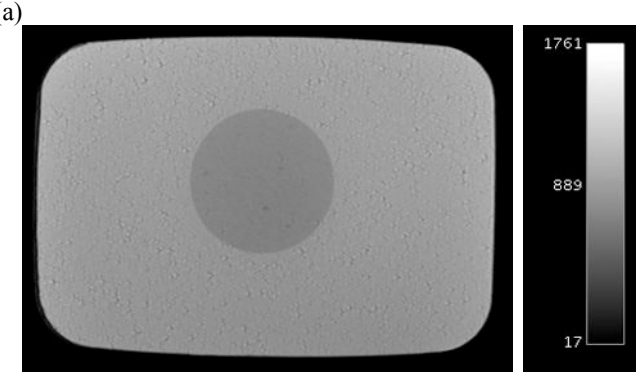

(b)

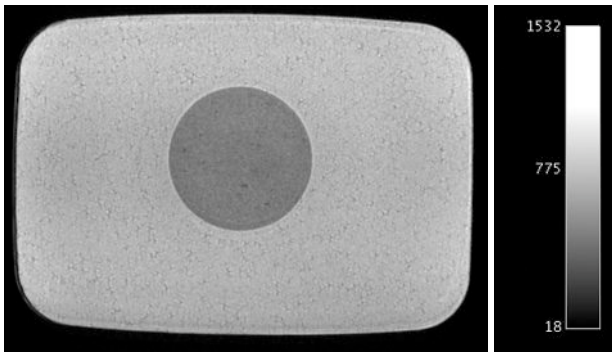

Fig. 4. (a) Reconstructed coronal MRI T_1–weighted image of the custom PET-US-CT-MRI phantom, representing 60 minutes of data. Voxel size is 0.4 mm x 0.4 mm x 3 mm. The dark gray circle shows the longer T_1 "prostate" surrounded by the shorter T1 "pelvis." (b) Reconstructed coronal MRI T_2–weighted image of the phantom, representing 60 minutes of data. Voxel size is 0.4 mm x 0.4 mm x 3 mm.

IV. Future Plans

We plan to make a PET-TRUS prostate phantom with a more realistic geometry using ^{68}Ge water in a finalized agar-gelatin mixture (as determined from above). The phantom will have structures simulating the prostate, rectal wall and urethra in a background gel with an opening for the TRUS probe (Fig. 5). The urethra is routinely simulated by filling a tube with ultrasound gel with some air bubbles. We will image this PET-TRUS prostate phantom with PET and TRUS to confirm that we have produced a phantom with the required properties. Since this PET-TRUS prostate phantom will be used only to validate image co-registration, the phantom does not have to exactly mimic the PET and TRUS properties of the prostate region.

(a) Top View:

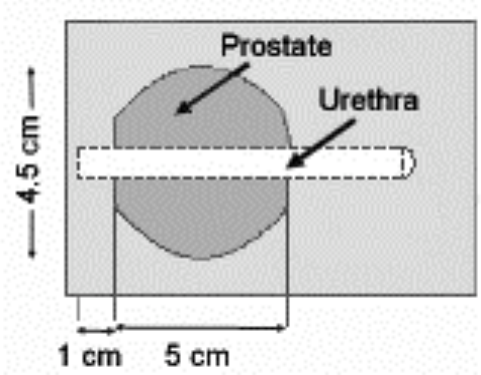

(b) Side View:

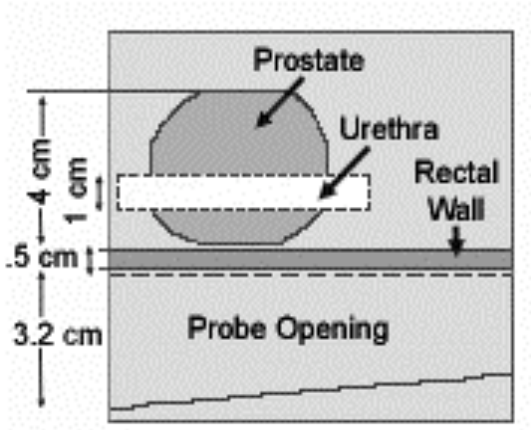

Fig. 5. Design drawing of the TRUS-PET prostate phantom that will be constructed at LBNL. The phantom will have structures simulating the prostate, rectal wall and urethra in a background gel with an opening for the TRUS probe.

If the agar-gelatin mixture does not work, other tissue mimicking materials could be used. Typical TMMs include agar, Zerdine™, urethanes, epoxies, liquids and natural materials. There are three TMMs commercially available: Zerdine™ from CIRs Inc., condensed-milk-based gel from Gammax RMI, and urethane-rubber-based material from ATS Labs. If necessary, we could investigate alternative phantom construction using radioactive water in condensed milk-agar-based mixtures [2] or poly(vinyl alcohol) cryogels [4].

V. Conclusions

We have successfully developed multi-modality phantoms, including a PET-US-CT-MRI phantom with two regions distinguishable by all four imaging modalities and long-term stability expected at room temperature. These phantoms had a relatively simple geometry, as their main purpose was to develop phantom construction methods. Our final multi-modality prostate phantom will be used to validate image co-registration for PET and TRUS prostate imaging. This prostate phantom will have a more realistic geometry (*e.g.*, rectal probe opening), but it does not have to exactly mimic the TRUS tissue properties or anatomy of the prostate region. Long-lived ^{68}Ge will be used for the final prostate phantom, to allow repeated use over at least a year.

VI. References

[1] C. L. de Korte, E. I. Cespedes, A. F. W. van der Steen, B. Norder and K. Te Nijenhuis, "Elastic and Acoustic Properties of Vessel Mimicking Material for Elasticity Imaging," *Ultrason. Imaging*, vol. 19, pp. 112-126, 1997.

[2] W. D. D'Souza, E. L. Madsen, O. Unal, K. V. Vigen, G. R. Frank, et al., "Tissue mimicking materials for a multi-imaging modality prostate phantom," *Med. Phys.*, vol. 28, pp. 688-700, 2001.

[3] J. E. Browne, K. V. Ramnarine, A. J. Watson and P. R. Hoskins, "Assessment of the acoustic properties of common tissue-mimicking test phantoms," *Ultrasound Med. Biol.*, vol. 29, pp. 1053-1060, 2003.

[4] K. J. M. Surry, H. J. B. Austin, A. Fenster and T. M. Peters, "Poly(vinyl alcohol) cryogel phantoms for use in ultrasound and MR imaging," *Phys Med Biol*, vol. 49, pp. 5529-5546, 2004.

[5] E. L. Madsen, M. A. Hobson, S. Hairong, T. Varghese and G. R. Frank, "Tissue-mimicking agar/gelatin material for use in heterogeneous elastography phantoms," *Phys. Med. Biol.*, vol. 50, pp. 5597-5618, 2005.

IEEE Medical Imaging and Nuclear Science Symposium Conference, October 2007

Multi-Modality Phantom Development

J.S. Huber, Q. Peng, W.W. Moses,

Lawrence Berkeley National Laboratory

Multi-modality imaging has an increasing role in the diagnosis and treatment of a large number of diseases, particularly if both functional and anatomical information is acquired and accurately co-registered. Although PET-CT has recently revolutionized the role of imaging in diagnosis and treatment for many kinds of cancer, ultrasound is the preferred imaging technology for many diseases such as prostate cancer. Since transrectal ultrasound (TRUS) is an integral part of diagnosis and treatment for prostate cancer, we are developing a dual imaging system that will acquire PET and TRUS data during the same patient imaging session and accurately co-register the images. In order to validate our methods, we will use a novel custom PET-TRUS prostate phantom. We present our initial PET-ultrasound phantom development, including PET and ultrasound images of a simple phantom, as well as discuss of our future phantom construction plans. We will use agar-gelatin tissue mimicking material mixed with radioactive water solutions. Although we are currently focused on prostate imaging, this phantom development is applicable to all PET-ultrasound imaging applications. In addition, we discuss how to make a PET-ultrasound phantom also MRI and/or CT compatible.

(Currently 1260 characters with spaces. Maximum of 1500 allowed?)

Acknowledgments:
This work was supported in part by the U.S. Department of Energy under Contract No. DE-AC02-05CH11231, and in part by Department of Defense grant number W81XWH-07-1-0020.

Address correspondence to:
Jennifer Huber
Lawrence Berkeley National Laboratory
1 Cyclotron Rd., Mail Stop 55-121
Berkeley, CA 94720
(510) 486-6445
(510) 486-4768 (FAX)
jshuber@lbl.gov